Faculty of Aerospace Engineering

Measuring and modeling the role of time margins on drivers' pedal control inputs during cornering speed adaptation

Virgílio Gruppelaar

July 12, 2017

TU Delft Delft University of Technology

Challenge the future

Measuring and modeling the role of time margins on drivers' pedal control inputs during cornering speed adaptation

Master of Science Thesis

For obtaining the degree of Master of Science in Aerospace Engineering
at Delft University of Technology

Virgílio Gruppelaar

July 12, 2017

Faculty of Aerospace Engineering · Delft University of Technology

Delft University of Technology

Delft University Of Technology
Department Of
Control and Simulation

The undersigned hereby certify that they have read and recommend to the Faculty of Aerospace Engineering for acceptance a thesis entitled **"Measuring and modeling the role of time margins on drivers' pedal control inputs during cornering speed adaptation"** by **Virgílio Gruppelaar** in partial fulfillment of the requirements for the degree of **Master of Science**.

Dated: July 12, 2017

Readers:

M. M. (René) van Paassen

David A. Abbink

Max Mulder

Contents

Part I

Scientific article

Measuring and modeling the role of time thresholds in drivers' pedal control inputs during cornering speed adaptation

Virgílio Gruppelaar
Control and Simulation, Faculty of Aerospace Engineering
Delft University of Technology
email: virgilio@quintadoriodao.com

***Abstract*—Reducing conflicts between drivers and assistance systems has become an important issue in recent times, resulting in a need for a better understanding of how humans drive. Current models of driver speed choice on curved roads do not model accelerator and brake pedal deflections, and consequently do not account for the fact that deceleration usually occurs in two distinct phases. The contribution of this work lies in the combination of studies of driver's visual fixations during curve driving with research on how drivers use time thresholds as safety margins, resulting in a more realistic computational driver model that uses thresholds on a single visual perceptual variable to trigger the release of the accelerator and the application of the brakes. A simulator experiment showed that, after individualization of the thresholds using a binary classification method, the model is capable of accurately capturing the speed adaptation of 15 human drivers on single lane roads with multiple curves.**

ACRONYMS

ADAS	Advanced Driver Assistance Systems
ETP	Extended Tangent Point
FN	False Negative
FP	False Positive
HMI	Human-Machine Interaction
HSC	Haptic Shared Control
MCC	Matthews Correlation Coefficient
OP	Occlusion Point
TETP	Time to Extended Tangent Point
TLC	Time to Line Crossing
TN	True Negative
TP	True Positive
TP	Tangent Point
VAF	Variance Accounted For

LIST OF SYMBOLS

Greek Symbols

δ_a	Accelerator pedal deflection [-]
$\delta_{a,EB}$	Minimum accelerator pedal deflection needed to overcome engine braking [-]
δ_b	Brake pedal deflection [-]

Roman Symbols

$\mathrm{d}T_a$	TETP rate of change for re-acceleration [-]
K_a	Accelerator pedal depression gain [-]
K_b	Brake pedal depression gain [-]
K_d	Accelerator pedal release gain [-]
T_b	Minimum TETP margin before start of braking phase [s]
T_d	Minimum TETP margin before start of deceleration phase [s]
V	Vehicle speed [ms^{-1}]
V_{max}	Speed limit on current road section [ms^{-1}]

I. INTRODUCTION

DRIVING a car on a curved road is a task most people are familiar with. As they steer their vehicle along the road, drivers adapt their speed to suit the road they are driving on. However, despite a large wealth of research on driver modeling, the mechanisms that govern this speed adaptation are not yet well explored. Over the past decade, the focus of automobile research has shifted to Advanced Driver Assistance Systems (ADAS) and automated driving. In order to avoid conflicts between driver and automation, these systems must understand driver's intentions. In the context of speed choice, understanding how drivers control their speed on a curving road becomes essential.

Field studies show a correlation between curve radius and speed [1, 2, 3]. Small radius curves are taken at low speeds, with a marked increase in speed up to radii of 100m, while curves of radius larger than 300m show little evidence of any speed adaptation at all, and are essentially treated as straight road sections [4, 5]. Other geometrical factors that can influence speed choice are the road width [6], the lengths of the straight road sections between curves, the curve deflection angle, the presence of other curves in close proximity, and the curve superelevation [7]. In addition to this, the lateral position of the vehicle on the road can alter the effective turn radius, impacting drivers' speed choice [8].

When approaching a turn that requires speed adaptation, drivers have two distinct methods of decelerating: either by releasing the accelerator pedal, taking advantage of engine braking, rolling resistance and drag, or by pressing the brake pedal [1]. The deceleration phase generally begins on the straight road segments, and in many cases continues into the entry of the curve, while drivers usually begin to accelerate before having completely exited the turn [7, 8].

In the context of road design and road safety, many studies model the speed at which a driver can safely negotiate a turn based on the geometrical characteristics of said turn. While

this is a useful limit for assistance systems to take into account as an upper boundary, it does not provide information about a driver's desired speed and is consequently not directly usable in ADAS applications [9]. We wish to model the manner in which drivers themselves choose their speed, depending on their preferences of driving style, risk, or safety margins.

Drivers deliberately stay well within the dynamic capabilities of the vehicles they drive [10], performing a tradeoff between comfort, mostly measured by lateral acceleration, and speed [11, 12]. However, in most situations drivers tend to slow down before reaching a corner [1, 10, 13], which means that some sort of estimation or anticipation of the lateral acceleration must take place.

There are several approaches to modeling this anticipation. The vast majority of these propose a direct relationship between road curvature and speed, fitting parameters to experimental data [2, 9, 14]. Bosetti et al. [1] developed a model relating speed to road radius based on the two-thirds power law relating velocity and curvature of human hand movements. Reymond et al. [15] argue that drivers have a maximum estimated lateral acceleration and adapt their speed accordingly, taking into account a safety margin on the maximum tolerable path curvature deviation, but do not provide any explanation on how drivers estimate this maximum limit.

These models can provide good fits to experimental data of individual curves, and can estimate maximum velocity envelopes with good accuracy. However, the models currently found in literature have their limitations. As seen in the naturalistic driving studies described above, curvature is not the only geometric factor that influences speed. In addition, the actual path geometry can significantly vary with the lateral position of the vehicle during the turn [8]. In order to account for the effects of the geometry of the turn, adjacent road segments, and lateral position, model complexity will increase [4, 7]. Another issue with these models is that human drivers have been shown to be poor judges of road curvature [16], which means that different cues must play a role.

As described previously, speed control in curves consists of three different phases: engine braking, braking, and acceleration. Geometrical models limit themselves to describing the desired speed in curves, ignoring approach and exit phases. In order to design effective ADAS systems, the modeling of driver preferred pedal actuation in all three cornering segments is essential.

The combination of these issues means that in order to gain insight into the actual mechanisms regulating speed choice, a different approach is necessary. During driving, humans tend to control their risk by employing certain safety margins [17]. In situations where speed needs to be adjusted, these are usually time margins such as the Time to Line Crossing (TLC) in lane keeping [18] or the Time Headway and Time To Contact in car following [19]. Contrasting with their poor performance in judging distances, velocities, and curvatures [16], humans can very accurately judge visual angles and time margins to target or contact points [20]. This leads us to believe that speed adjustment in turns is very likely dependent on a time margin to a salient point.

Godthelp and van Winsum [18] used this approach, arguing that speed and curvature are traded off in order to maintain a constant TLC. However, later research showed that the TLC is not constant throughout turns of different radius [6, 15]. In addition, similarly to the previously mentioned geometry based approaches, this model does not provide insight into the different phases of longitudinal control in curve negotiation, and does not describe pedal actuation.

Human drivers tend to manage their risk with as little cognitive and physical effort as possible [21]. This means that unless there is a factor requiring immediate action in order to stay within their acceptable risk limits, humans prefer not to take any action. In the context of this research, this suggests that we should not aim at developing a model of driver speed control that aims at keeping a constant safety margin, such as the TLC model, but rather use time thresholds that trigger specific actions, such as the release of the accelerator pedal or the application of the brakes.

Land and Lee [22] introduced the idea that the Tangent Point (TP) on the inside of a curve is key to curve negotiation, and a substantial amount of research has shown that drivers focus their gaze towards the area containing the apex of the curve, employing what is called TP orientation [23]. However, driver eye movement studies have shown that drivers do not fixate only on this point, but also scan areas further up the road in a controlled pattern [24]. A particular area of interest is the *far road triangle* [25], comprised of the TP, the Occlusion Point (OP), which is the furthest point of the road that is not blocked by obstacles in the field of vision, and the point where the driver's line of vision through the TP intersects the opposite lane edge, the Extended Tangent Point (ETP).

The contribution of this work lies in combining existing studies into driver visual behavior with research on drivers' tendency to use time margins to control their speed, by developing a model for speed choice based on ETP perception. The model uses threshold values to distinguish between braking, acceleration and gas pedal release.

Section II describes the approach taken in designing the model, the developed speed control algorithm, and predictions from simulation. Section III explains the identification procedure used to individualize the model parameters. To validate the model, an experiment was set up and performed, as shown in Section IV. The results from this experiment are shown in Section V and discussed in Section VI.

II. Model design

The Time to Extended Tangent Point (TETP), defined as the time it would take for the vehicle to reach the ETP in a straight line, while maintaining its speed, could be an excellent candidate for the development of a simple, yet accurate model of speed choice in curve driving. This time margin can be interpreted as a measure of how much the road opens up after a turn, as illustrated in Figure 1. The curve on the right of this figure is less tight than the one on the left, and leads to less speed adaptation. Consequently, on the right example the ETP is further away from the car than on the sharp curve on the left, causing a larger TETP value.

The ETP position also captures variations in the car position on the road, as seen in Figure 2. On the left, the vehicle is

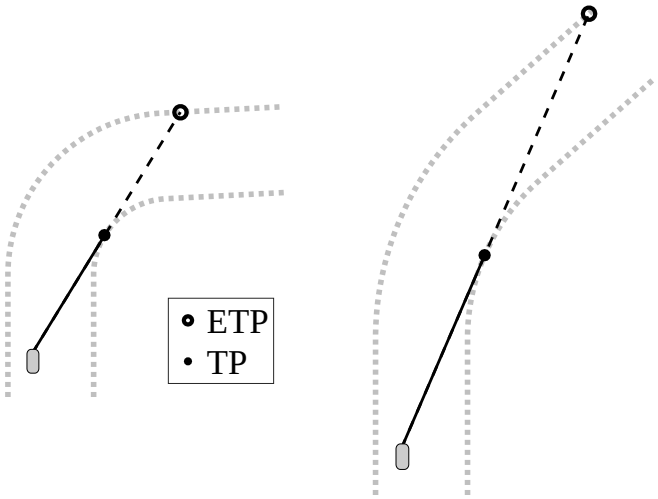

Fig. 1. ETP position on curves of different radii and deflection angles.

driving through the turn, and the location of the ETP changes with the car as it moves from position 1 to position 2. This way, a model based on the ETP will be able to represent the speed variation throughout the entire turn. On the right of Figure 2 the influence of lateral position on the ETP is shown. When the vehicle is close to the inside of the turn (2), it effectively makes the turn tighter than when the car is on the outside (1). This is represented by the comparatively shorter distance to the ETP in case 2, which will lead to lower TETP values.

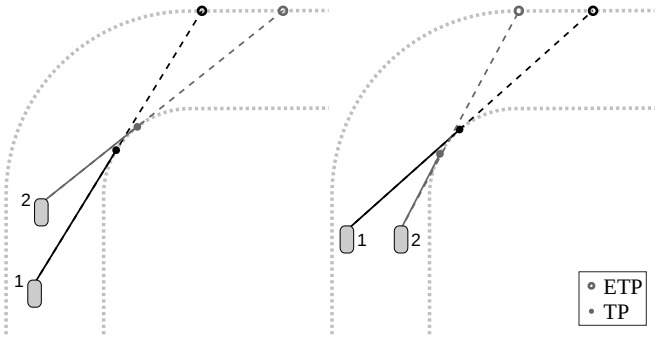

Fig. 2. Change of ETP position with changes in vehicle longitudinal and lateral positions.

A. Preliminary findings

A preliminary analysis of data obtained from an earlier experiment on the influence of steering guidance on speed choice, performed at the Human-Machine Interaction (HMI) Laboratory of the Delft University of Technology [26], showed that drivers used two different time margins for the two phases of speed regulation: they first released the accelerator at a certain TETP, and only when the TETP went below a certain lower value would they begin to press the brake pedal.

The study of mid-corner and corner exit behavior also showed a correlation between speed and TETP. Close to the end of the decelerating or braking phases, the TETP decreased more slowly until eventually becoming constant, before increasing again as a consequence of the road opening up after the turn. Drivers appeared not to use the same thresholds when accelerating as when slowing down, but became comfortable once the rate of change of the TETP approached zero. Then, drivers began accelerating, and only if the TETP started decreasing again did they resume decelerating or braking.

The curves in this experiment had large radii (minimum of 300m), and therefore many of the subjects did not adapt their speed throughout the experiment. Therefore, a new experiment in which all drivers are required to adapt their speed will be necessary to confirm or reject this hypothesis.

However, this experiment did show that, as would be expected, each driver is different. Some drivers never adapted their speed to the given road, while others felt the need to brake in certain curves. This can be attributed to the idea that different drivers feel comfortable at different TETP values. By identifying these different thresholds, and combining them with different gains on the pedal actuation, it could be possible to use a TETP based approach to model each driver's individual preferences and driving styles.

The combination of these findings lead us to select TETP thresholds as the primary perceptual variables for the development of a model of driver speed control through pedal actuation.

B. Model architecture

The TETP is determined following the method described in Appendix A. After calculation of the TETP, its value is used in a speed control model. The model is divided into five phases: *acceleration*, *deceleration*, *braking*, *brake release*, and *re-acceleration*. Two thresholds on the TETP value, one for deceleration and one for braking, and one threshold on the TETP rate of change determine which of the five phases of the model is active. A typical example of how the model works is shown in Figure 3, where a simulated vehicle (see Section II-E for details) negotiates a 150m radius left turn with a target speed of 27ms^{-1} on the straight sections. In this figure, we can clearly see the differences between the phases of the model.

Initially, the vehicle is above both the deceleration and braking TETP thresholds, and therefore the *acceleration* phase is active. In this phase, the accelerator pedal deflection is only dependent on the ratio between the current speed and the target speed. Since the vehicle is already driving at the target speed, the gas pedal deflection is just enough to overcome engine braking, rolling resistance and drag, and therefore the vehicle maintains its speed.

Once the TETP goes under the deceleration threshold, the model enters the *deceleration* phase, where it gradually decreases the accelerator pedal deflection. If the TETP goes under the braking threshold, the *braking* phase starts.

If the model is either in the *deceleration* or the *braking* phase, the rate of change of the TETP becomes the most important factor in the decision of when the model stops decelerating or begins releasing the brake pedal.

During the *braking* phase, once the rate of change of the TETP approaches zero, the model switches to the *brake release*

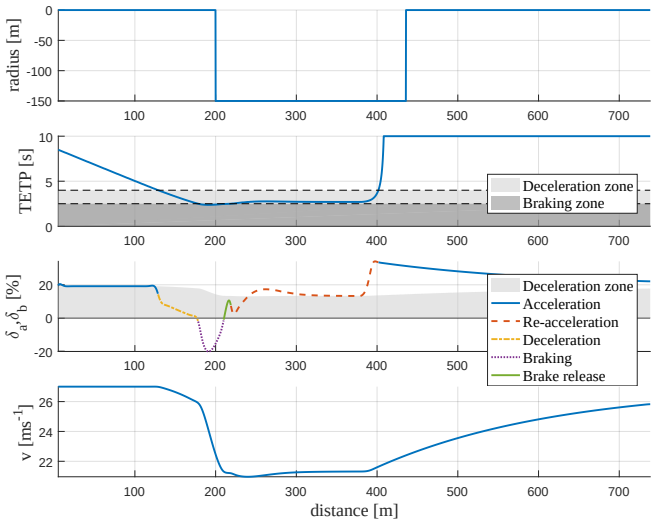

Fig. 3. Simulated TETP, pedal deflections, and speed on a 150m radius left turn (negative radius in the figure). Positive pedal deflections correspond to the accelerator pedal, while negative deflections represent brake actuation. The shaded area represents the deceleration zone, that is, the accelerator pedal position values that correspond to a zero or negative acceleration.

phase. In this phase the model begins releasing the brakes, and can even apply a small deflection to the accelerator pedal once the brakes have been completely released. The accelerator pedal deflection during the *brake release* phase can never be above the deceleration zone shown in the figure.

If the TETP value is in between the deceleration and braking thresholds, but its rate of change is positive or close to zero, the *re-acceleration* phase will activate. This phase represents the mid-corner behavior, when the vehicle has already slowed down to the desired corner speed, but is still inside the corner and therefore cannot accelerate without limitations.

When all TETP thresholds have been cleared, the model returns to the *acceleration* phase, accelerating back to the target speed.

The remainder of this section will describe the model parameters, followed by a more detailed description of how these parameters affect the choice of the model phase, and how pedal deflections are calculated in each of the five phases. Finally, the results of a sensitivity analysis performed on the model parameters are shown.

C. Model parameters

To capture the three distinct methods that drivers use to adapt their speed during cornering, the model regulates vehicle speed using six driver dependent parameters: two thresholds on the TETP and one threshold on the TETP rate of change to determine the model phase, and three actuation gains to describe the magnitude of the corresponding pedal actuations in each phase. The parameters are:

- T_d [s]: The minimum TETP drivers keep before releasing the accelerator pedal, and entering the *deceleration* phase.
- K_d [-]: The accelerator pedal release gain. Determines how quickly the driver lets go of the gas pedal during the *deceleration* phase.
- T_b [s]: The minimum TETP drivers keep before pressing the brake pedal, and entering the *braking* phase.
- K_b [-]: The brake pedal depression gain. Determines how strongly the driver presses the brake pedal during the *braking* phase.
- $\mathrm{d}T_a$ [-]: The rate of change of TETP at which the driver feels comfortable to begin accelerating out of a turn. Determines when the *brake release* and *re-acceleration* phases begin, if the model is already in the *braking* or *deceleration* phases, respectively.
- K_a [-]: The accelerator pedal depression gain. Determines how strongly the driver presses the accelerator pedal during the *acceleration*, *brake release* and *re-acceleration* phases.

In addition to these parameters, the model requires the following information from the vehicle properties and the road ahead:

- V: current vehicle speed.
- V_{max}: maximum speed, determined by either car characteristics, the speed limit on the current road section, or other external factors.
- TETP: Current time to the extended tangent point.
- $\frac{\mathrm{dTETP}}{\mathrm{d}t}$: Rate of change of the TETP, de-noised with a moving average filter.
- $\delta_{a,EB}$: Accelerator pedal position needed to overcome engine braking, that is, the pedal position at which the vehicle acceleration is $0\mathrm{ms}^{-2}$. This value depends on the current speed and the engine characteristics.

D. Speed control algorithm

The algorithm the model uses to select one of the five phases, based on the three thresholds T_d, T_b and $\mathrm{d}T_a$, is described in Figure 4.

In each of the five phases, the model finds a desired brake and accelerator pedal deflection, δ_a and δ_b respectively. The way these deflections are calculated for each phase is described below. These values are bound between the *released* and *fully depressed* states, corresponding to values of 0 and 1. If the found value in any of the model phases is outside of this range, it set to the nearest value between 0 and 1.

1) *Acceleration*: If the current TETP is above the deceleration threshold T_b, the model will go into the *acceleration* phase, where the brake pedal deflection is $\delta_b = 0$ and the accelerator pedal deflection, δ_a, is limited only by the maximum speed on the road segment, as described by Equation (1).

$$\delta_a = \delta_{a,EB} + K_a \left(1 - \frac{V}{V_{max}}\right) \tag{1}$$

2) *Deceleration*: If the TETP is below the deceleration limit T_d, but above the braking limit T_b, the model is in the *deceleration* phase. In this case, the brake pedal deflection continues to be zero, while the desired accelerator pedal deflection is a function of how far the TETP is from both thresholds, as described by Equation (2). The resulting value is bound between

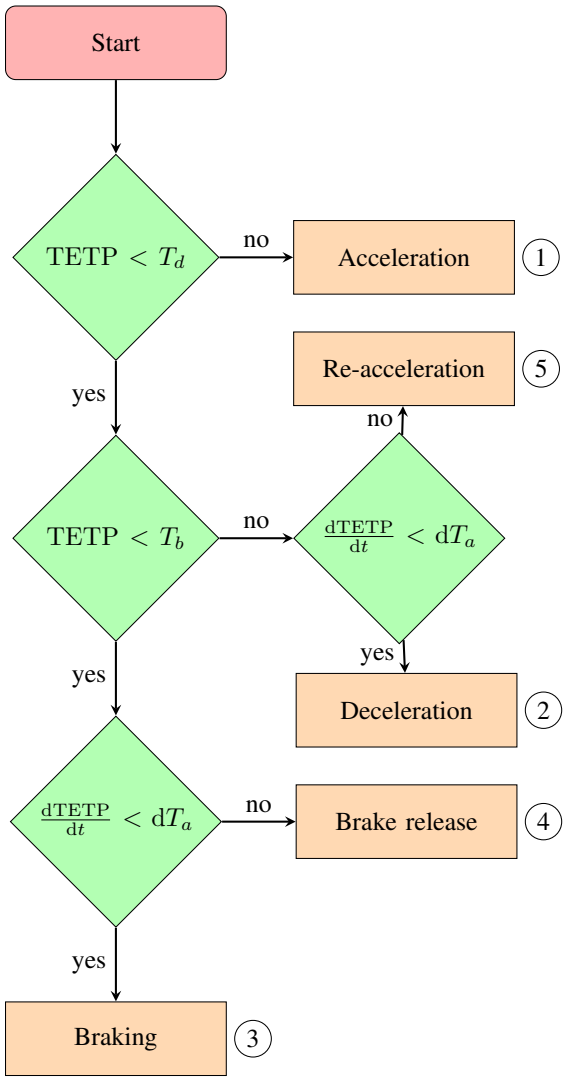

Fig. 4. Model phase decision flowchart

the accelerator pedal deflection required to maintain the current speed, $\delta_{a,EB}$, and 0.

$$\delta_a = \min\left(\delta_{a,EB}, K_d\left(\frac{\mathrm{TETP} - T_b}{T_d - T_b}\right)\right) \tag{2}$$

This phase will continue until either the TETP goes under the braking threshold T_b and the *braking* phase starts, or the moving average of the rate of change of the TETP approaches zero, at which point the *re-acceleration* phase begins.

3) *Braking*: If the TETP is below the braking threshold, the accelerator pedal deflection is set to zero, while the brake pedal deflection is dependent on the ratio between the current TETP and T_b, as described in Equation (3).

$$\delta_b = K_b\left(1 - \frac{\mathrm{TETP}}{T_b}\right) \tag{3}$$

4) *Brake release*: As the vehicle brakes, the TETP will gradually stop decreasing. If the rate of change of TETP becomes larger than $\mathrm{d}T_a$ while the braking phase is active, the *brake release* phase begins. The brake pedal deflection is the same as in the *braking* phase (Equation (3)), with the added limitation that the deflection cannot increase while this phase is active. While the vehicle is braking, there should be no accelerator pedal actuation (δ_a= 0). During this phase, once δ_b becomes 0, the model will begin pressing the accelerator pedal. The deflection δ_a is then the minimum value between the pedal position from the acceleration phase, and a direct function of the rate of change of the TETP, as determined by Equation (4).

$$\begin{aligned}\delta_a = \min\Bigg(&\delta_{a,EB} + K_a\left(1 - \frac{V}{V_{max}}\right),\\ &K_a\left(\frac{\mathrm{dTETP}}{\mathrm{d}t} - \mathrm{d}T_a\right)\Bigg)\end{aligned} \tag{4}$$

5) *Re-acceleration*: This phase is entered when the TETP is between T_b and T_d, but its rate of change is above $\mathrm{d}T_a$. In this case, the driver feels confident enough in their safety to begin accelerating again. The brake pedal deflection is $\delta_b = 0$, while the accelerator pedal is the minimum value between the one found for the acceleration phase, and the value derived from Equation (5). This calculation is similar to the one in the deceleration phase, but uses the acceleration gain K_a instead of K_d.

$$\begin{aligned}\delta_a = \min\Bigg(&\delta_{a,EB} + K_a\left(1 - \frac{V}{V_{max}}\right),\\ &K_a\left(\frac{\mathrm{TETP} - T_b}{T_d - T_b}\right)\Bigg)\end{aligned} \tag{5}$$

These five phases are combined into a pedal trace, which can then serve as input to a vehicle model, a driver assistance system, or any other desired application.

E. Simulation results

In order to verify that the model can produce realistic pedal deflections in simulation, it was coupled with the lateral control model developed by Sentouh et al. [27]. The simulated vehicle characteristics and the engine model are described in Appendix B. A realistic assumption for the speed control model parameter set, shown in Table I was used, and the simulation was performed for a variety of road geometry combinations.

TABLE I
SPEED CONTROL MODEL PARAMETERS USED IN SIMULATION

T_d [s]	T_b [s]	K_d [-]	K_b [-]	K_a [-]	$\mathrm{d}T_a$ [-]
4	2.5	0.1	4	1	-0.25

An analysis of the sensitivity of the model to changes in the different parameters was performed. Each parameter was varied individually, while the others were kept to the values in Table I. The effects of the parameters on pedal actuation and speed, for the same curve as Figure 3, are shown in Figure 5.

For the TETP thresholds (Figures 5a and 5b), the results correspond to expectations: a larger threshold value means

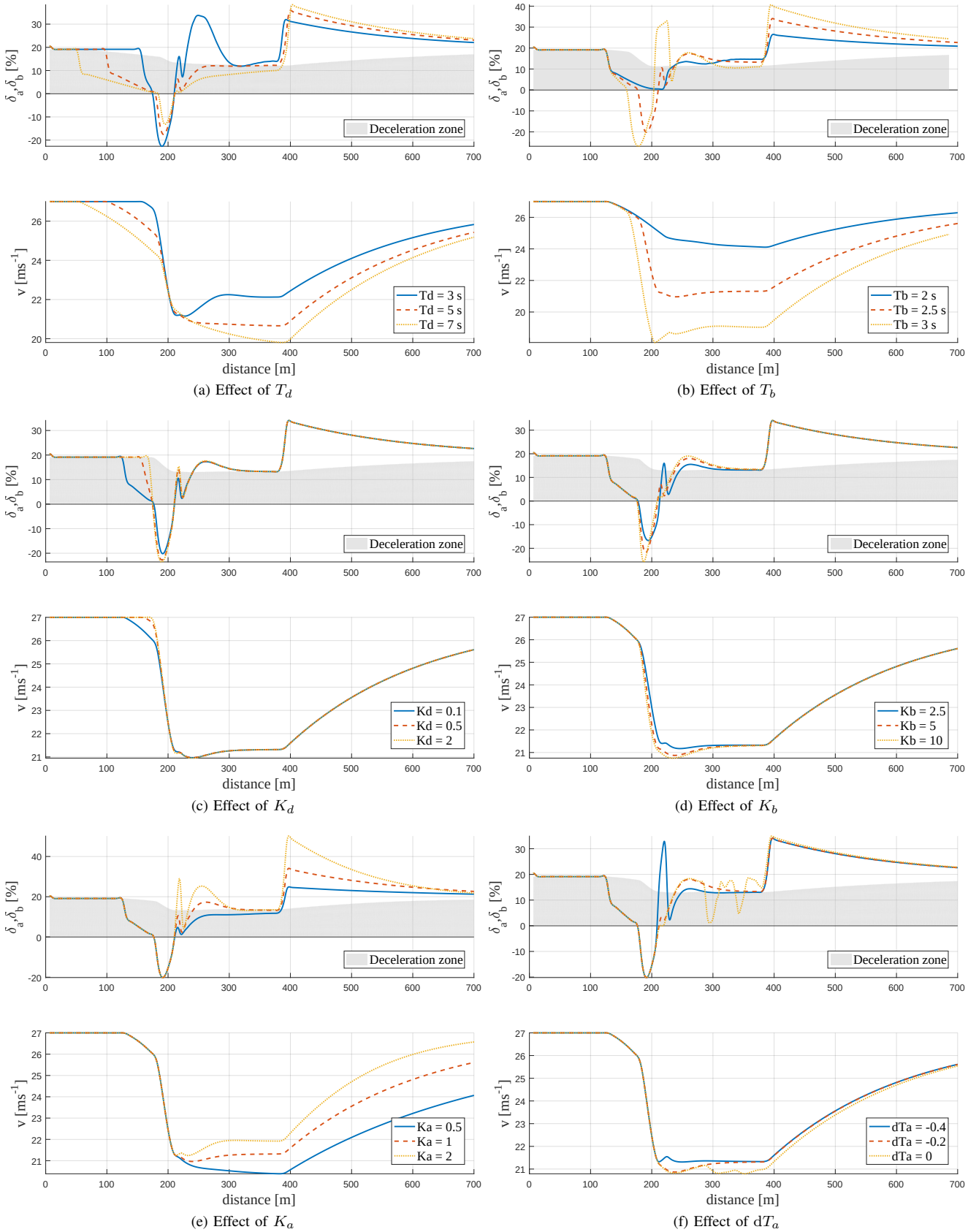

(a) Effect of T_d

(b) Effect of T_b

(c) Effect of K_d

(d) Effect of K_b

(e) Effect of K_a

(f) Effect of $\mathrm{d}T_a$

Fig. 5. Sensitivity of the model to changes in parameter values.

an earlier onset of engine braking or brake pedal actuation. Since the magnitudes of the pedal depressions are affected by different ratios of the current TETP to the thresholds, we see differences in the pedal traces at every time step. For the speed, we can conclude that T_d has more of an influence on the smoothness of the speed curve, while T_b determines how much the model slows down.

The main effects of K_b and K_a (Figures 5d and 5e) are relatively straightforward: larger values imply larger magnitudes for brake pedal depression in the brake phase, and for the accelerator pedal depression during the acceleration, brake release, and re-acceleration phases. K_d affects the magnitude of the deceleration, with lower values corresponding to faster releases of the gas pedal. Since this value is limited on the upside by the engine braking pedal position (Equation (2)), in practice higher values of K_d will correspond to later releases, as shown in Figure 5c.

Finally, $\mathrm{d}T_a$ determines when and how strongly the model accelerates in the brake release and re-acceleration phases. Lower values result in peaks in accelerator pedal depression as the TETP stops decreasing, but this strong, quick depression will make the TETP decrease again. This could result in oscillations, so values lower than -0.5 should be avoided.

III. Identification procedure

The model can be individualized by identifying the different driver dependent parameters. This identification is performed in two steps: in the first step the TETP thresholds for pedal actuation are determined, followed by a second identification process for the three pedal actuation gains and the $\mathrm{d}T_a$ threshold.

A. TETP thresholds

For the identification of the two TETP thresholds, T_d and T_b, a binary classification approach was taken. In the case of deceleration, pedal actuations can be classified as *accelerating*, when the pedal deflection is large enough to overcome engine braking, rolling resistance and drag, and *decelerating*, when the pedal deflection is lower. For braking the two classifications are *braking* and *not braking*. The goal of the identification process then becomes finding the values of T_d and T_b that can predict these classifications, based on the TETP values, with the highest accuracy.

Many different methods to measure the performance of a classifier exist, and the choice of the appropriate one depends greatly on the characteristics and goals of the classifications. In our specific application, because drivers use the brake pedal for only a very small proportion of the total driving time, the sizes of the classifications of *braking* and *not braking* differ greatly in size. This difference in classification size can affect the performance of many of these metrics. Since the Matthews Correlation Coefficient (MCC) [28] is a measure the quality of fit of a classification that has been shown to perform well even when the sizes of the two classifications are very different [29], it was selected as the measure to evaluate the correlation between the observed pedal actuations and their respective predictions.

In order to use this criterion, we must first organize the observations into the categories True Positive (TP), False Positive (FP), True Negative (TN), and False Negative (FN), depending on whether the threshold correctly identifies the real driver behavior. A useful way to visualize this evaluation is in a confusion matrix, or error matrix [30]. The confusion matrices for deceleration and braking are shown in Tables II and III respectively. This evaluation is performed for a range of possible deceleration and braking threshold values (respectively T_d and T_b) from 0s to 10s.

For the gas pedal release TETP threshold, the four categories for each T_d candidate are set up as shown in Table II. For example, a true positive observation would be one where the gas pedal deflection is in the deceleration zone, and the TETP is under the chosen threshold T_d. Note that in each case a margin of 30% below the actual value of $\delta_{a,EB}$, denoted as $\tilde{\delta}_{a,EB}$, is used, to ensure that the method actually captures instances in which drivers consciously decide to slow down, rather than natural oscillations in gas pedal deflection.

TABLE II
CONFUSION MATRIX FOR ACCELERATOR PEDAL RELEASE

	$\mathrm{TETP} \leq T_d$	$\mathrm{TETP} > T_d$
$\delta_a \leq \tilde{\delta}_{a,EB}$	TP	FN
$\delta_a > \tilde{\delta}_{a,EB}$	FP	TN

Figure 6 shows an example of how this classification procedure works in a single turn. Instances when the TETP is under the T_d candidate value and the accelerator pedal is under $\tilde{\delta}_{a,EB}$, are classified as TP. When the driver first releases the accelerator pedal, the TETP has not yet passed under the threshold, which means that these points are FN. In this example, the driver's gas pedal deflection also goes above $\tilde{\delta}_{a,EB}$ before TETP goes above the candidate, leading to FP observations close to the time when the driver re-accelerates. All other points without additional markings are labeled as TN.

For the brake pedal case a similar set up is used. The classification parameters are displayed in Table III. However, since the goal of this approach is to find the time margins that trigger the onset of braking, we wish to exclude points counted as FN during with the drivers are already in the process of releasing the brakes. To do this, we subtract the number of occurrences of FN during which the brake pedal is being released from the number of FN found, and add the same value to the TN count.

TABLE III
CONFUSION MATRIX FOR BRAKE PEDAL DEPRESSION

	$\mathrm{TETP} \leq T_b$	$\mathrm{TETP} > T_b$
$\delta_b > 0$	TP	FN
$\delta_b = 0$	FP	TN

Once the confusion matrices are set up for each candidate value, the MCC is calculated according to Equation (6), where n_{TP}, n_{FP}, n_{TN} and n_{FN} are the number of occurrences of TP, FP, TN and FN, respectively. The candidate values with the corresponding highest MCC scores are chosen as T_d

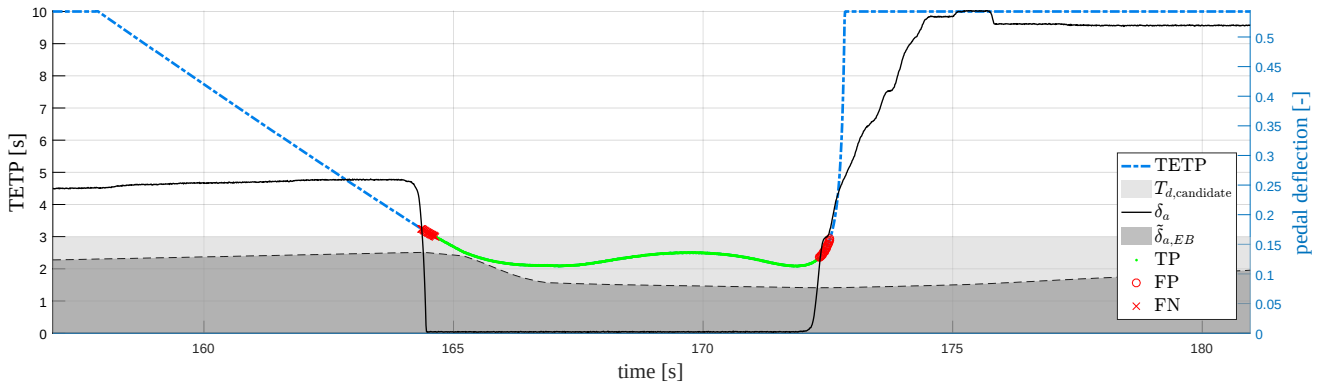

Fig. 6. Example of the classification procedure for accelerator pedal release

and T_b, taking care that the value of the time threshold for deceleration must always be higher than the one for braking.

$$MCC = \frac{n_{TP} \cdot n_{TN} - n_{FP} \cdot n_{FN}}{\sqrt{(n_{TP}+n_{FP})(n_{TP}+n_{FN})(n_{TN}+n_{FP})(n_{TN}+n_{FN})}} \quad (6)$$

B. Other parameters

Once the two time thresholds have been found using the procedure above, the speed choice model is ran for a range of values of the parameters $\mathrm{d}T_a$ (-0.5 to 0), K_a, K_d and K_b (all from 0.01 to 10). In order to find the optimal values, a non-linear least squares optimization is performed on the difference between the experimentally recorded accelerator and brake pedal traces, and the pedal traces resulting from the model. The combination of values that results in the best fit for each subject is chosen as that subject's parameter set.

IV. Experimental method

An experiment was set up at the fixed-base driving simulator in the HMI Laboratory, at the Faculty of Aerospace Engineering of the Delft University of Technology, in order to satisfy three main goals:

1) Show that a TETP based speed model can capture general trends of driver speed adaptation to road geometry.
2) Provide evidence for the three phases of speed adaptation, and show that TETP triggers can explain these phases more accurately than TLC.
3) Provide validation data in order to individualize the model, and measure its performance in reproducing individual drivers' speed control strategies.

A. Apparatus

The simulator, depicted in Figure 7, used passive accelerator and brake pedals, and the steering wheel had a passive spring, with simulated mass dynamics. A LCD screen was used to display speedometer information, while three projectors displayed the driving scene, generating a field of view close to 180 degrees. Realistic engine sound was played through speakers to aid in speed perception. The simulated vehicle was equipped with an automatic 4-speed gearbox.

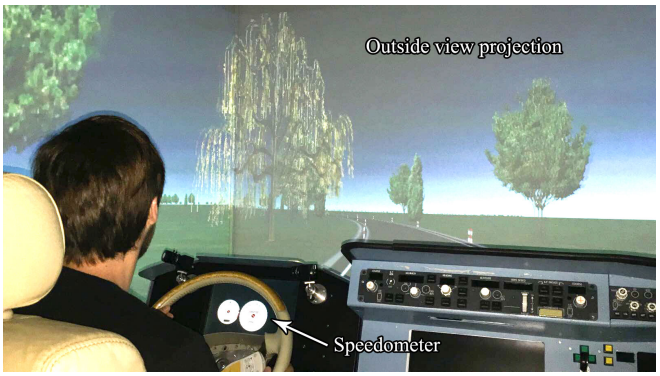

Fig. 7. The fixed-base driving simulator at the Faculty of Aerospace Engineering of the Delft University of Technology

B. Participants

A total of 16 subjects (3 female, 13 male) took part in the experiment. No financial compensation was offered. One male subject suffered from simulator sickness after two runs, therefore his data was removed from further analysis. The remaining subjects were a mix of experienced and novice young (25 ± 2 years old) drivers. They were in possession of driving licenses for 6.1 ± 2.6 years, and drove an average of 4600 ± 4200km per year.

C. Road design

Subjects drove on 6 different roads, in random order, with a posted speed limit of 100kmh^{-1}. These 6 roads correspond to different combinations of two road widths (3.6m and 2.4m), two corner radii (150m and 300m), and two deflection angles (45 and 90 degrees), connected by straight road segments. In addition, each road has one set of left and right connected turns (radii of 150m, deflection angles of 45 degrees), and finishes with a longer straight segment followed by a 90 degree 75m radius curve. Table IV shows the geometrical parameters of the roads designed for the experiment, and road 3 is shown in Figure 8 as an example. In order to improve speed perception, the road was lined with poles spaced at regular intervals, and trees were placed in the scenery.

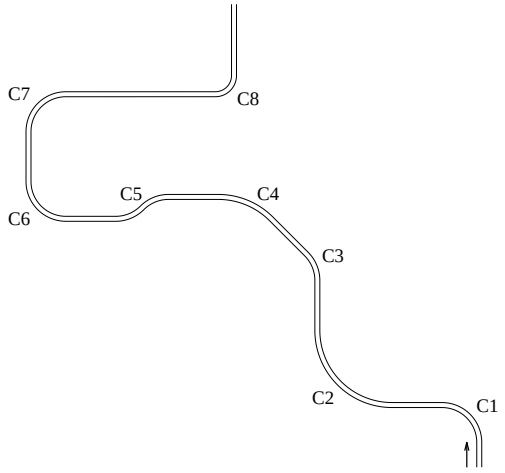

Fig. 8. Road 3 of the experiment (width not to scale).

Of the designed roads, four were used for identification (roads 1, 2, 3 and 5) and two for validation (roads 4 and 6) for all subjects.

TABLE IV
GEOMETRY OF THE ROADS USED IN THE EXPERIMENT

Road		1	2	3	4	5	6
Road width [m]		3.6	3.6	3.6	3.6	2.4	2.4
C1	radius [m]	300	300	150	150	300	300
	angle [^{o}]	90	90	90	90	90	90
	direction	R	L	R	L	R	L
C2	radius [m]	300	300	300	300	300	300
	angle [^{o}]	90	90	90	90	90	90
	direction	L	R	L	R	L	R
C3	radius [m]	150	150	150	150	150	150
	angle [^{o}]	45	45	45	45	45	45
	direction	R	L	R	L	R	L
C4	radius [m]	150	150	300	300	150	150
	angle [^{o}]	45	45	45	45	45	45
	direction	L	R	R	L	L	R
C5	radius [m]	150	150	150	150	150	150
	angle [^{o}]	45	45	45	45	45	45
	direction	LR	RL	LR	RL	LR	RL
C6	radius [m]	150	150	150	150	150	150
	angle [^{o}]	90	90	90	90	90	90
	direction	L	R	L	R	L	R
C7	radius [m]	150	150	150	150	150	150
	angle [^{o}]	90	90	90	90	90	90
	direction	R	L	L	R	R	L
C8	radius [m]	75	75	75	75	75	75
	angle [^{o}]	90	90	90	90	90	90
	direction	R	L	R	L	R	L

D. Experimental procedure and task

Subjects were informed of the experimental procedure and their task before the experiment, and this information was repeated to them before taking place in the simulator. Before driving, subjects filled in a short questionnaire.

Subjects were instructed to drive as they would in a real world driving situation, adapting their speed and steering behavior in order to stay within the lane boundaries. They were told the roads allowed only for one-way traffic, and that they could use all of the available road width. They were requested to treat the speed limit of 100kmh^{-1} in the same manner they would treat a speed limit on a real road.

Each road was approximately 4km in length, with the driving time depending on how fast the subjects drove. The total experimental time was approximately 30 minutes per subject.

Before the experiment, drivers were given time to familiarize themselves with the simulator by driving a road with similar characteristics to the ones used in the experiment twice. If drivers felt they needed more time to become comfortable with the conditions after these two runs, they were given extra time. No subjects drove more than three familiarization runs.

V. RESULTS

This section describes how the model satisfied the three experimental goals. First, we measured the ability of the TETP model to capture the general trend of speed adaptation to corners with different geometrical features in naturalistic driving. The second evaluation concerns the different phases of braking, and shows that drivers do indeed use TETP triggers to control their brake and gas pedal activity, and not TLC. Finally, we measured the performance of the individualized driver model for each subject of the experiment.

A. Naturalistic driving

To analyze the effect of road geometry on speed and TETP, the curves of the experiment were segmented, and driving data were averaged over identical segments. In the figures shown in this section, the number of identical segments that were averaged is denoted by n. The direction of the turn was not found to have a significant influence on the minimum ($p = 0.87$) and average ($p = 0.74$) speeds in curves. However, the minimum TETP margin drivers kept on right turns was approximately 0.1s smaller on right turns when compared to left turns ($p = 0.003$), therefore in further analysis left and right turns are treated separately.

For all subjects and each combination of geometrical factors (curve radius, road width, curve deflection angle, and turn direction) the most critical situations in terms of minimum speed and minimum TETP were found. In order to determine whether the model can produce the same trends as the experimental results show, the model was run over the two validation roads using a reasonable assumption for the parameters, shown on the last row of Table V, and the results were compared with the experimental data.

Figure 9 shows the results of this comparison for the minimum curve speed. It can be seen that the model captures the general trend of the experimental data, showing higher speeds for larger road widths and larger radii. The chosen parameters result in minimum curve speeds that are close to the lower range of minimum speeds kept by drivers on small radius curves.

The results for the minimum and average TETP kept in each segment are shown in Figures 10a and 10b. The parameter

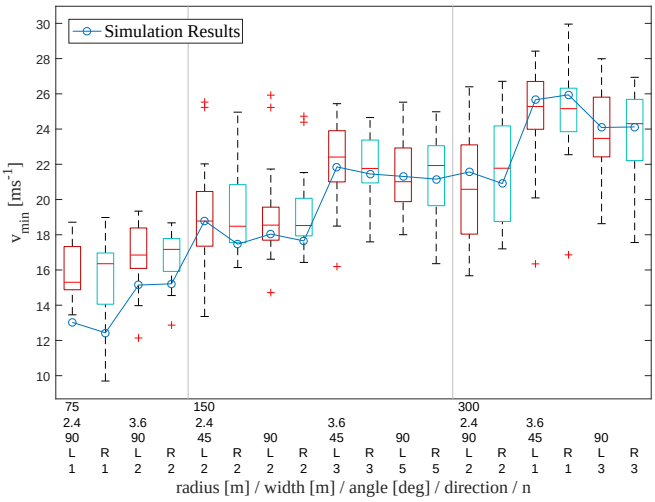

Fig. 9. Variation of experimental and modeled minimum curve speed with curve radius, road width, curve deflection angle, and turn direction. The boxes represent experimental data, while the line represents model simulation results using a typical parameter set. n is the number of identical segments that the experimental data were averaged over.

assumption results in TETP values on the high side of the experimental data, but the model captures the trend of the variation of both minimum and average TETP with curve geometry quite well.

The same experimental data can also be used to verify the interaction of geometrical factors on speed and safety margins found in literature. Since the number of segments was not balanced, a repeated measures ANOVA with a Bonferroni correction ($\alpha = 0.05$) was performed to find significant differences between the various combinations.

No statistically significant interactions of curve deflection angle or road width on speed were found in this experiment. The radius effect was significant ($p < 0.0121$) for all combinations on the same road width excluding the 300m radius curves.

On wide roads, the combinations with radius of 300m showed significantly higher minimum TETP values than all other combinations ($p < 0.0174$). For the curves with radii of 75m and 150m, no combinations of geometric factors showed significant differences to all other combinations, and no patterns of significance caused by any of the factors were found.

The average TETP in curves was only decreased significantly ($p < 0.0189$) with decreasing road width for the 75m radius turns, while no other combination of curves with the same radius, deflection angle and direction showed an influence of road width. For all of the curves of 150m radius, a higher deflection angle resulted in lower average TETP ($p < 0.0000$).

B. TETP thresholds

Figure 11 shows how TETP, TLC (values above $10s$ are ignored and set to $10s$), speed, and pedal deflection interact during approach, mid-corner, and exit of a curve.

As predicted, the pedal trace clearly shows the distinct deceleration methods. As the car approaches the curve, the TETP decreases linearly. The driver releases the gas pedal once a certain TETP threshold, indicated by the dashed vertical line, has been passed, at approximately 50m before the corner. After releasing the gas pedal, the TETP continues to decrease, eventually making the driver apply the brakes (solid vertical line). Once the TETP stops decreasing, the driver feels comfortable enough to begin re-accelerating, and after the TETP has increased past any thresholds, the driver eventually increases the acceleration.

The figure shows the value of using TETP triggers for modeling speed adaptation: at a TETP of approximately $3s$ the driver releases the gas pedal, followed by braking at a TETP of approximately $2.3s$. It also provides evidence that the TETP is a better candidate than the TLC for curve speed modeling applications. The TLC shows considerable variability, even on straight segments of road, as it depends on the steering inputs of the driver. On the other hand, the TETP depends only on the speed, the position of the vehicle, and the road geometry. The figure also shows that the minimum TLC value is reached at the exit of the corner, when the driver is already accelerating out of the turn.

The TETP thresholds for decelerating and for braking, T_d and T_b respectively, were calculated using the method described in Section III for each subject on each of the six roads individually, in order to determine whether the driver's speed adaptation strategy varies with road width. The results are displayed in Figure 12, and show that neither of the thresholds changed significantly with road width: $p(T_d) = 0.14$, $p(T_b) = 0.73$.

C. Model validation

For each subject, data from the four roads designed for identification were used to identify the driver dependent parameters, using the procedure detailed in Section III. The identified model parameters for each subject of the experiment are shown in Table V, along with their means and standard deviations. Both K_a and $\mathrm{d}T_a$ do not exhibit a large variance between subjects when compared to the other parameters.

The model was validated using two different approaches: first a single 75m radius turn, followed by an analysis of the performance over a 4km long winding road.

1) Single turn: In literature, speed control models are usually judged on their performance in a single turn [2, 6, 9]. In this case, the model was initialized on a straight segment approximately 500m before a 75m radius 90 degree turn. The results of this validation are given in Table VI, while Figure 13 shows an example of the model performance. In this example, the model tracks the speed and pedal deflections with great accuracy, and the only significant mismatch is the fact that the real driver releases the gas pedal slightly earlier than the model and coasts for approximately 50m before applying the brakes. The braking event timing is extremely accurate, with a small difference in magnitude of brake pedal actuation caused by the difference in speed at the onset of braking due to the extra coasting. The short release of the accelerator pedal on curve exit is also reproduced.

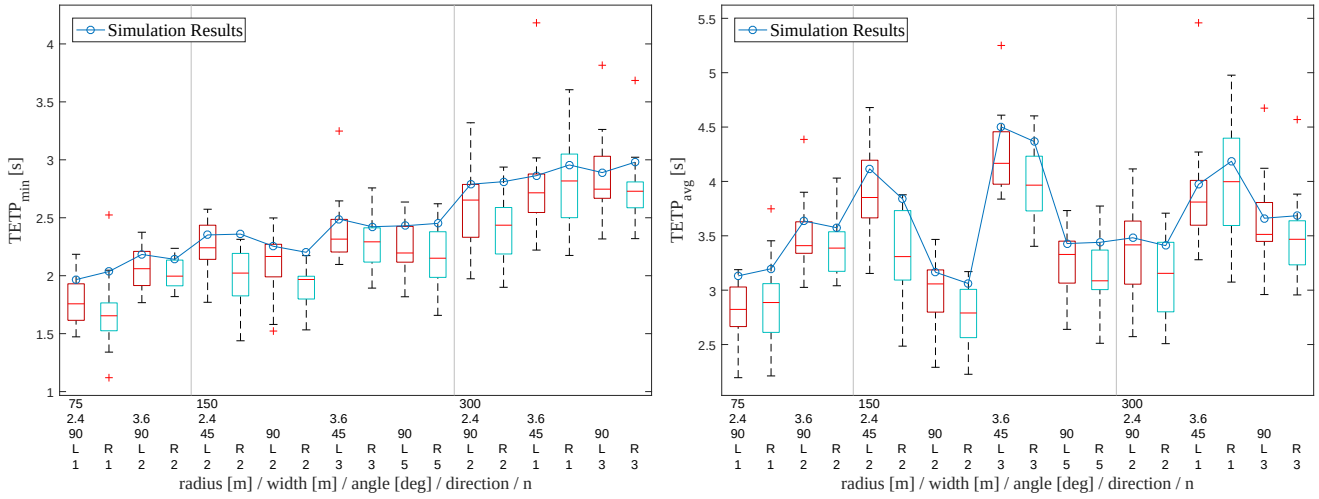

(a) Minimum TETP in curves

(b) Average TETP in curves

Fig. 10. Comparison of experimental and modeled minimum TETP with curve radius, road width, curve deflection angle, and turn direction. The boxes represent experimental data, while the line represents model simulation results using a typical parameter set. n is the number of identical segments that the experimental data were averaged over

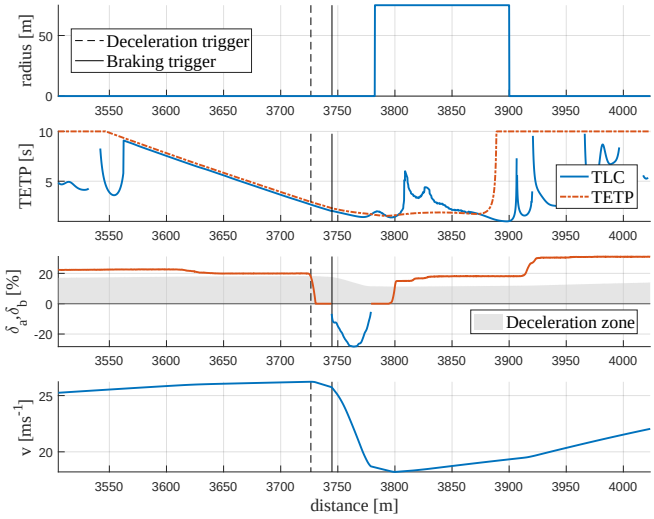

Fig. 11. Typical example (S15) of the variation of TETP, TLC, speed, and pedal deflections on a 75m radius right turn. Positive pedal deflections correspond to the accelerator pedal, while negative deflections represent brake actuation. The shaded area represents the deceleration zone, that is, the accelerator pedal position values that correspond to a zero or negative acceleration.

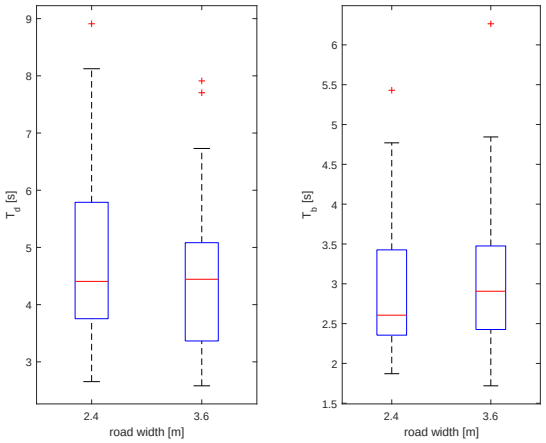

Fig. 12. Change in T_d and T_b with road width. The time thresholds are identified for each subject on each road, resulting in 60 measurements for the wide road and 30 for the narrow road in each case.

Validation results showed that, for most subjects, the TETP based model can accurately track driver speed choice in an isolated turn, with an average speed Variance Accounted For (VAF) above 60%. The acceleration and gas pedal deflection VAF values are lower, but the fact that they are, on average, above 30% can be seen as a corroboration the speed results. The brake pedal deflection VAF values are low, but this can be attributed to the fact that there are only few occasions where drivers actually use the brake pedal, resulting in low variance overall. This can cause small differences in the variance to result in low VAF values.

The VAF results show large variability, with a standard deviation of the speed VAF of approximately 30%. For four of the subject/road combinations the speed VAF is below 25%: this occurs for both validation runs of subject 6, the narrow road run of subject 8, and the wide road run of subject 9. Two of these runs are exemplified in Figure 14.

In the case of subject 8, shown in Figure 14b, the model performs as expected, but slows down slightly later and more strongly than the real driver. The intrinsic variability of human behavior means that drivers will not perform the same task in the same manner every time, leading to poor performance of the model in this instance.

The cases of subjects 6 and 9 are different, as exemplified in Figure 14a, and show that the model, and especially the modeling of the relationship between TETP and pedal actuation, must still be improved. These two subjects use

TABLE V
IDENTIFIED PARAMETERS FOR EACH SUBJECT

Subject	T_d [s]	T_b [s]	K_d [-]	K_b-	K_a [-]	dT_a [-]
1	3.7780	3.0710	0.9989	5.1329	1.0031	-0.2500
2	4.8200	2.1230	0.9923	4.9843	0.9988	-0.2495
3	4.3380	2.8460	0.1649	4.1200	1.0027	-0.2480
4	3.8540	2.7940	0.8327	4.7101	0.9988	-0.2487
5	4.6340	3.5960	0.1579	4.3751	0.9930	-0.2496
6	7.1480	3.9040	1.0440	4.6086	0.9916	-0.2497
7	5.6200	3.8060	0.0595	4.9297	0.9983	-0.2500
8	3.2780	2.4930	0.5274	4.7574	0.9910	-0.2543
9	8.3930	6.2850	0.2233	4.9901	1.0001	-0.2500
10	4.8890	2.6760	0.7218	5.2828	1.0269	-0.2408
11	4.7600	2.2770	2.8536	0.9874	0.8727	-0.0118
12	3.9150	1.2150	0.0450	4.8248	0.9969	-0.2501
13	5.1480	4.7130	0.7592	4.9988	1.0000	-0.2500
14	3.4920	2.6490	0.1816	2.9510	0.9552	-0.2462
15	3.0750	1.9780	0.1936	0.5795	0.8721	-0.1391
Mean	4.6673	3.2597	0.6504	4.1488	0.9801	-0.2259
StdDev	1.4342	1.1286	0.7130	1.4776	0.0460	0.0657
Simulation	3.8	2.8	1	5	1	-0.25

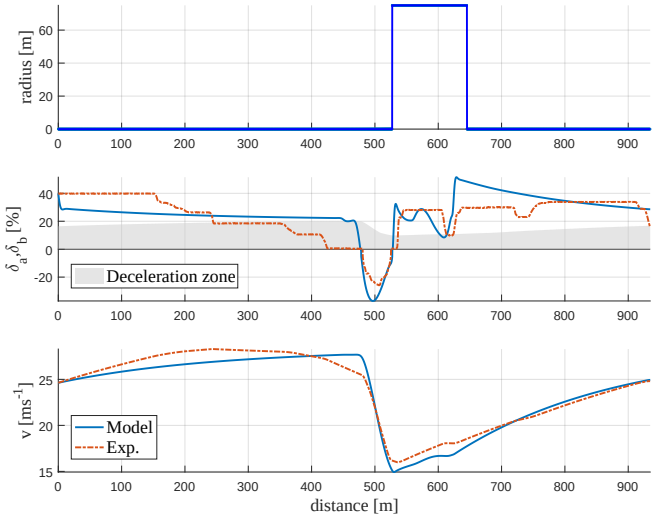

Fig. 13. Example (S4) of the performance of the model on an isolated 75m radius turn. Positive pedal deflections correspond to the accelerator pedal, while negative deflections represent brake actuation. The shaded area represents the deceleration zone, that is, the accelerator pedal position values that correspond to a zero or negative acceleration.

larger values of T_d, for different reasons. Subject 6 drove at consistently high speeds ($v_{avg} = 26.8\text{ms}^{-1}$), but released the accelerator pedal relatively early and braked as little as possible, while subject 9 drove at comparatively slow speeds ($v_{avg} = 20.1\text{ms}^{-1}$) throughout the experiment and started the brake phase early, as evidenced by a T_b value of 6.29s.

In conclusion, the model captures a typical driver on a single turn with good accuracy, but there is room for improvement in the way extreme cases are dealt with.

2) Entire road: In the second validation approach, the model is initialized at the beginning of a 4km curved road with various combinations of turn geometry, and the speed tracking performance is evaluated over the entire length of the road. The results of the model performance evaluation are displayed in Table VII.

Figure 15 shows an example of good model performance, where the largest mismatch between the model and the

TABLE VI
EVALUATION OF THE TETP SPEED CONTROL MODEL PERFORMANCE FOR A WIDE AND A NARROW ISOLATED TURN WITH 75M RADIUS.

Subject	VAF(v) [%]	VAF(a) [%]	VAF(δ_a) [%]	VAF(δ_b) [%]
S1W	90.23	70.51	44.85	65.492
S1N	85.06	77.57	48.96	77.40
S2W	85.76	31.11	45.27	0
S2N	80.84	0	22.43	0
S3W	88.29	14.40	50.49	0
S3N	78.36	0	37.03	0
S4W	96.04	78.19	24.95	73.65
S4N	87.14	67.15	40.56	53.75
S5W	93.95	53.79	46.25	37.16
S5N	90.50	50.19	36.38	29.53
S6W	0	25.89	8.07	9.57
S6N	0	0	38.88	0
S7W	50.84	34.20	51.15	0
S7N	73.88	61.65	44.44	42.86
S8W	73.37	48.54	54.25	0
S8N	11.18	0	19.43	0
S9W	0	0	35.85	0
S9N	34.80	0	55.83	0
S10W	77.42	36.47	49.41	0
S10N	63.77	0	38.06	0
S11W	64.67	24.06	23.85	25.91
S11N	77.31	70.26	29.72	85.83
S12W	81.42	54.74	52.01	30.60
S12N	35.62	9.12	46.97	0
S13W	36.60	0	44.67	0
S13N	62.65	6.56	40.75	14.09
S14W	82.03	25.83	24.13	0
S14N	67.24	57.39	53.32	36.62
S15W	54.63	28.26	28.31	0
S15N	91.78	23.38	47.64	0
Mean	63.85	31.64	39.46	19.41
StdDev	29.68	27.18	12.02	27.53

experimental data is an excessive slowdown of the model during the first curve. For the pedal trace comparison, the figure shows acceptable model performance, reproducing most deceleration and acceleration events well. The human driver shows additional variability on the straight segments, that the model does not capture. The three braking events are well reproduced, but the model brakes in three additional situations.

Analyzing the model performance on the complete road, it stands to reason that the VAF values would be lower. The average speed VAF is approximately halved, while the values for the other three measures decrease more. Aside from the increased influence of inherent human variability on the results caused by driving for longer periods of time, this reduced model performance can be attributed to at least two additional causes.

Since the model is only given the initial conditions (speed, acceleration, pedal deflections) at the start of the road, errors at the beginning can accumulate: for example, if the model slows down more than the real driver in a turn, and accelerates out of the turn at the same rate as the real driver, the modeled TETP will be different than the real TETP at the entrance of the next turn, causing different behavior.

Another issue that reduces model performance in some situations relates to the target speed on straight sections. In the validation procedure, this target was set to the maximum speed that the driver reached during the entire run, on the assumption that drivers would drive close to the given speed limit on all straight sections. This proved not to be the case for all subjects,

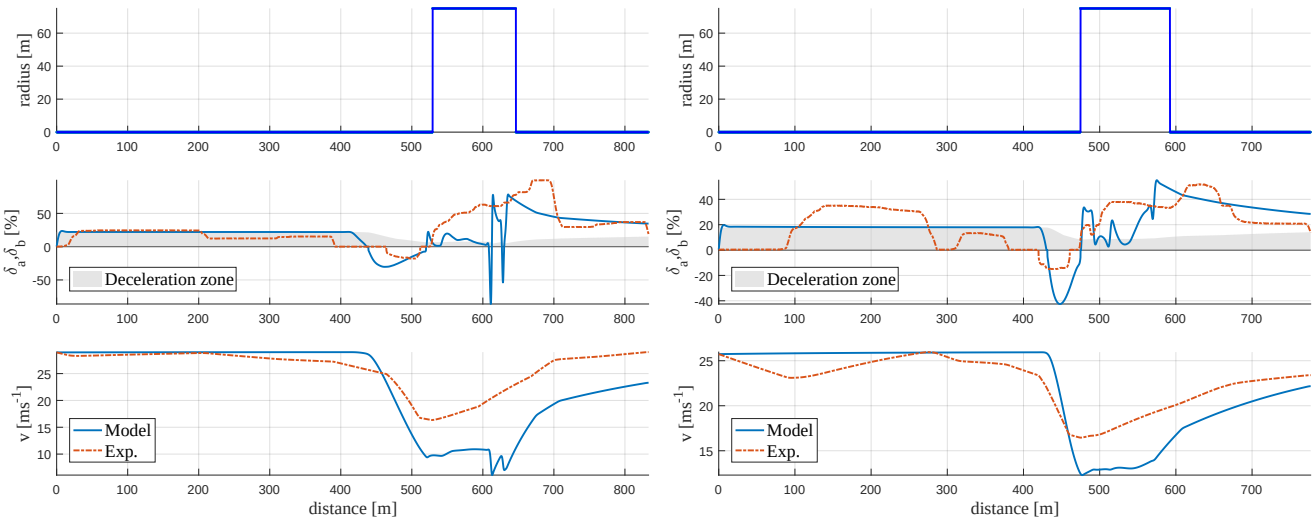

(a) Subject 6, narrow road

(b) Subject 8, narrow road

Fig. 14. Two examples of decreased model performance.

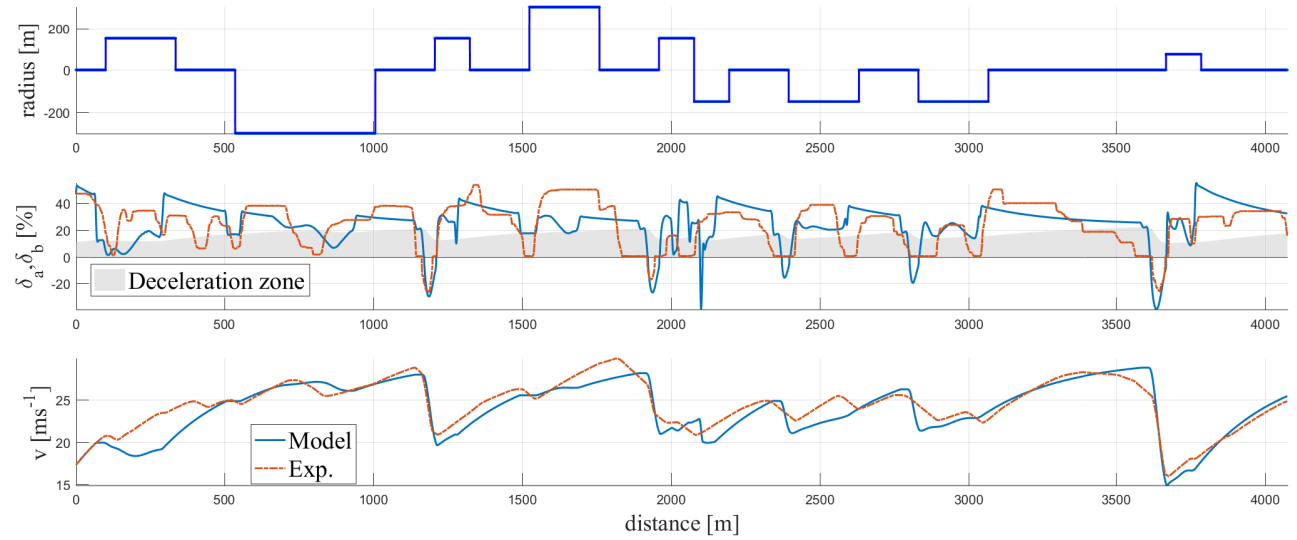

Fig. 15. Example (S4) of the performance of the model on a 4km length wide road. Positive pedal deflections correspond to the accelerator pedal, while negative deflections represent brake actuation. The shaded area represents the deceleration zone, that is, the accelerator pedal position values that correspond to a zero or negative acceleration.

as shown for subject 12 on a wide road in Figure 16. In this case, the maximum speed (27.87ms^{-1}) was achieved on the penultimate straight, but on previous straights the speed is considerably lower. This causes the model to accelerate more than the real driver, and since a higher speed results in a lower TETP, also brake earlier and harder. An improvement of this part of the model would ensure better results, but speed control on straight roads is outside of the scope of this research.

Despite these flaws, an average speed VAF of 35.6% shows that the developed model can still reproduce speed control along a 4km curved road with satisfactory accuracy. Furthermore, when excluding the two subjects (6 and 9) with known issues described in this section, this average VAF increases to 46.1%.

VI. Discussion

A. Naturalistic driving

In literature, curves with radii of 300m or higher are generally not considered to require speed adaptation [4, 5]. This experiment showed the same results, with the radius of the road only influencing speed for curves of radius smaller than 300m. Similarly, the minimum TETP kept by drivers was only significantly higher on the segments of radius higher than 300m. This can be seen as evidence that drivers allow for the same risk, measured as the TETP, on all curves that require speed adaptation.

TABLE VII
EVALUATION OF THE TETP SPEED CONTROL MODEL PERFORMANCE FOR A WIDE AND A NARROW 4KM ROAD.

Subject	VAF(v) [%]	VAF(a) [%]	VAF(δ_a) [%]	VAF(δ_b) [%]
S1W	60.76	25.43	28.39	4.53
S1N	68.54	48.56	42.46	36.69
S2W	45.87	6.23	4.74	0
S2N	73.55	0	6.47	0
S3W	58.65	0	29.29	0
S3N	73.55	0	6.47	0
S4W	80.87	21.74	7.06	2.44
S4N	73.55	0	6.47	0
S5W	51.17	0	29.48	0
S5N	73.55	0	6.47	0
S6W	0	0	0	0
S6N	0	0	0	0
S7W	24.67	0	25.04	0
S7N	34.68	0	30.00	0
S8W	14.80	0	0	0
S8N	0	0	0	0
S9W	0	0	0	0
S9N	0	0	1.12	0
S10W	64.06	27.35	30.37	0
S10N	50.89	6.89	34.09	0
S11W	66.05	5.45	19.28	0.52
S11N	17.09	7.11	10.80	7.30
S12W	0	0	0	0
S12N	0	0	0	0
S13W	9.99	0	0	0
S13N	0	0	16.28	0
S14W	60.54	5.97	21.21	0
S14N	0	0	0	0
S15W	50.87	33.61	33.12	0
S15N	40.88	29.24	27.09	2.27
Mean	35.6402	8.7438	16.5597	1.7917
StdDev	29.1154	13.2987	14.7633	6.7843

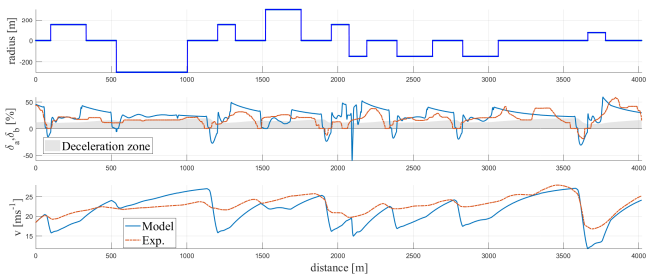

Fig. 16. Example of decreased model performance due to target speed mismatch (S12, wide road).

The average TETP kept in turns showed more dependence on road geometry than the minimum TETP. While the curve deflection showed no significant influence on the minimum TETP, the average TETP was lower for curves with a higher deflection angle. This shows that higher angle curves cause drivers to maintain a higher TETP risk for longer periods of time, but the maximum TETP risk does not change significantly.

However, these conclusions require further confirmation, as the experiment was not designed to answer these questions, and therefore did not have enough repetitions of all combinations of geometrical parameters. In order to conclusively determine the effect of road width on speed and TETP, a different experiment, with more repetitions, should be performed.

The findings on driver strategy showed no statistically significant differences between the TETP thresholds used by drivers on wide and narrow roads. This indicates that drivers maintained the same strategy independently of the width of the road.

B. Time to Line Crossing

Godthelp and van Winsum [18] proposed that drivers trade off steering performance and speed in order to maintain a constant TLC. Subsequent studies showed that for larger radii, the TLC is not constant [1, 6, 15], and the same was found in this experiment. However, we argue that drivers do not strive for a constant safety margin, but merely intervene once a safety margin passes a certain threshold. While the TLC provides excellent information on the criticality of the task, and we believe that the TLC is an important factor in regulating speed and steering actions in order to maintain lane position, it does not appear to be suited to use as a threshold for speed adaptation to curves. Even though TLC and TETP generally coincide on turn entry, the TLC usually reaches its minimum value close to turn exit, when the TETP value has already increased considerably and the driver is accelerating out of the curve.

An interesting conclusion can be drawn from the observation that as the vehicle approaches a turn, the TETP and TLC values almost coincide, with the TLC being consistently slightly lower. Since the TLC is a measure of the time the vehicle would take to cross the road edge if it would maintain the current trajectory, this can be regarded as evidence that drivers steer towards an area adjacent to the tangent point in curve driving: when drivers aim their car in a straight line towards the tangent point, the TLC will be measured at the next intersection of this straight line with the road edge. This is the same principle as the ETP, which is simply the continuation of the visual line from the driver to the TP onto the next road edge. If drivers do not aim at the TP, but at an area just to the inside of the curve from it, the TLC value will be calculated to a point slightly closer to the driver than the ETP, resulting in a slightly lower TLC value than the TETP value, which agrees with the results of this experiment.

C. Model performance

The model performance evaluation suggests that a TETP threshold based approach for speed modeling is very promising, and that the current model can reproduce speed behavior with good accuracy on single turns. Since no speed models that take into account driver pedal actuation currently exist, it is difficult to evaluate how good this performance is in comparison to models from literature.

However, there is still room for improvement in the model of the relationship between TETP and pedal actuation. The equations for pedal deflection described in Section II serve as good initial estimations for this relationship, but further research should focus on improving these.

The evaluation method itself is also a factor: evaluating brake pedal deflection tracking with VAF is a flawed approach. The low amount of braking events result in low overall variance, causing small mismatches in brake timing to result in

low VAF. Further research into pedal deflection models should use a different evaluation procedure, such as the amount of braking events that were correctly modeled, and a measure of the time and magnitude differences in the application of the brakes of the model when compared with experimental data.

Furthermore, the model suffers from two known issues that should be first priority in any future development of the model.

The first one can be seen in Figure 14a, where the oscillation in pedal actuation that occurs close to turn exit is worthy of note. When the TETP value is under the engine braking threshold, denoted as *deceleration zone* in the figure, the rate of change of TETP takes on great importance in the drivers evaluation of whether it is safe to accelerate. In these cases, where the TETP can vary considerably while remaining under the threshold, the current implementation is flawed as it relies on a hard threshold on the rate of change of the TETP. Further research is necessary on how exactly this rate of change relates to pedal actuation is necessary. Furthermore, in real driving mid-corner speed control is likely to be governed by the lateral acceleration drivers feel instead of the rate of change of a visual parameter, casting doubt on the usefulness of research into mid-corner speed behavior in a fixed-based driving simulator.

Observing Figure 15, the second flawed behavior of the model can be identified. In the curve-countercurve section, just after 2000m, the model brakes strongly, at the same time as the real driver begins accelerating out of the turn. This is due to the way the ETP is determined by the model. The issue is illustrated in Figure 17: as the driver approaches the curve apex, their line of sight past the tangent point intersects the road edge on the same side of the TP, meaning that there is no ETP on the other lane edge (case 1 in the figure). Without an ETP, the model assumes it is free to accelerate, but once the TP has moved to the opposite side of the road (case 3 in the figure) the algorithm detects an ETP again, causing a large change in TETP. At this point the TETP is still under T_d, which as described above means that the rate of change of the TETP has a great influence on speed control. This sudden decrease in TETP causes sudden, hard braking. Modifying the ETP detection algorithm to allow this point to be on the same side of the road of the TP does not solve this problem, as the sudden switch between ETP sides once the driver is past the TP causes the same issue, and the TETP becomes very small as the driver approaches the turn, causing excessive slowdown (case 2 in the figure). A new way to deal with the switching of sides of the ETP must be found in future work.

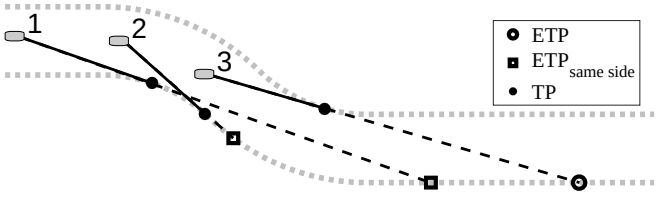

Fig. 17. Diagram illustrating the flaw in the ETP detection algorithm for a counter-countercurve scenario

D. Practical applications and future work

While this model incorporates much of the current state-of-the-art of research into human's visual targets when driving, some effects could benefit from further investigation. Research has shown that drivers don't limit their look-ahead fixations to the far-road triangle, but occasionally look at points further ahead, allowing the anticipation of the need for speed adaptation [31].

Another aspect that could affect speed control in a similar manner is the effect of memory in driving. Not much research has been performed on this subject, however Lappi et al. [25] argue that memory has an important influence on where drivers look. Visual perception during driving occurs in a intermittent fashion: drivers monitor different targets, rotating their gaze over the various salient points. On a familiar road, drivers will know when to look at certain points to obtain crucial information. In the case of speed adaptation, this could result in lower safety margins, as drivers will be aware of the points at which they have to pay more attention to their current TETP, enabling them to detect crossings of the threshold with more accuracy. However, these effects are currently not well known, and further research into the interaction of visual strategies with memory is necessary.

The experiment was conducted on a single-lane road, making it easier for drivers to visualize the location of the ETP. A possible topic for further research is investigating how driving on a dual-lane road, where drivers must keep to one side, affects these results.

The TETP threshold based model showed good performance reproducing results of a fixed-base simulator experiment. However, many of the experimental subjects reported that the lack of motion affected their speed perception, especially during braking. Reymond et al. [15] compared speed adaptation behavior in static and dynamic simulators, and argue that drivers use similar strategies in both cases, but that the factors influencing these strategies are affected by an underestimation of speed in fixed-based simulators. In the context of TETP as a cue for speed adaptation, we expect the driver specific thresholds to be affected by this underestimation. It would be worthwhile to conduct an experiment in a dynamic simulator. The addition of motion should result in lower speeds, and therefore higher TETP thresholds, without affecting the overall strategy.

Another issue stemming from the lack of motion feedback in the performed experiment concerns the mid-corner phase. In the current implementation of the model, the rate of change of the TETP is the main indicator governing speed in this phase. While this results in a model that performs well, we expect the lateral acceleration felt by the driver to be the dominant factor in mid-corner speed choice. We recommend an experiment in a moving-base driving simulator to investigate speed control in the mid-corner phase. However, we do not expect the felt lateral acceleration to significantly alter drivers' behavior on corner approach and exit.

The developed model offers significant advantages over models found in literature in the context of the current push towards better ADAS and self-driving vehicles. By modeling

the driver's pedal actuation, we enable future research toward a haptic pedal assistance system similar to the one developed by Mulder et al. [32] for car following. We envision a future Haptic Shared Control (HSC) system that enables the driver to feel the severity of upcoming turns through forces on the gas pedal. Such a system has the potential to improve safety and driving performance on curved roads.

However, for this model to be applicable to HSC systems, the current knowledge of the neuromuscular dynamics of driver's pedal actuation must be combined with the visual perception model described in this paper [33]. With such an approach, the realism of the modeled pedal actuation triggered by TETP safety margins can be greatly improved.

VII. Conclusion

To the best of our knowledge, this research is the first to directly relate visual perception to pedal actuation when driving on a curved road. Using two thresholds on a single perceptual variable, the time to extended tangent point, the developed model is able to accurately capture the different phases of deceleration and acceleration caused by curves.

This approach offers several advantages over traditional models of speed choice in curved roads. Previous research has shown that in car following and lane keeping, time safety margins are the primary method used for speed regulation. The developed speed model brings curve driving into the larger framework of risk-based speed adaptation. Furthermore, by directly modeling the pedal actuation instead of the resulting speed, new methods of assisting drivers during cornering using haptic shared control can be developed.

Appendix A
ETP detection

To control speed based on TETP, we must first determine the location of the extended tangent point. In order to enable the model to be implemented in future ADAS applications, it must include a feasible method of finding the necessary information.

In this case, the algorithm used to find the ETP is based on a method for locating the TP of a curve developed by Gallen and Glaser [34]. This method uses a car-mounted camera to sample discrete locations of points on both lane edges at a regular interval, calculates the angle between the current vehicle location and these points, and finds the point at which this derivative passes through zero. This zero crossing means that the angle from the car to the side of the road changes direction, denoting the tangent point of the curve. This procedure is illustrated in Figure 18a, where the black points are the candidates the algorithm searches through until a zero derivative of the change in angle from one point to the next is found. The TP location is shown in dark gray.

The TP finding method was extended in a similar fashion to enable the detection of the ETP, by calculating the angles between the car and the road points on the opposite lane edge of the TP. When this angle equals the angle to the TP, we have found the ETP. This is illustrated by Figure 18b. However, since the discrete road sampling points do not necessarily match, it is possible that an angle exactly equal to the TP angle does not exist. To solve this, the point on the opposite road edge where the difference between its angle and the angle from the car to the TP crosses zero is used.

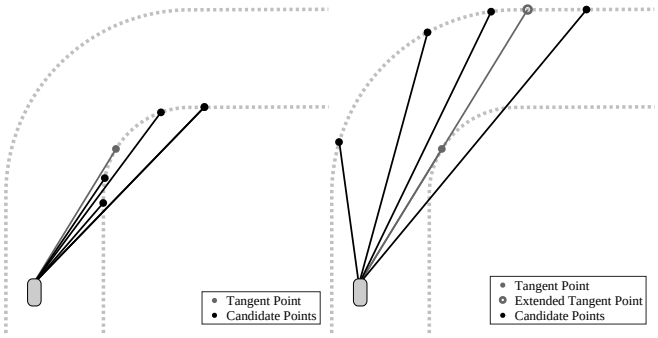

(a) TP search procedure (b) ETP search procedure

Fig. 18. Illustration of the methods to find the tangent point and the extended tangent point.

Appendix B
Vehicle characteristics

The characteristics of the vehicle used in simulation are shown in Table VIII.

TABLE VIII
Simulated vehicle characteristics

Vehicle mass	1600 kg
Front tire cornering stiffness	30000 N·rad^{-1}
Rear tire cornering stiffness	30000 N·rad^{-1}
Vehicle yaw moment of inertia	3136 kg·m^3
Front wheelbase	1.4 m
Rear wheelbase	1.4 m
Steering wheel rotational inertia	0.5 kg·m^2
Steering wheel stiffness	16.8
Steering system damping	5 kg·m
Steering gear ratio	15

A. Longitudinal vehicle model

The vehicle acceleration is calculated according to Equation (7), where v is the current vehicle speed, G is the contribution of the gas pedal to the vehicle acceleration, shown in Equation (8), and B is the brake contribution, shown in Equation (9).

$$a = \frac{4\,(G - B) - \left(K_{res} \cdot v^2 + 200\right)}{M + 100 + K_{in} \cdot \mathrm{gearratio}^2} \tag{7}$$

$$G = 0.9 \cdot \mathrm{gearratio}\,(K_{\mathrm{rpm},1} \cdot \mathrm{rpm} - K_{\mathrm{rpm},2} \cdot \mathrm{rpm}) \cdot \left(K_{g,1} \cdot \delta_a + K_{g,2} \cdot \delta_a^2 + K_{g,1} \cdot \delta_a^3\right) \tag{8}$$

$$B = K_{b,2} \cdot p_b + K_{b,3} \cdot p_r \tag{9}$$

The various parameter values are described in Table IX.

The simulated vehicle uses a four speed automatic gearbox with the gear ratios displayed in Table X and fixed shift points depending on the gas pedal position, velocity and current gear.

TABLE IX
LONGITUDINAL VEHICLE MODEL PARAMETERS

Parameter	Value	
$K_{\mathrm{rpm},1}$	0.1186	
$K_{\mathrm{rpm},2}$	0.00001252	
$K_{g,1}$	3.944358	
$K_{g,2}$	-5.12919	
$K_{g,3}$	2.178	
p_b	0	if $\delta_b < \delta_{b,\mathrm{threshold}}$
	$200 \cdot \delta_b$	if $\delta_b \geq \delta_{b,\mathrm{threshold}}$
$\delta_{b,\mathrm{threshold}}$	0.05	
p_r	p_b	if $p_b < p_{b,\mathrm{threshold}}$
	$30 + K_{b,1}\,(p_b - 30)$	if $p_b \geq p_{b,\mathrm{threshold}}$
$p_{b,\mathrm{threshold}}$	30	
$K_{b,1}$	0.5	
$K_{b,2}$	29.43	
$K_{b,3}$	14.0283	
M	1600 kg	
K_{res}	1.7504	
K_{in}	1.65289256198347	

TABLE X
SIMULATED VEHICLE GEAR RATIOS

Gear	1	2	3	4
Ratio	11.37	6.31	4.08	2.83

ACKNOWLEDGMENT

The author would like to thank Dr. Erwin Boer for providing the initial inspiration to use the extended tangent point in a speed control model.

The author is also grateful to Dr. René van Paassen, Dr. David Abbink and Dr. Max Mulder for being a constant source of encouragement, support and assistance during the research process, and Mario Coppola, Melle Gruppelaar, Chris Möckel and Ren Smis for their help in reviewing this article.

REFERENCES

[1] P. Bosetti, M. Da Lio, and A. Saroldi, "On the human control of vehicles: an experimental study of acceleration," *European Transport Research Review*, vol. 6, no. 2, pp. 157–170, 2013.

[2] M. Shino, H. Yoshitake, M. Hiramatsu, T. Sunda, and M. Kamata, "Deviated state detection method in driving around curves based on naturalistic driving behavior database for driver assistance systems," *International Journal of Automotive Technology*, vol. 15, no. 5, pp. 749–755, aug 2014.

[3] S. Cafiso and G. Cerni, "A new approach to define continuous Speed Profile Models for two lane rural roads," *Transportation Research Record*, vol. 23-09, no. July, pp. 1–22, dec 2012.

[4] Y. Shao, J. Xu, B. Li, and K. Yang, "Modeling the Speed Choice Behaviors of Drivers on Mountainous Roads with Complicated Shapes," *Advances in Mechanical Engineering*, vol. 7, no. 2, pp. 862 610–862 610, feb 2015.

[5] A. Takahashi and M. Akamatsu, "Speed Choice Model of Curve Entering Based on Naturalistic Driving Data," in *European Conference on Human Centred Design for Intelligent Transport Systems*, 2012.

[6] A. M. C. Odhams and D. J. Cole, "Models of driver speed choice in curves," in *7th International Symposium on Advanced Vehicle Control (AVEC 04)*, 2004.

[7] A. Montella, L. Pariota, F. Galante, L. L. Imbriani, and F. Mauriello, "Prediction of Drivers ' Speed Behaviour on Rural Motorways Based on an Instrumented Vehicle Study," *Transportation Research Record: Journal of the Transportation Research Board*, no. 2434, pp. 52–62, 2014.

[8] B. Turner, J. Woolley, and P. Cairney, "An analysis of driver behaviour through rural curves: Exploratory results on driver speed," in *Australasian Road Safety Conference*, 2015.

[9] D. Zhang, Q. Xiao, J. Wang, and K. Li, "Driver curve speed model and its application to ACC speed control in curved roads," *International Journal of Automotive Technology*, vol. 14, no. 2, pp. 241–247, mar 2013.

[10] D. Lechner and C. Perrin, "The actual use of the dynamic performances of vehicles," *Proc. of the Institution of Mechanical Engineers, Part D: Journal of Automobile Engineering*, vol. 207, no. 44, pp. 249–256, 1993.

[11] M. L. Ritchie, W. K. McCoy, and W. L. Welde, "A Study of the Relation between Forward Velocity and Lateral Acceleration in Curves During Normal Driving," *Human Factors: The Journal of the Human Factors and Ergonomics Society*, vol. 10, no. 3, pp. 255–258, jun 1968.

[12] G. D. Herrin and J. B. Neuhardt, "An Empirical Model for Automobile Driver Horizontal Curve Negotiation," *Human Factors: The Journal of the Human Factors and Ergonomics Society*, vol. 16, no. 2, pp. 129–133, apr 1974.

[13] E. Bertolazzi, F. Biral, M. Da Lio, A. Saroldi, and F. Tango, "Supporting drivers in keeping safe speed and safe distance: The SASPENCE subproject within the European framework programme 6 integrating project PReVENT," *IEEE Transactions on Intelligent Transportation Systems*, vol. 11, no. 3, pp. 525–538, 2010.

[14] W. H. Levison, A. Bittner, J. Campbell, and C. Schreiner, "Modification and Partial Validation of the Driver/Vehicle Module," *Transportation Research Record: Journal of the Transportation Research Board*, vol. 1803, pp. 52–58, jan 2002.

[15] G. Reymond, A. Kemeny, J. Droulez, and A. Berthoz, "Role of Lateral Acceleration in Curve Driving : Driver Model and Experiments on a Real Vehicle and a Driving Simulator," *Human Factors: The Journal of the Human Factors and Ergonomics Society*, vol. 43, no. 3, pp. 483–495, 2001.

[16] B. N. Fildes and T. J. Triggs, "The Effect of Road Curve Geometry on Curvature Matching Judgements," *Australian Road Research*, vol. 12, no. 5, pp. p. 63–70, 1984.

[17] H. Summala, "Risk control is not risk adjustment: the zero-risk theory of driver behaviour and its implications," *Ergonomics*, vol. 31, no. 4, pp. 491–506, 1988.

[18] H. Godthelp and W. van Winsum, "Speed Choice and Steering Behavior in Curve Driving," *Human Factors: The Journal of the Human Factors and Ergonomics Society*, vol. 38, no. 3, pp. 434–441, 1996.
[19] D. A. Abbink, E. R. Boer, and M. Mulder, "Motivation for continuous haptic gas pedal feedback to support car following," *IEEE Intelligent Vehicles Symposium, Proceedings*, pp. 283–290, 2008.
[20] E. R. Boer, "Car following from the driver's perspective," *Transportation Research Part F: Traffic Psychology and Behaviour*, vol. 2, no. 1999, pp. 201–206, 2000.
[21] H. Summala, "Towards Understanding Motivational and Emotional Factors in Driver Behaviour: Comfort Through Satisficing," in *Modelling Driver Behaviour in Automotive Environments: Critical Issues in Driver Interactions with Intelligent Transport Systems*, 2007, pp. 189–207.
[22] M. F. Land and D. N. Lee, "Where we look when we steer," *Nature*, vol. 369, no. 6483, pp. 742–744, 1994.
[23] E. R. Boer, "Tangent point oriented curve negotiation," in *Proceedings of the 1996 IEEE Intelligent Vehicles Symposium*, no. 617. Tokyo: IEEE, 1996, pp. 7–12.
[24] E. Lehtonen, O. Lappi, and H. Summala, "Anticipatory eye movements when approaching a curve on a rural road depend on working memory load," *Transportation Research Part F: Traffic Psychology and Behaviour*, vol. 15, no. 3, pp. 369–377, 2012.
[25] O. Lappi, P. Rinkkalla, and J. Pekkanen, "Systematic Observation of An Expert Driver's Gaze Strategy - An On-Road Case Study," *Frontiers in Psychology*, vol. 8, no. April, 2017.
[26] T. Melman, J. C. de Winter, and D. A. Abbink, "Does haptic steering guidance instigate speeding? A driving simulator study into causes and remedies," *Accident Analysis and Prevention*, vol. 98, pp. 372–387, 2017.
[27] C. Sentouh, P. Chevrel, F. Mars, and F. Claveau, "A Human-Centred Approach of Steering Control Modelling," in *Proceedings of the 21st IAVSD Symposium on Dynamics of Vehicles on Roads and Tracks*, Stockholm, Sweden, 2009, pp. 1–12.
[28] B. W. Matthews, "Comparison of the predicted and observed secondary structure of T4 phage lysozyme," *Biochimica et Biophysica Acta (BBA)-Protein Structure*, vol. 405, no. 2, pp. 442–451, 1975.
[29] D. M. W. Powers, "Evaluation: From Precision, Recall and F-Factor to ROC, Informedness, Markedness & Correlation David," *Journal of Machine Learning Technologies*, vol. 2, no. December, pp. 37–63, 2007.
[30] S. V. Stehman, "Selecting and interpreting measures of thematic classification accuracy," *Remote Sensing of Environment*, vol. 62, no. 1, pp. 77–89, 1997.
[31] E. Lehtonen, O. Lappi, H. Kotkanen, and H. Summala, "Look-ahead fixations in curve driving." *Ergonomics*, vol. 56, no. 1, pp. 34–44, 2013.
[32] M. Mulder, M. Mulder, M. M. van Paassen, and D. A. Abbink, "Haptic gas pedal feedback," *Ergonomics*, vol. 51, no. 11, pp. 1710–1720, 2008.
[33] D. A. Abbink, D. Cleij, M. Mulder, and M. M. van Paassen, "The Importance of Including Knowledge of Neuromuscular Behaviour in Haptic Shared Control," in *IEEE International Conference on Systems, Man, and Cybernetics*, Seoul, South Korea, 2012, pp. 3350–3355.
[34] R. Gallen and S. Glaser, "Vision Based Tangent Point Detection Algorithm, Evaluation and Validation," in *MVA2009 IAPR Conference on Machine Vision Applications*, Yokohama, Japan, 2009, pp. 518–522.

Appendix A

Additional results

A-1 Naturalistic Driving Data

A-1-1 TETP distribution

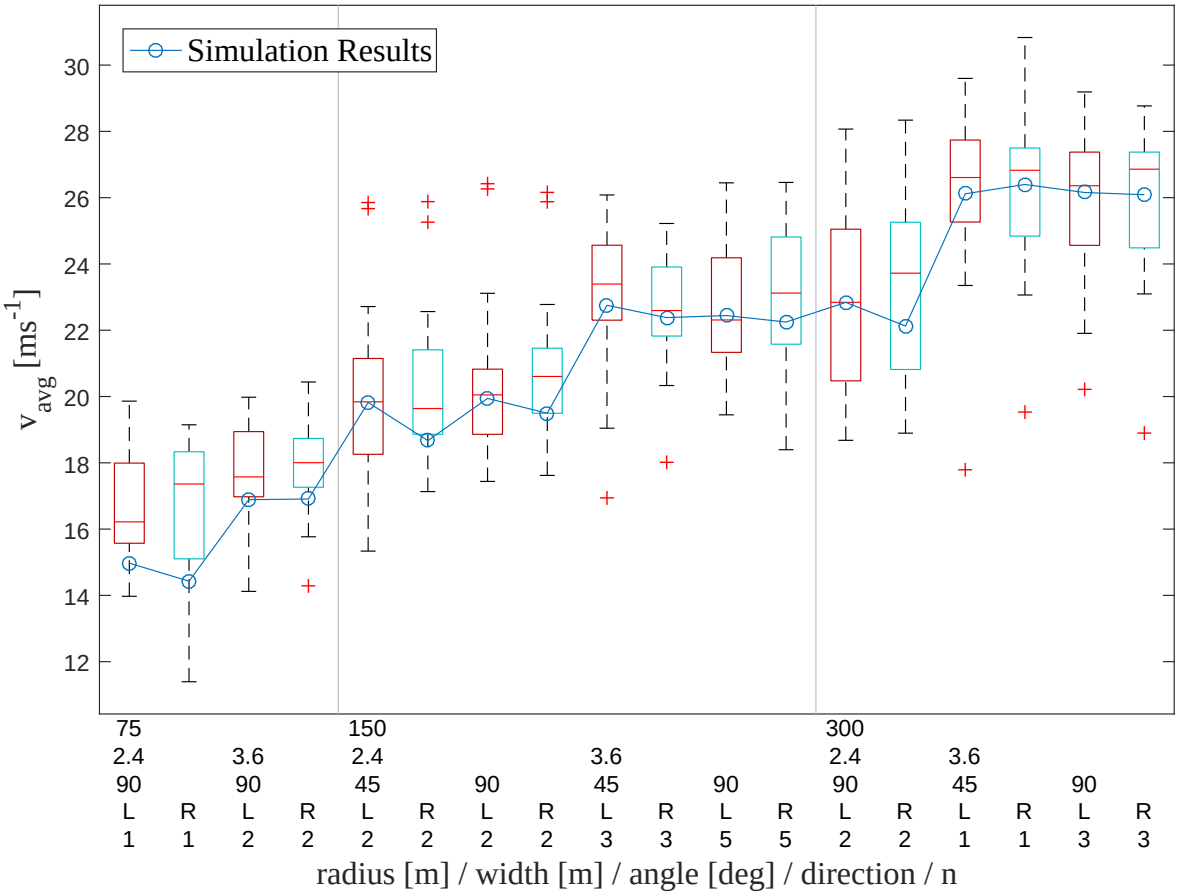

Figure A-1: Variation of experimental and modeled average curve speed with curve radius, road width, and curve deflection angle. The boxes represent experimental data, while the line represents model simulation results using a typical parameter set. n is the number of identical segments that the experimental data was averaged over.

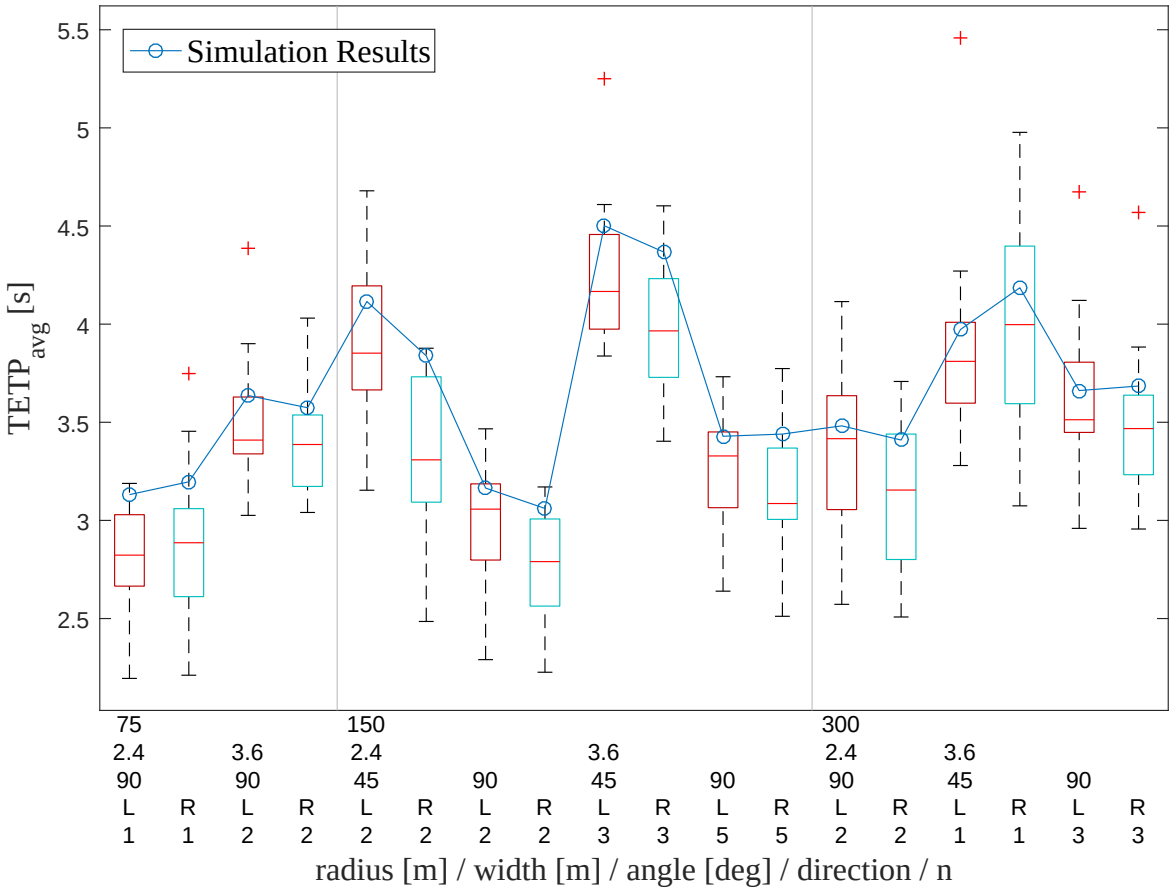

Figure A-2: Variation of experimental and modeled average TETP with curve radius, road width, and curve deflection angle. The boxes represent experimental data, while the line represents model simulation results using a typical parameter set. n is the number of identical segments that the experimental data was averaged over.

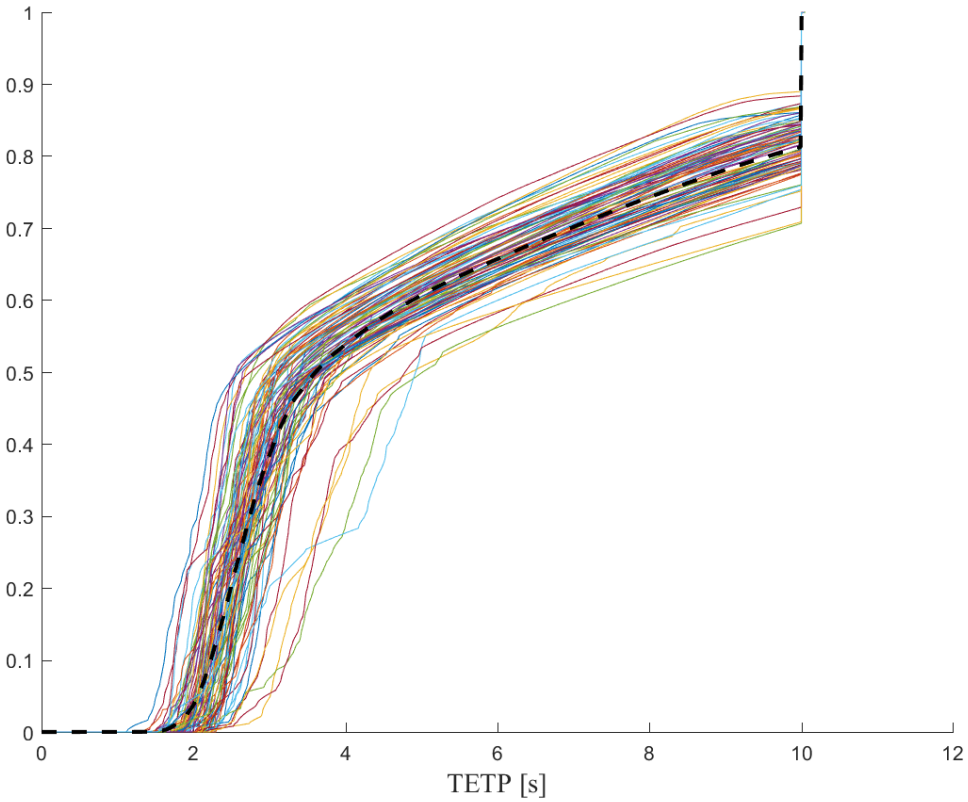

Figure A-3: Comulative distribution function of the experimental TETP values.

A-1-2 TLC distribution

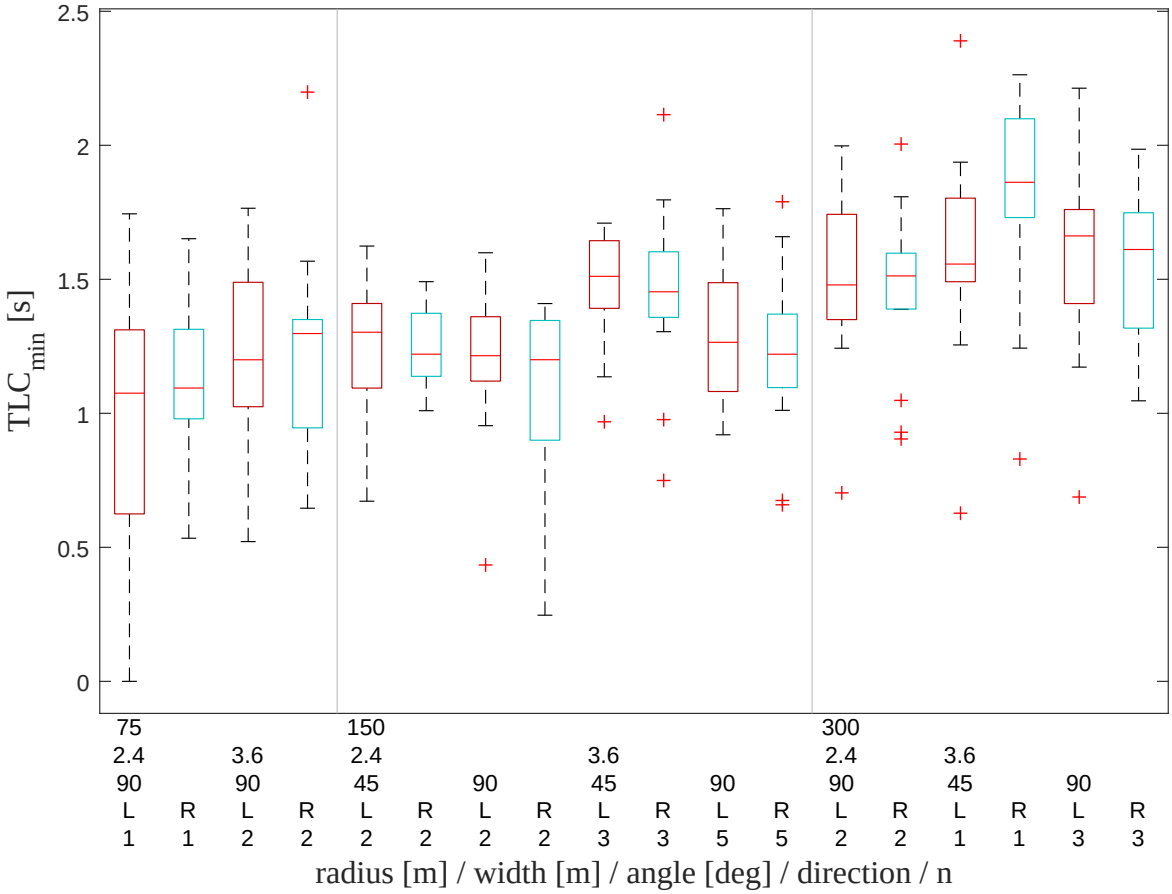

Figure A-4: Variation of experimental minimum TLC with curve radius, road width, and curve deflection angle. n is the number of identical segments that the experimental data was averaged over.

A-1-3 Corner entry lateral position

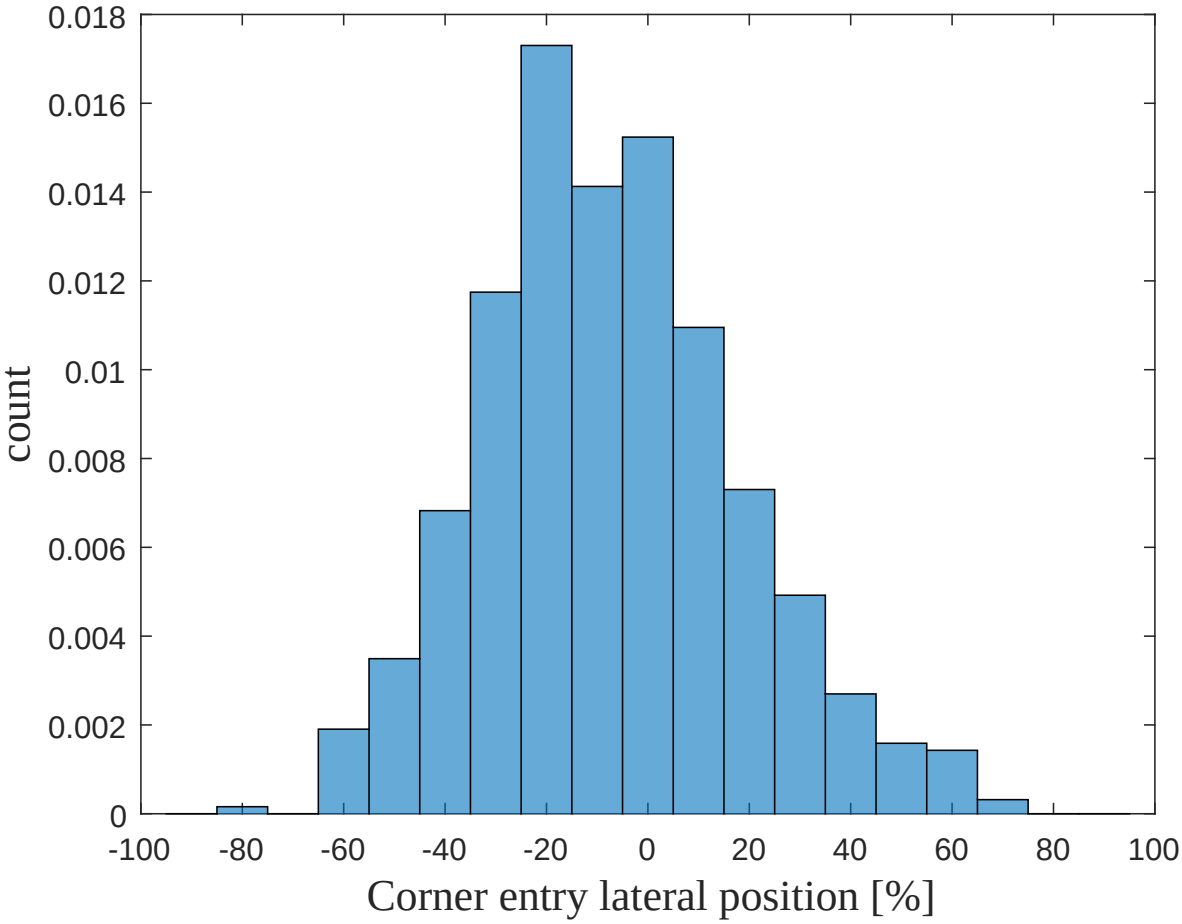

Figure A-5: Distribution of lateral position on corner entry. Positive values correspond to the inside of the curve.

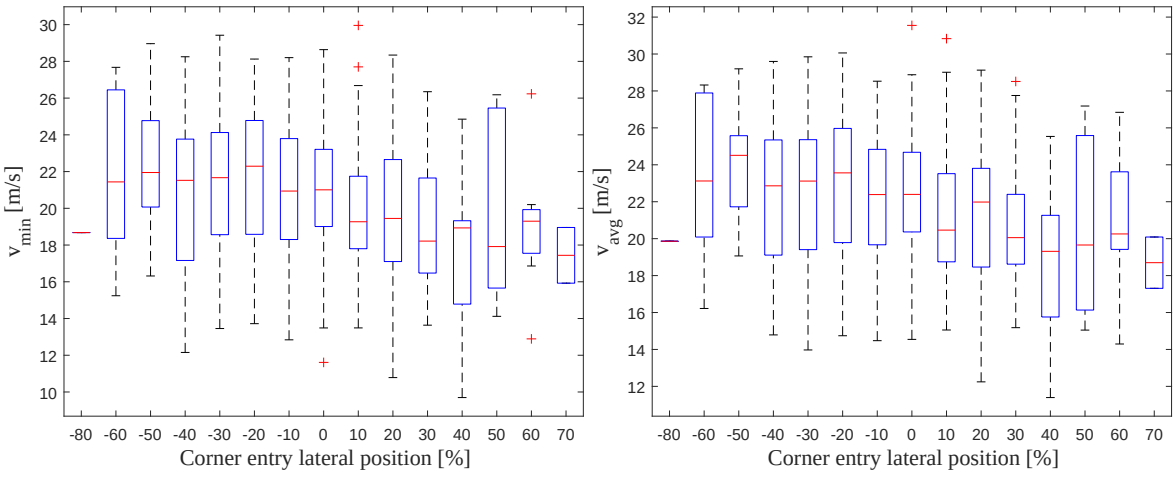

(a) Minimum speed **(b)** Average speed

Figure A-6: Influence of corner entry lateral position on speed.

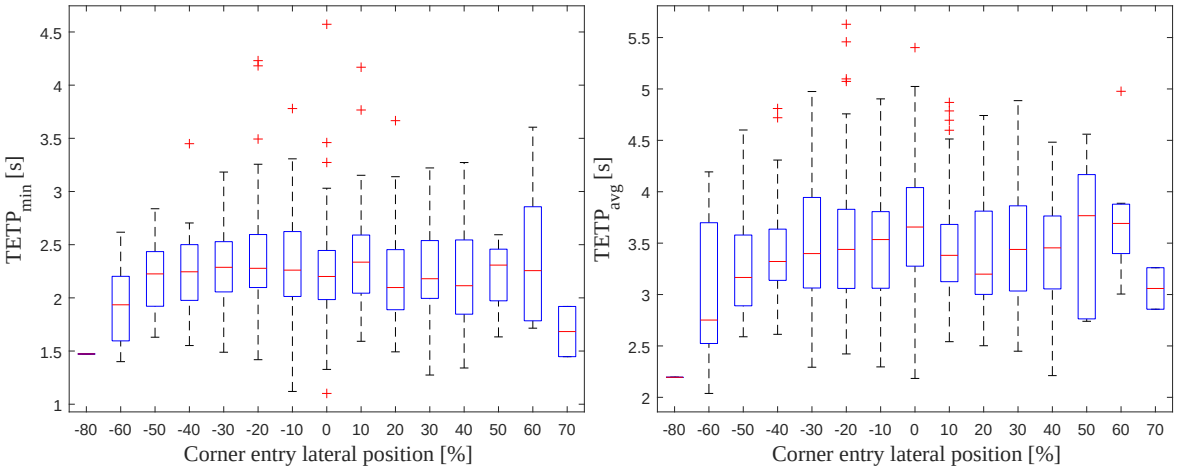

(a) Minimum TETP **(b)** Average TETP

Figure A-7: Influence of corner entry lateral position on TETP.

A-2 Comparison with speed models from literature

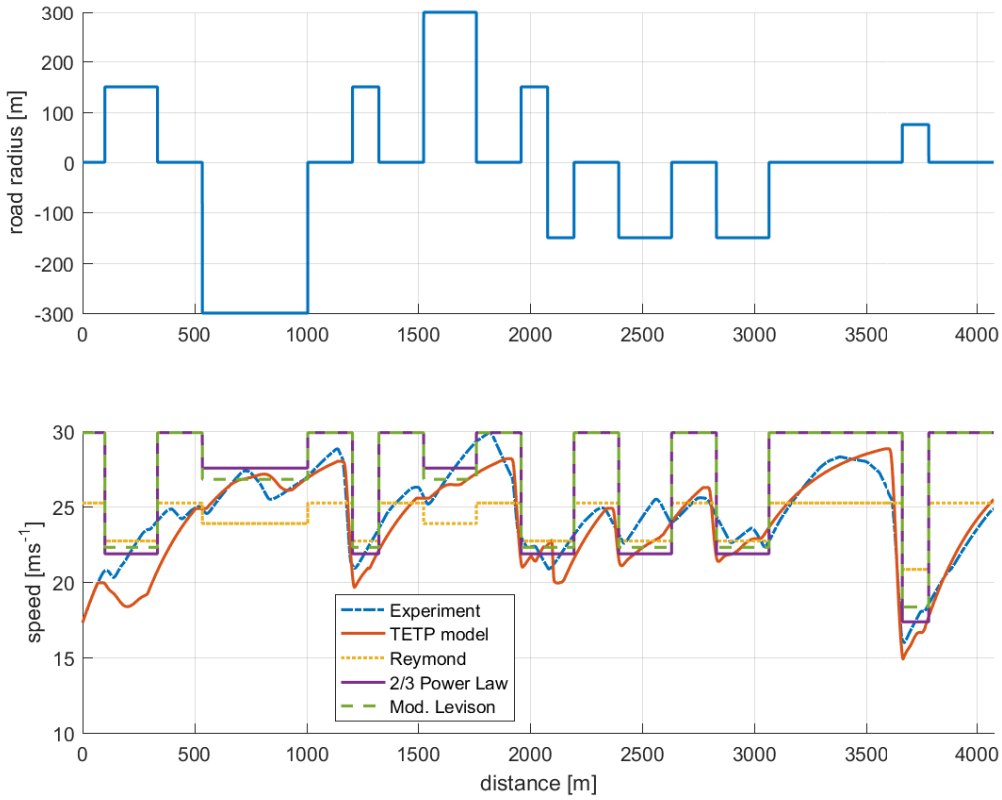

Figure A-8: Example of the performance of the speed traces model compared to speed models from literature on a wide road.

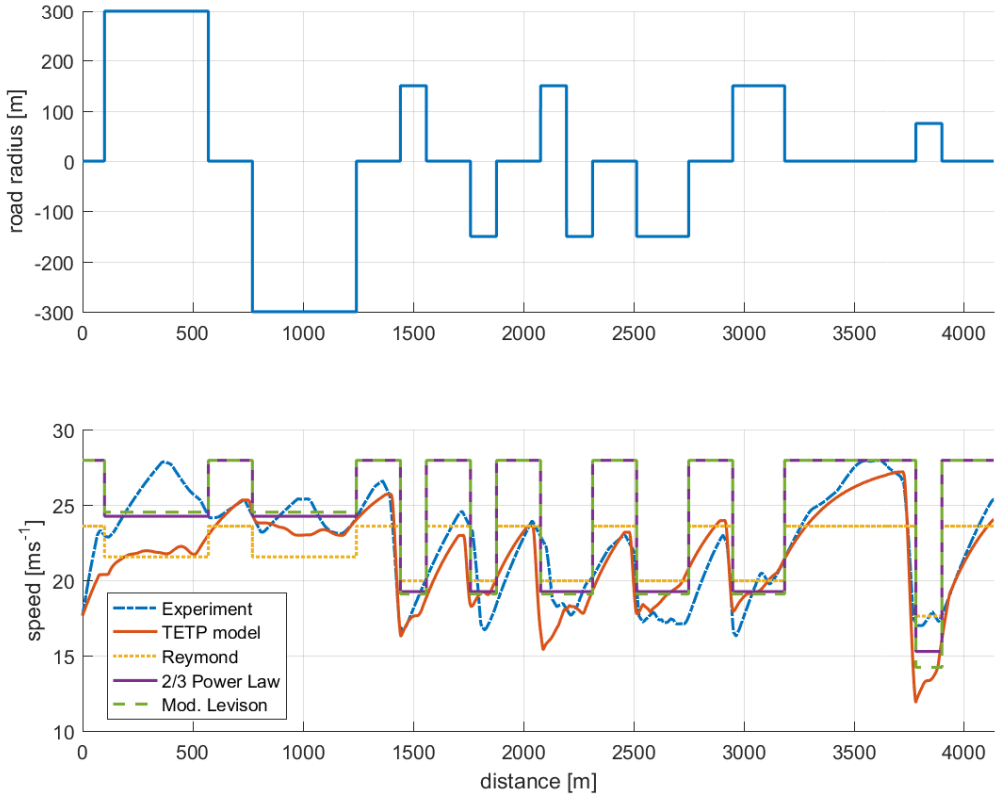

Figure A-9: Example of the performance of the speed traces model compared to speed models from literature on a narrow road.

A-3 Validation results

A-3-1 One-size-fits-all

Table A-1: Evaluation of the TETP speed control model performance using one size fits all parameters, for a wide and a narrow isolated turn with 75m radius.

Subject	VAF(v) [%]	VAF(a) [%]	VAF(δ_a) [%]	VAF(δ_b) [%]
S1W	83.9984	52.7750	46.4160	44.0683
S1N	77.4808	37.6299	48.0066	27.5818
S2W	81.2230	28.0760	35.2275	17.2190
S2N	76.0380	0	8.7645	0
S3W	84.2929	11.4482	47.3604	0
S3N	73.5175	0	31.0089	0
S4W	93.1904	60.1026	13.7231	58.2829
S4N	79.4801	24.6845	37.0417	28.3169
S5W	86.0351	66.9624	44.4168	64.3211
S5N	83.8478	10.0237	23.6368	0
S6W	37.2780	0	8.7107	0
S6N	0	0	34.0794	0
S7W	69.1493	48.5896	50.3959	50.1537
S7N	65.6990	0	40.2361	0
S8W	37.9508	50.0059	51.5619	37.7024
S8N	0	0	8.8674	0
S9W	41.0526	0	29.7754	0
S9N	65.9650	0	27.9564	0
S10W	65.9536	57.4405	54.4612	40.0552
S10N	50.0293	0	29.7506	0
S11W	82.4061	44.2498	27.4842	54.3628
S11N	85.3967	25.7527	20.7641	39.8858
S12W	82.2511	10.8720	48.5510	0
S12N	45.2254	0	29.3959	0
S13W	72.9518	0	36.8107	0
S13N	69.0362	0	30.2461	0
S14W	79.6948	32.0052	26.6636	0
S14N	55.6956	33.5170	32.2785	30.7032
S15W	76.9361	38.9459	10.6036	38.7862
S15N	45.6322	46.0113	0	41.8926
Mean	64.9136	22.6364	31.1398	19.1111
StdDev	23.6519	22.9214	14.5959	22.4896

Table A-2: Evaluation of the TETP speed control model performance using one size fits all parameters, for a wide and a narrow 4km road.

Subject	VAF(v) [%]	VAF(a) [%]	VAF(δ_a) [%]	VAF(δ_b) [%]
S1W	48.1693	38.7364	27.0199	37.0238
S1N	65.2888	49.4318	43.9695	42.4603
S2W	51.8377	0	0	0
S2N	45.8621	0	0	0
S3W	52.1381	0	28.7364	0
S3N	50.9090	0.6289	34.9081	0
S4W	69.3718	23.2617	0	16.0650
S4N	36.5311	26.4561	14.2744	20.2106
S5W	62.8130	25.5786	24.9349	15.0642
S5N	70.5461	25.4575	31.2277	0
S6W	0	0	0	0
S6N	0	0	0	0
S7W	44.6311	0	28.3741	0
S7N	31.6654	0.6498	30.2304	0
S8W	6.1971	0	0	0
S8N	0	0	0	0
S9W	37.4627	0	0	0
S9N	38.4808	0	7.4605	0
S10W	74.5454	62.2211	37.8046	55.6249
S10N	59.0856	25.1909	30.8161	0
S11W	44.0862	0	0	0
S11N	13.3079	0	0	0
S12W	46.3758	0	3.2952	0
S12N	0	0	0	0
S13W	57.8899	0	0	0
S13N	19.0420	0	18.2488	0
S14W	57.5191	20.3771	30.9927	0
S14N	0	0	0	0
S15W	23.6682	0	20.4302	0
S15N	36.6694	0	0	0
Mean	38.1365	9.9330	13.7574	6.2150
StdDev	23.6970	17.0694	15.2062	14.3869

A-3-2 Individualized parameters - isolated curve

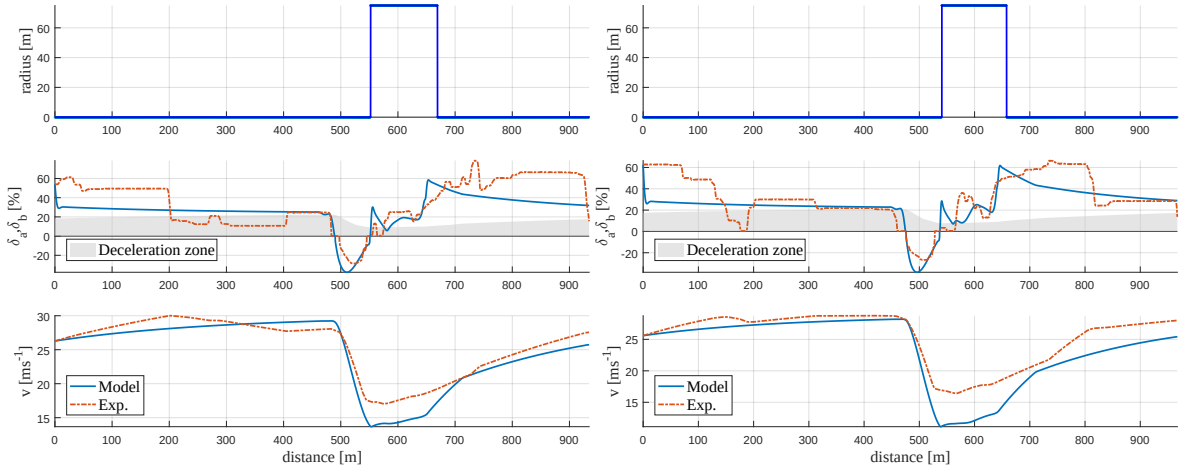

(a) Wide road **(b)** Narrow road

Figure A-10: Performance of the model on an isolated 75m radius turn for subject 1. Positive pedal deflections correspond to the accelerator pedal, while negative deflections represent brake actuation. The shaded area represents the accelerator pedal position values that correspond to engine braking.

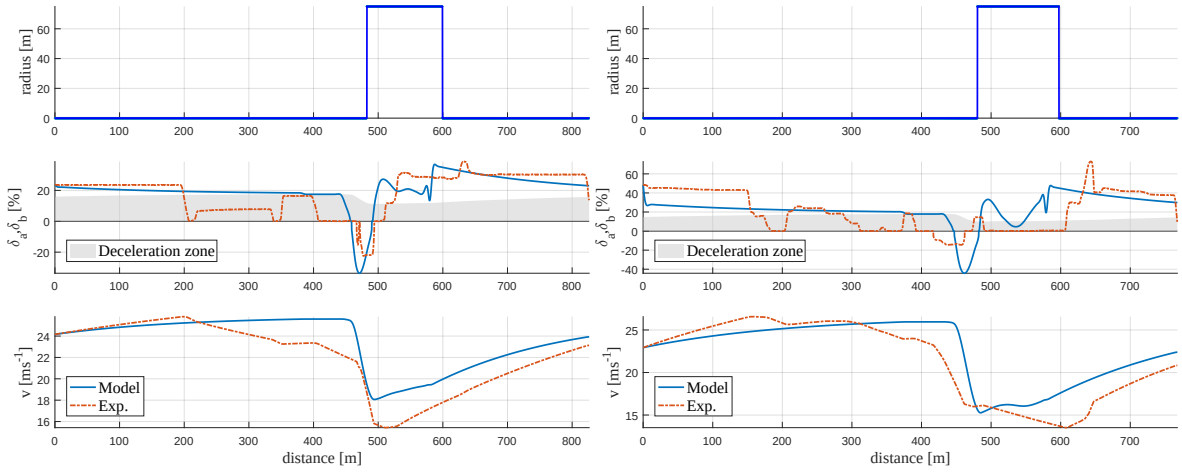

(a) Wide road **(b)** Narrow road

Figure A-11: Performance of the model on an isolated 75m radius turn for subject 2. Positive pedal deflections correspond to the accelerator pedal, while negative deflections represent brake actuation. The shaded area represents the accelerator pedal position values that correspond to engine braking.

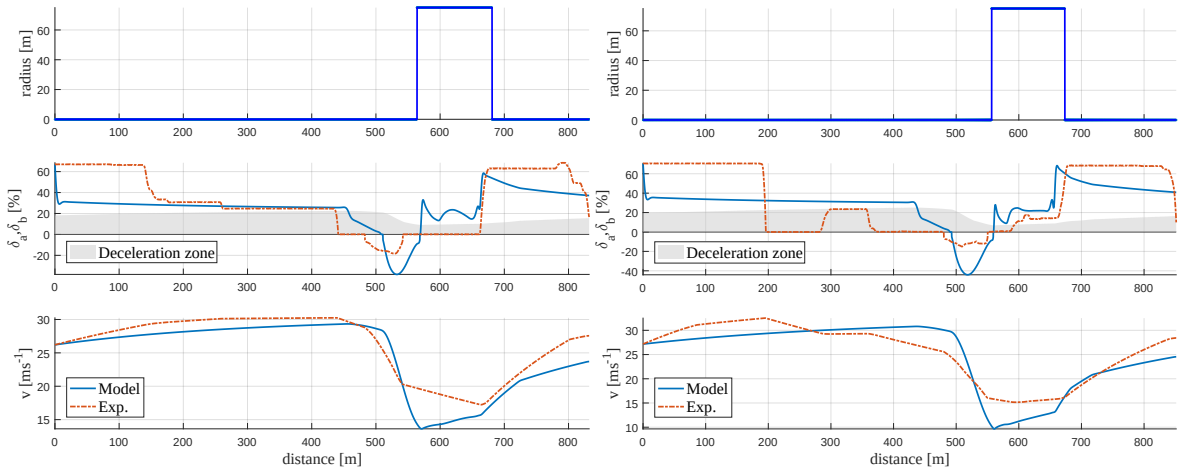

(a) Wide road **(b)** Narrow road

Figure A-12: Performance of the model on an isolated 75m radius turn for subject 3. Positive pedal deflections correspond to the accelerator pedal, while negative deflections represent brake actuation. The shaded area represents the accelerator pedal position values that correspond to engine braking.

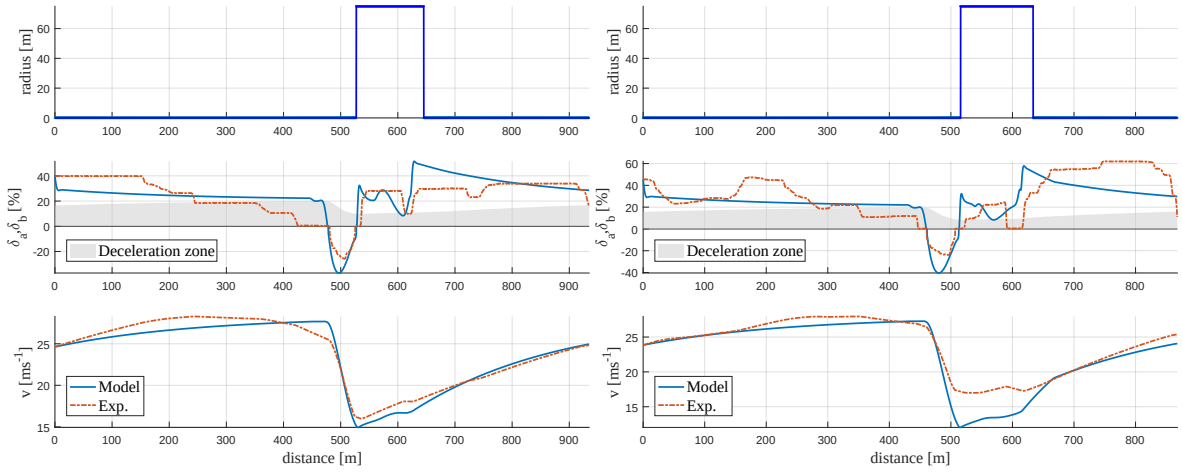

(a) Wide road **(b)** Narrow road

Figure A-13: Performance of the model on an isolated 75m radius turn for subject 4. Positive pedal deflections correspond to the accelerator pedal, while negative deflections represent brake actuation. The shaded area represents the accelerator pedal position values that correspond to engine braking.

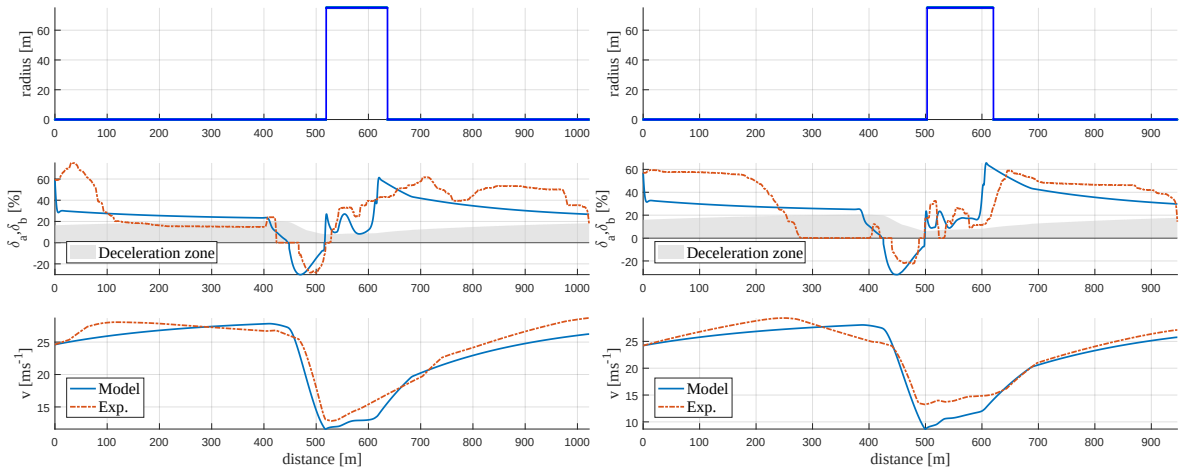

(a) Wide road **(b)** Narrow road

Figure A-14: Performance of the model on an isolated 75m radius turn for subject 5. Positive pedal deflections correspond to the accelerator pedal, while negative deflections represent brake actuation. The shaded area represents the accelerator pedal position values that correspond to engine braking.

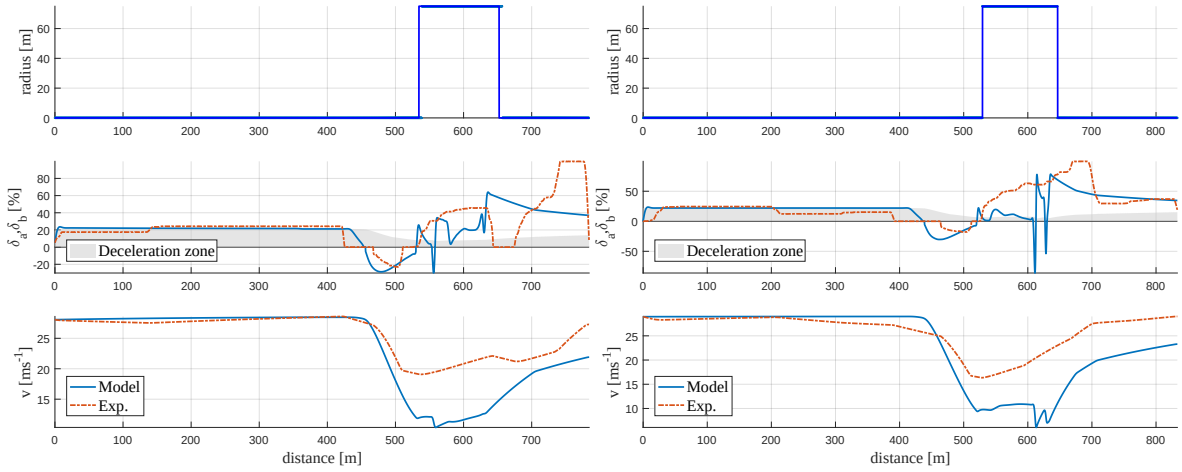

(a) Wide road **(b)** Narrow road

Figure A-15: Performance of the model on an isolated 75m radius turn for subject 6. Positive pedal deflections correspond to the accelerator pedal, while negative deflections represent brake actuation. The shaded area represents the accelerator pedal position values that correspond to engine braking.

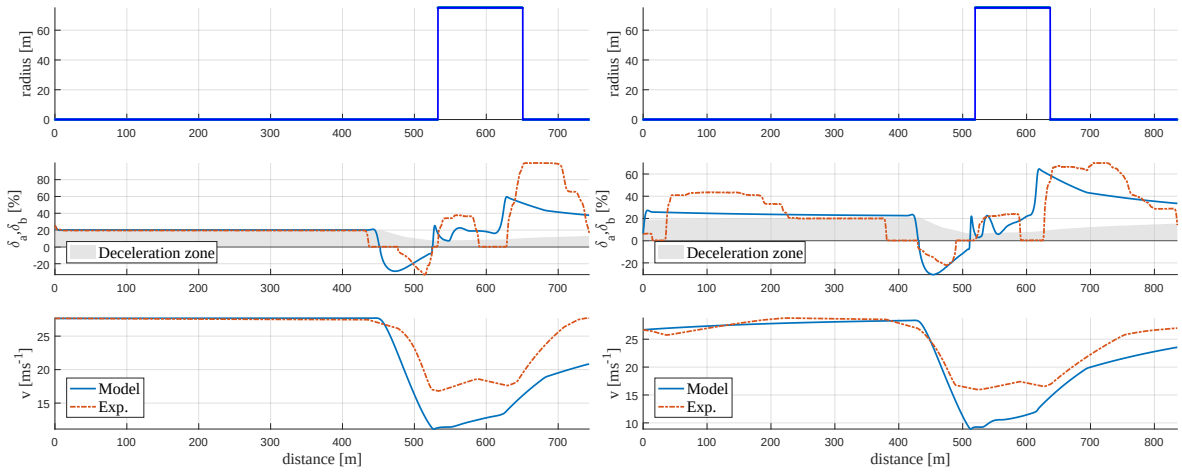

(a) Wide road **(b)** Narrow road

Figure A-16: Performance of the model on an isolated 75m radius turn for subject 7. Positive pedal deflections correspond to the accelerator pedal, while negative deflections represent brake actuation. The shaded area represents the accelerator pedal position values that correspond to engine braking.

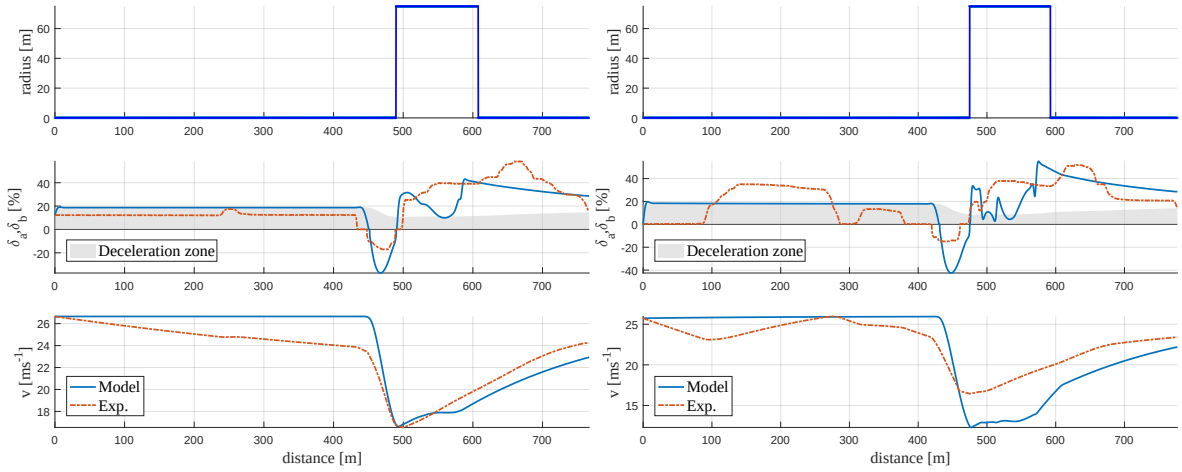

(a) Wide road **(b)** Narrow road

Figure A-17: Performance of the model on an isolated 75m radius turn for subject 8. Positive pedal deflections correspond to the accelerator pedal, while negative deflections represent brake actuation. The shaded area represents the accelerator pedal position values that correspond to engine braking.

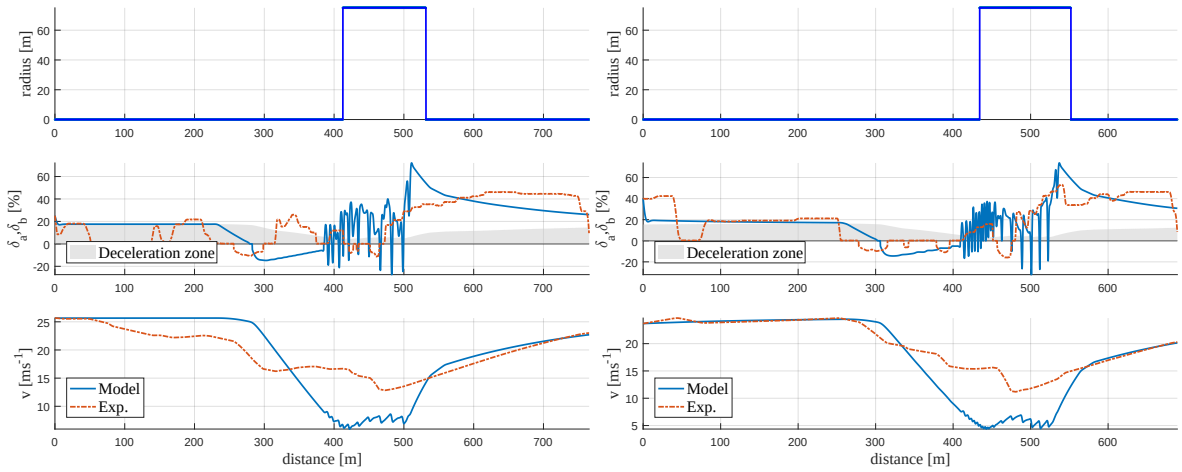

(a) Wide road **(b)** Narrow road

Figure A-18: Performance of the model on an isolated 75m radius turn for subject 9. Positive pedal deflections correspond to the accelerator pedal, while negative deflections represent brake actuation. The shaded area represents the accelerator pedal position values that correspond to engine braking.

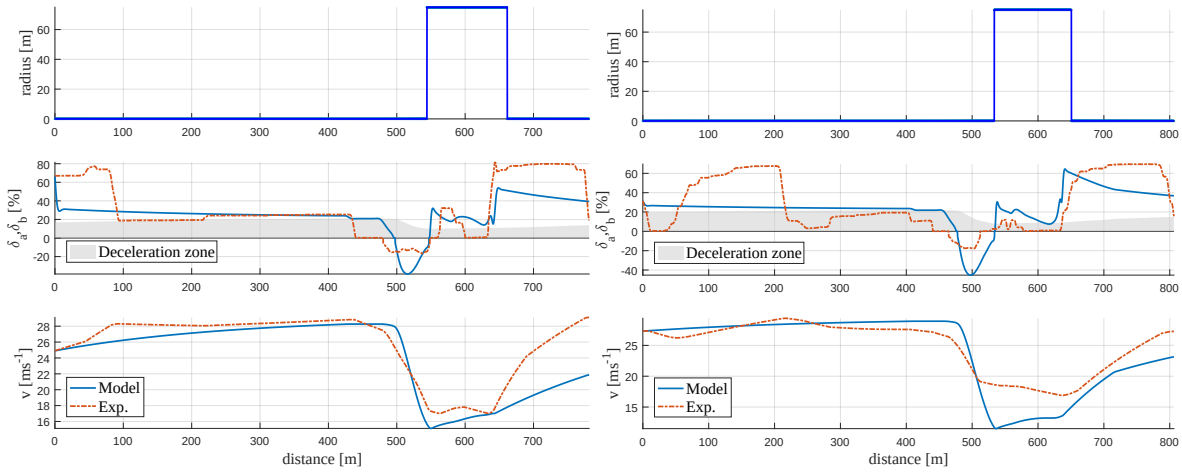

(a) Wide road **(b)** Narrow road

Figure A-19: Performance of the model on an isolated 75m radius turn for subject 10. Positive pedal deflections correspond to the accelerator pedal, while negative deflections represent brake actuation. The shaded area represents the accelerator pedal position values that correspond to engine braking.

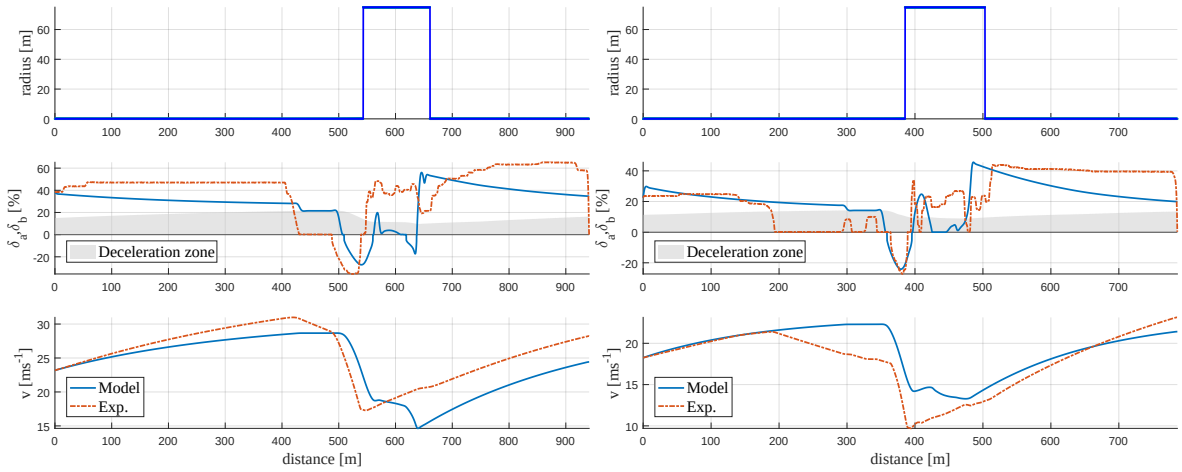

(a) Wide road **(b)** Narrow road

Figure A-20: Performance of the model on an isolated 75m radius turn for subject 11. Positive pedal deflections correspond to the accelerator pedal, while negative deflections represent brake actuation. The shaded area represents the accelerator pedal position values that correspond to engine braking.

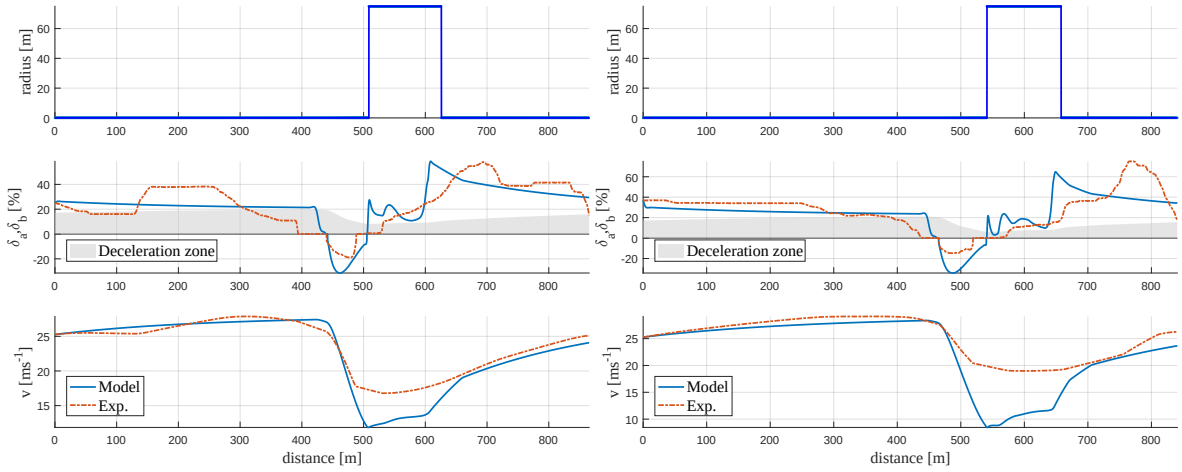

(a) Wide road **(b)** Narrow road

Figure A-21: Performance of the model on an isolated 75m radius turn for subject 12. Positive pedal deflections correspond to the accelerator pedal, while negative deflections represent brake actuation. The shaded area represents the accelerator pedal position values that correspond to engine braking.

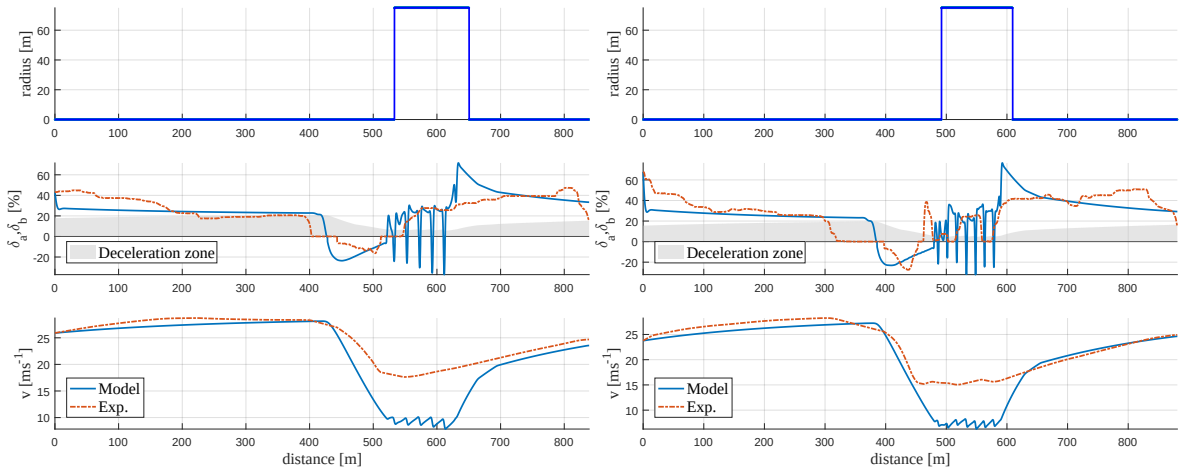

(a) Wide road **(b)** Narrow road

Figure A-22: Performance of the model on an isolated 75m radius turn for subject 13. Positive pedal deflections correspond to the accelerator pedal, while negative deflections represent brake actuation. The shaded area represents the accelerator pedal position values that correspond to engine braking.

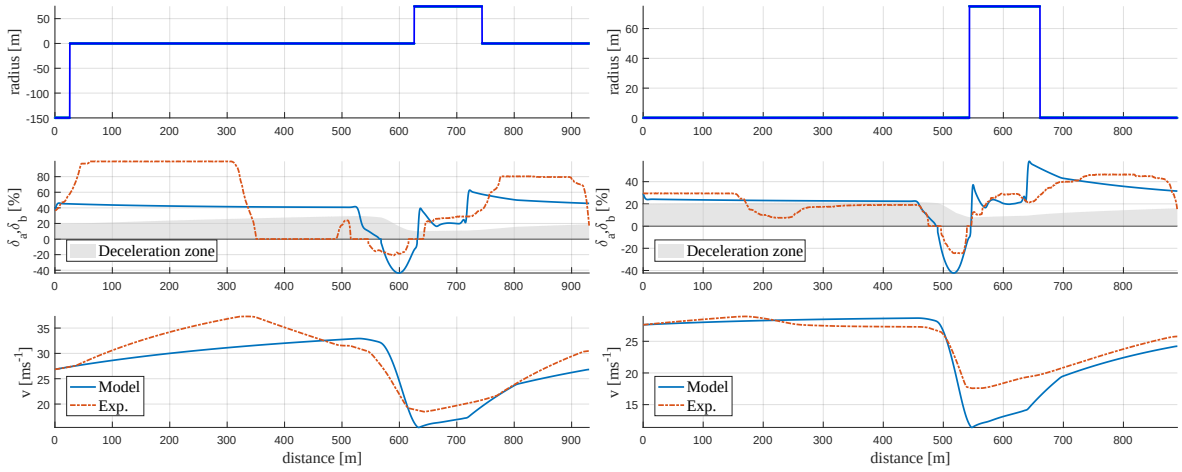

(a) Wide road **(b)** Narrow road

Figure A-23: Performance of the model on an isolated 75m radius turn for subject 14. Positive pedal deflections correspond to the accelerator pedal, while negative deflections represent brake actuation. The shaded area represents the accelerator pedal position values that correspond to engine braking.

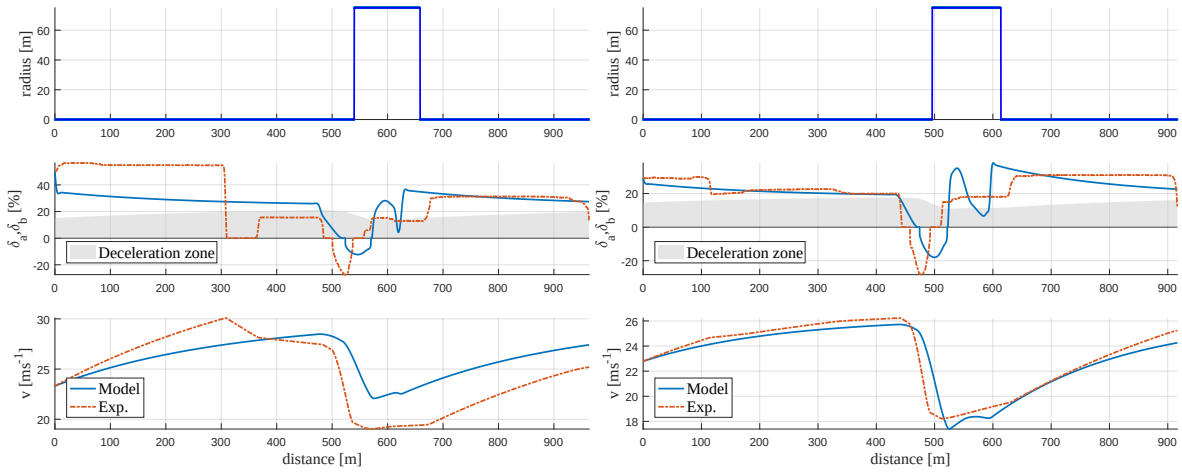

(a) Wide road **(b)** Narrow road

Figure A-24: Performance of the model on an isolated 75m radius turn for subject 15. Positive pedal deflections correspond to the accelerator pedal, while negative deflections represent brake actuation. The shaded area represents the accelerator pedal position values that correspond to engine braking.

A-3-3 Individualized parameters - complete road

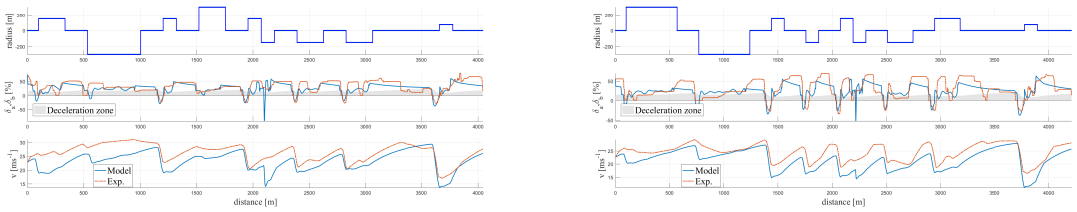

(a) Wide road **(b)** Narrow road

Figure A-25: Performance of the model on a 4km length road for subject 1. Positive pedal deflections correspond to the accelerator pedal, while negative deflections represent brake actuation. The shaded area represents the accelerator pedal position values that correspond to engine braking.

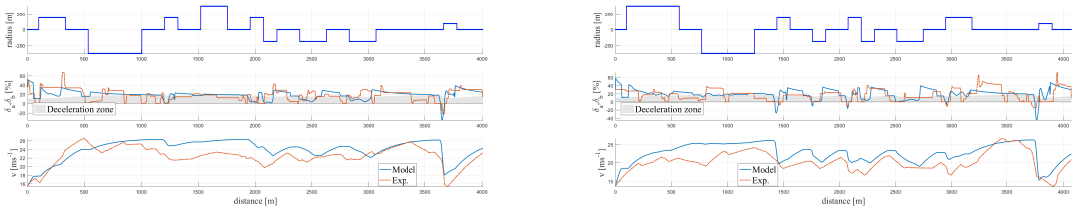

(a) Wide road **(b)** Narrow road

Figure A-26: Performance of the model on a 4km length road for subject 2. Positive pedal deflections correspond to the accelerator pedal, while negative deflections represent brake actuation. The shaded area represents the accelerator pedal position values that correspond to engine braking.

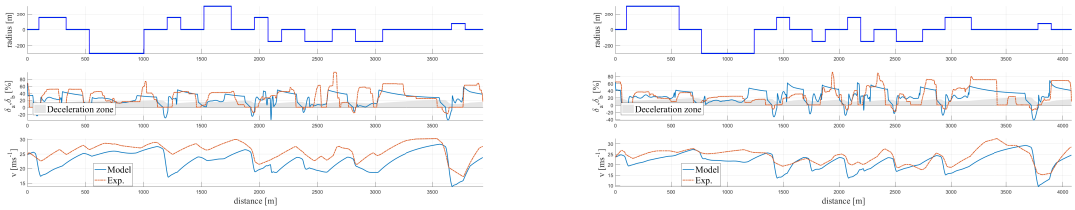

(a) Wide road **(b)** Narrow road

Figure A-27: Performance of the model on a 4km length road for subject 3. Positive pedal deflections correspond to the accelerator pedal, while negative deflections represent brake actuation. The shaded area represents the accelerator pedal position values that correspond to engine braking.

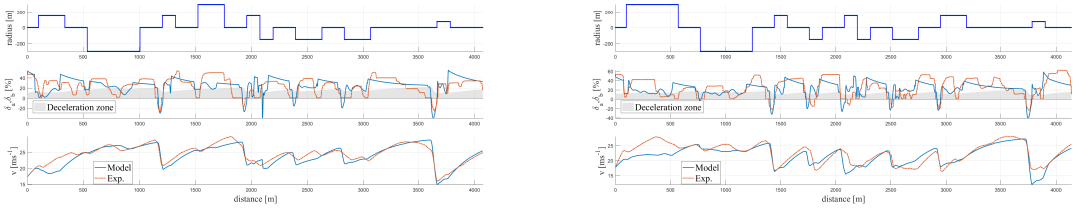

(a) Wide road **(b)** Narrow road

Figure A-28: Performance of the model on a 4km length road for subject 4. Positive pedal deflections correspond to the accelerator pedal, while negative deflections represent brake actuation. The shaded area represents the accelerator pedal position values that correspond to engine braking.

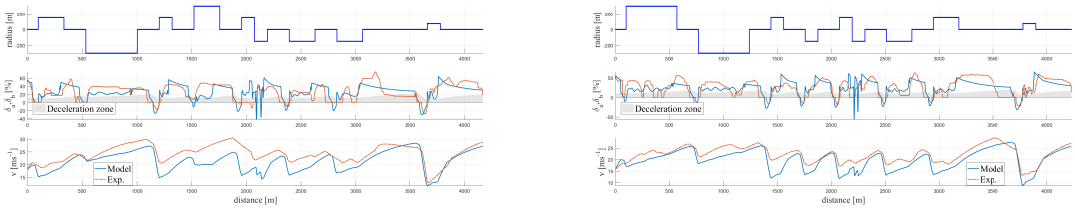

(a) Wide road **(b)** Narrow road

Figure A-29: Performance of the model on a 4km length road for subject 5. Positive pedal deflections correspond to the accelerator pedal, while negative deflections represent brake actuation. The shaded area represents the accelerator pedal position values that correspond to engine braking.

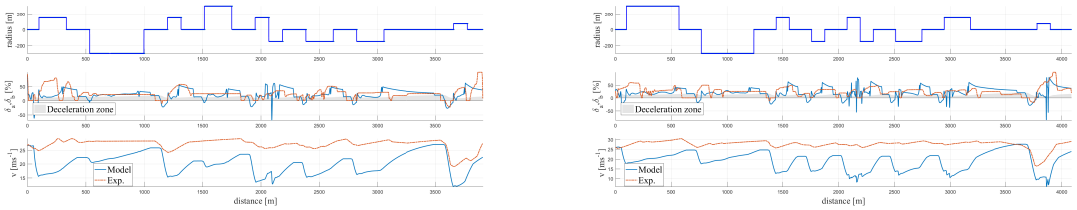

(a) Wide road **(b)** Narrow road

Figure A-30: Performance of the model on a 4km length road for subject 6. Positive pedal deflections correspond to the accelerator pedal, while negative deflections represent brake actuation. The shaded area represents the accelerator pedal position values that correspond to engine braking.

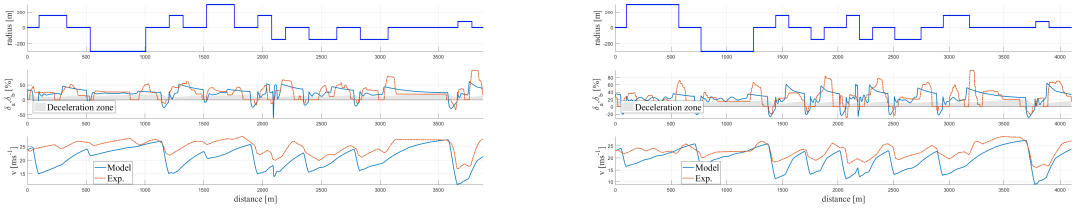

(a) Wide road **(b)** Narrow road

Figure A-31: Performance of the model on a 4km length road for subject 7. Positive pedal deflections correspond to the accelerator pedal, while negative deflections represent brake actuation. The shaded area represents the accelerator pedal position values that correspond to engine braking.

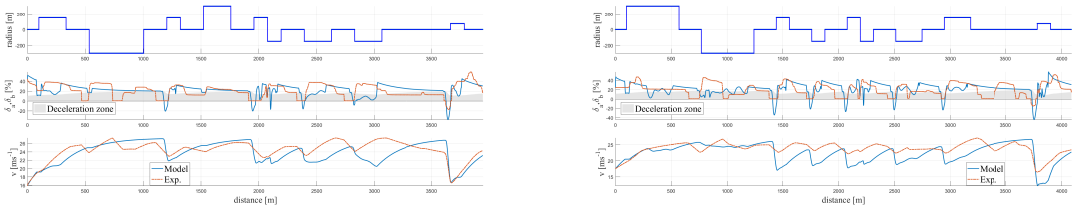

(a) Wide road **(b)** Narrow road

Figure A-32: Performance of the model on a 4km length road for subject 8. Positive pedal deflections correspond to the accelerator pedal, while negative deflections represent brake actuation. The shaded area represents the accelerator pedal position values that correspond to engine braking.

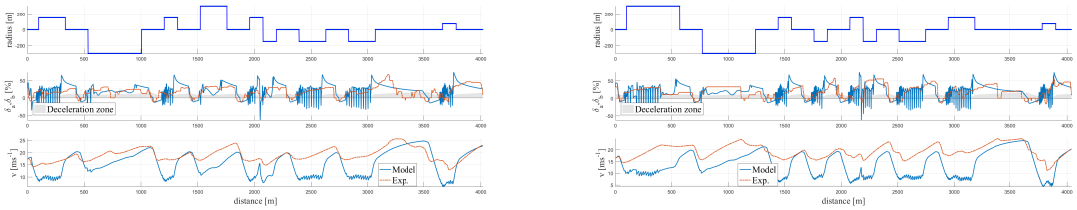

(a) Wide road **(b)** Narrow road

Figure A-33: Performance of the model on a 4km length road for subject 9. Positive pedal deflections correspond to the accelerator pedal, while negative deflections represent brake actuation. The shaded area represents the accelerator pedal position values that correspond to engine braking.

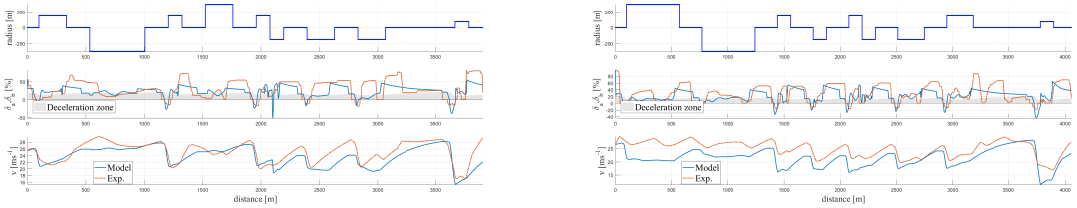

(a) Wide road **(b)** Narrow road

Figure A-34: Performance of the model on a 4km length road for subject 10. Positive pedal deflections correspond to the accelerator pedal, while negative deflections represent brake actuation. The shaded area represents the accelerator pedal position values that correspond to engine braking.

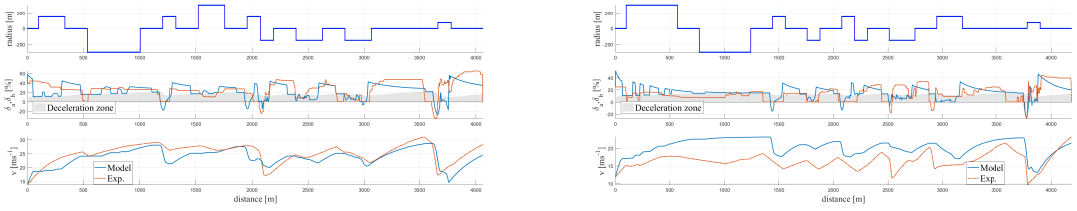

(a) Wide road **(b)** Narrow road

Figure A-35: Performance of the model on a 4km length road for subject 11. Positive pedal deflections correspond to the accelerator pedal, while negative deflections represent brake actuation. The shaded area represents the accelerator pedal position values that correspond to engine braking.

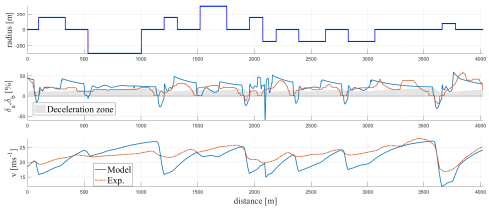

(a) Wide road

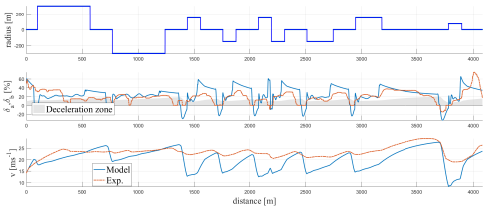

(b) Narrow road

Figure A-36: Performance of the model on a 4km length road for subject 12. Positive pedal deflections correspond to the accelerator pedal, while negative deflections represent brake actuation. The shaded area represents the accelerator pedal position values that correspond to engine braking.

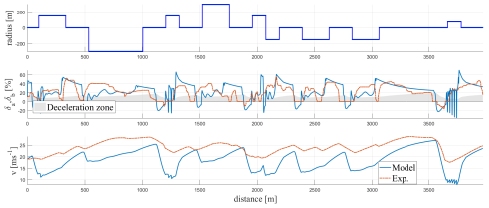

(a) Wide road

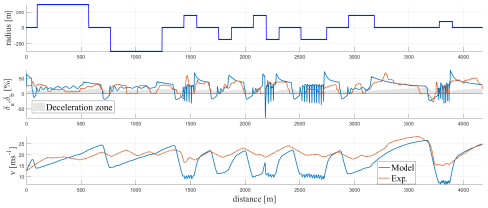

(b) Narrow road

Figure A-37: Performance of the model on a 4km length road for subject 13. Positive pedal deflections correspond to the accelerator pedal, while negative deflections represent brake actuation. The shaded area represents the accelerator pedal position values that correspond to engine braking.

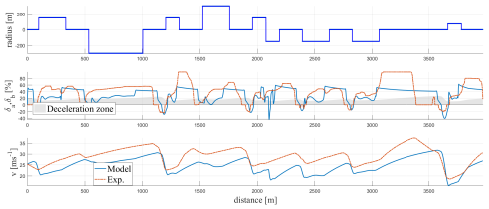

(a) Wide road

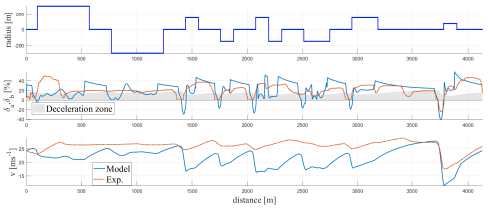

(b) Narrow road

Figure A-38: Performance of the model on a 4km length road for subject 14. Positive pedal deflections correspond to the accelerator pedal, while negative deflections represent brake actuation. The shaded area represents the accelerator pedal position values that correspond to engine braking.

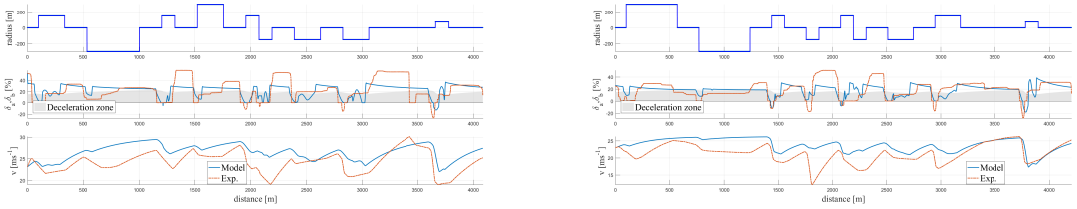

(a) Wide road **(b)** Narrow road

Figure A-39: Performance of the model on a 4km length road for subject 15. Positive pedal deflections correspond to the accelerator pedal, while negative deflections represent brake actuation. The shaded area represents the accelerator pedal position values that correspond to engine braking.

Part II

Preliminary Thesis

How do drivers combine speed choice and steering behavior during curve negotiation, and how can knowledge of this interaction be applied in the design of haptic assistance?

Preliminary Master of Science Thesis

For obtaining the degree of Master of Science in Aerospace Engineering
at Delft University of Technology

Virgílio Gruppelaar

September 27, 2016

Faculty of Aerospace Engineering · Delft University of Technology

Acronyms

AOI	Area Of Interest
ETP	Extended Tangent Point
FP	Future Path
GTO	Golgi Tendon Organ
HCR	Human Compatible Reference
HMM	Hidden Markov Model
HSC	Haptic Shared Control
MPC	Model Predictive Control
NMS	Neuromuscular System
RF	Retinal Flow
RMSE	Root Mean Square Error
RVS	Road-Vehicle-Steering
TETP	Time to Extended Tangent Point
TLC	Time to Line Crossing
TP	Tangent Point
TPA	visual angle to the tangent point
TTP	Time To Collision
TTP	Time to Tangent Point
VAF	Variance Accounted For
VD	Visual Direction

List of Symbols

Greek Symbols

α	Velocity gain factor
ΔC	Path curvature safety margin
δ_{SW}	Current steering wheel angle
$\hat{\delta}_{SW}$	Driver desired steering wheel angle
Γ	Lateral acceleration during curve driving
τ_p	Padé approximation of human processing time delay
Θ	Angle between current vehicle heading and a specified reference point
θ_{far}	Angle between current vehicle heading and the far point
θ_{near}	Angle between current vehicle heading and the near point

Roman Symbols

C	Path curvature
K_a	Driver visual anticipation gain
K_c	Driver visual compensation gain
K_r	Gain of driver internal model of steering column stiffness
K_t	Stiffness of driver's holding of the steering wheel
L	Vehicle wheelbase
$\|T\|$	Distance to target point
T_I	Driver near angle visual compensation lag time constant
T_L	Driver near angle visual compensation lead time constant
T_N	Driver neuromuscular time constant

v	Tangential velocity
y_{lat}	Lateral position from the lane center line

Contents

Chapter 1

Introduction

For many people, driving a car is a familiar task, and for most of the past century the manner in which it is performed has not changed considerably. However, in recent times a large amount of attention has been devoted to developing assistive or automated systems that can take away a part, or all, of the workload involved in driving a car. Gordon and Lidberg (2015) provide a comprehensive overview of the state of driving automation, and conclude that while a lot of focus is placed on the research of fully automated vehicles, these are still a long way from being implemented on the roads, and would required complete overhauls of the current personal transportation infrastructure for effective large scale implementation. In addition, as argued by Flemisch et al. (2012), even if technology advances as far as to enable these systems, there is no guarantee that they will provide significant benefits to the human operator, due to the well known *ironies of automation* (Bainbridge, 1983).

Current state of the art systems automate some aspects of the driving task, but once they reach their limits drivers are prompted to take over at short notice. This places the driver in a supervisory role, a task humans have been shown to perform poorly at (Mulder, Abbink, & Boer, 2012). When asked to intervene, drivers take time to insert themselves into a manual control role, resulting in delays that could cause accidents. This is know as the human-out-of-the-loop problem (Flad, Otten, Schwab, & Hohmann, 2014a; Flemisch et al., 2012).

A promising approach to support drivers without causing them to lose situational awareness is Haptic Shared Control (HSC) (Abbink, Mulder, & Boer, 2012; Mars, Deroo, & Hoc, 2014). As the name indicates, HSC entails a shared control approach, in which the human operator and the assistance system communicate their intentions and actions to each other through a haptic interface. In the context of the driving task, these haptic interfaces can be implemented on, for example, the gas pedal (Mulder, Mulder, van Paassen, & Abbink, 2008), or the steering wheel (Mulder, Abbink, & Boer, 2008).

For the proper development of any assistance system, but especially in the case of a system that interacts closely with a human operator, it is essential that the system is based on a solid understanding of the underlying human behavior. The aim of this work is to address haptic shared control systems applied to curve driving. While there is a significant body of recent

research into such systems for assistance in cornering at constant speeds (Mulder, Abbink, & Boer, 2008; Saleh, Chevrel, Claveau, Lafay, & Mars, 2013; Flad, Otten, Schwab, & Hohmann, 2014b), not much focus has been placed on the issue of variable speeds. However, as can be noted by observing any curved road, human drivers do not drive through turns at the same speeds that they negotiate straight sections of road, but rather adapt their speed in some way. This work focuses on HSC applications to variable speed corner driving.

van Paassen, Boink, Abbink, Mulder, and Mulder (n.d.) specify four essential design choices that must be addressed in order to design a successful haptic shared control implementation. All of these choices are important, but in order to limit the scope of this research, the focus will lie on the first design choice, the generation of an appropriate Human Compatible Reference (HCR). Human drivers control their vehicles by applying torques on the steering wheel and the gas pedal, and if necessary, by applying a force on the brake pedal. However, driver models for steering generally use the available information of the environment to produce a desired steering wheel angle for vehicle control. If no other torques or forces are present, then this approach is valid and the steering wheel angle corresponds directly to the applied torque. However, as noted by Abbink, Cleij, Mulder, and van Paassen (2012), in the case that the human is sharing control with a system that applies assistance, it is essential to know how humans will react to this assistance in order to be able to design effective systems. It follows from that statement that, for HSC systems, an appropriate HCR for steering consists of steering wheel torques, and an appropriate HCR for speed control consists of pedal torques. Furthermore, in order to to provide effective assistance at variable speeds, knowledge must be gathered about the changes in human driving behavior with speed. To that end, the research question that this literature review aims to answer is: *How do drivers combine speed choice and steering behavior during curve negotiation, and how can knowledge of this interaction be applied in the design of haptic assistance?*

The answer to this question is provided over the next chapters. The first chapter gives a summary of an extensive literature survey into how drivers take corners, followed by a preliminary analysis, through simulation, of one of the models described in literature. Finally, the conclusion will address the future work that remains to be done in order to answer this question.

Chapter 2

How do drivers corner?

In order to develop an assistance system, first one must understand the task to be accomplished, in this case how a driver negotiates a corner. This chapter will address the state of the art of the available literature on this topic, in three different sections. Before delving into how speed affects cornering, one must first understand the dynamics behind the simpler steering task at constant speed. The first section of this chapter concerns this. The second section aims to explain how corners affect the choice of speed by the driver, and to provide a way of modeling speed choice. Finally, the third section explores the combination of the two previous ones, that is, how does the speed choice affect the steering behavior.

2-1 Steering at constant speed

For the purposes of this work, steering is divided into two separate parts: the perception of the road ahead, including the neurological processing required to generate an intended steering angle; and the neuromuscular actuation that transforms this desired angle into physical torques on the steering wheel.

This section is divided into four parts. The first describes the most important models of the perception component of steering developed since the introduction of the idea of two level of steering. This is followed by short overview of the current debate on where drivers actually look during steering. The last two sections describe two different approaches in modeling of drivers' neuromuscular behavior during curve driving. The first one concerns the classical models of the neuromuscular system, while the final section describes the idea of using motion primitives to explain the control of the steering wheel.

2-1-1 The two levels of steering

Since Donges (1978) first proposed a two level model of human steering behavior, it has been accepted that human steering can be divided, in general terms, into two patterns of behavior.

The first level is the preview function, where drivers use what is called *guidance information* from the visual field to predict the desired path of the vehicle, that is, the *forcing function* that they wish to follow. The second level is where drivers use visual information on the deviations of the vehicle's current path from the desired path, the so called *stabilization information*, in order to stabilize the vehicle's motion around the forcing function.

The model developed by Donges (1978) uses the curvature of the desired path, extracted from the drivers' visual field, as the guidance information. This information is then used in the first level of control, a feedforward *anticipatory open-loop control*. The stabilization information is divided into three parts: the lateral deviation between the driver and the desired path, the heading angle error, and the difference in current to desired path curvatures, or path curvature error. These three perceived parameters are combined in the *compensatory closed-loop control* level in order the generate a correcting steering angle to ensure the vehicle keeps to the desired path in a stable fashion. In a simulator experiment, drivers drove a curved course, and were verbally instructed to maintain certain speeds. The model was found to predict the low frequency behavior of the drivers well, but some high-frequency behavior remained unaccounted for. This was attributed to a non-linear driver noise, called remnant by McRuer, Allen, Weir, and Klein (1977).

Land and Lee (1994) provided a very important contribution by being one of the first works to link steering behavior with driver's gaze direction. By monitoring eye movements during real driving, they discovered that drivers consistently look in the direction of the Tangent Point (TP) of the curve they are steering around, which is the point where the gaze direction is tangential to the road edge on the inside of the curve. Drivers focus on the TP because it is a very good reference point in order to estimate the curvature of the road ahead, as described in equation (2-1) where Θ is the visual angle between the current heading and the TP, and y_l is the distance between the intended path and the inside lane edge, as shown in figure 2-1. Many driver models have been developed based on this idea, but in recent times the notion that drivers use the TP for steering has become the target of much discussion, as will be described further below.

$$\rho = \frac{1}{R} \approx \frac{\Theta^2}{2y_l} \tag{2-1}$$

In further vision-based experiments, Land and Horwood (1995) used partial visual occlusion to determine what parts of the road are essential for successful steering. It was found that when driving at moderate to high speeds, in this case $16.9m/s$, successful curve negotiation requires both a near and a far segment of the road to be visible. Only showing the driver a distant part of the road resulted in a good match of the overall road curvature, but a poor performance in terms of lateral position in lane. Only showing a near region resulted in very jerky driving, but lateral position was better maintained. An intermediate view provided better performance than either of the previous, but at this speed the accuracy was 20% lower than when the entire road was visible. When driving the road segment at a lower speed of $12m/s$, accuracy was actually improved with only a near part of the road visible.

Eye movement tracking showed that driver tend to focus on a far part of the road segment, and use their peripheral vision to monitor the near segment. The findings support the two-level model of steering developed by Donges (1978).

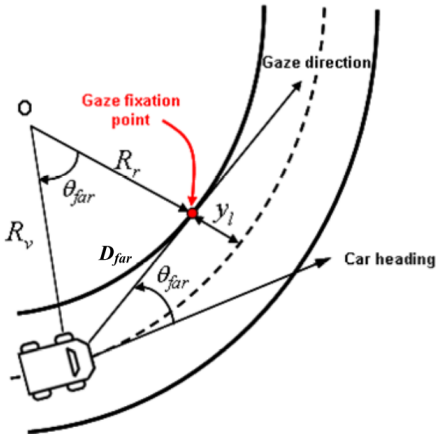

Figure 2-1: Relationship between the visual far point angle and the turn radius for curvature estimation purposes. (Sentouh et al., 2009a)

Boer (1996) developed a model that is instead based a target point that is adjacent to the TP, where no estimation of the actual road curvature is made. Instead, drivers use the distance $|T|$ to the target point and the angle Θ between the current vehicle heading and the target point direction to intermittently calculate the optimal curvature trajectory. Optimizing the trajectory means taking the path that generates the lowest lateral acceleration. This can be achieved either by lowering the speed or choosing the path with the lowest curvature. Since in this work the speed was kept constant, the model computes a maximum curvature path. This path predicts that drivers will steer to the opposite side of the curve direction before entering the turn, start their steering movements before the start of the curve, and come closer to the inner lane edge at the curve midpoint. Steering along this trajectory is guided by targets on the path that are intermittently updated. These targets lie next to the TP at a certain lateral distance into the lane that depends on the longitudinal distance $|T|$. The driver uses an internal model of the relationship between the steering wheel angle and the change in heading of the vehicle, and adapts the intermittence time to ensure that the vehicle does not exceed a maximum distance from the line between the driver and the target point before the next intermittent update. Experiments showed that driver appear to use a lateral acceleration minimization strategy, and that the model correctly predicts the anticipation time in steering into a curve and the distance to the lane edge at the curve midpoint. However, driver did not appear to steer in the opposite direction of the curve before entry, suggesting that they do not completely optimize their path.

Hildreth, Beusmans, Boer, and Royden (2000), used a slightly modified version of the model of Boer (1996) and compared it to a series of experiments that used visual occlusion to gain insight on the visual cues used for steering in lane correction maneuvers. The model was successful in reproducing the human steering behavior, even under complete occlusion periods of up to 2 seconds.

Salvucci and Gray (2004) note that the models presented by Donges (1978) and Land and Lee (1994) requires an accurate estimation of curvature, a task at which humans have been demonstrated to perform poorly (Fildes & Triggs, 1984). In these models, the inaccuracies introduced by the erroneous curvature estimation can be compensated by the closed-loop second level of steering. However, Godthelp (1986) showed that in general, drivers were able

to successfully steer around corners, even under a long visual occlusion of $1.5s$ that began just after the driver started a steering motion on curve entry. This indicates that it is likely that drivers to not attempt to judge curvature while negotiating a turn.

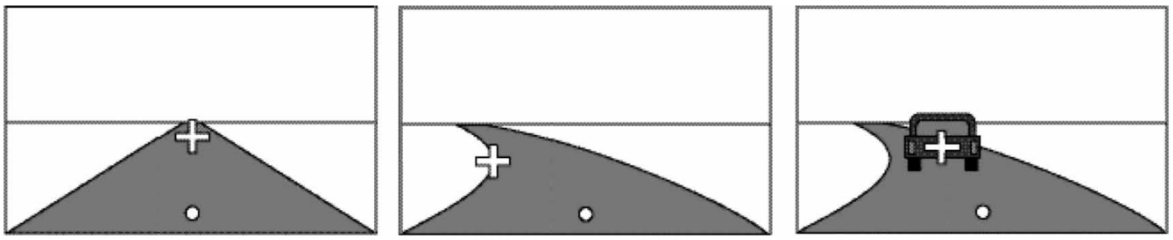

Figure 2-2: Near (circle) and far (cross) points for three different scenarios. (Salvucci & Gray, 2004)

This prompted Salvucci and Gray to develop an explicit two point model of steering, shown in figure 2-2. The near point represents the center of the lane at a close, fixed distance in front of the driver. This point is not necessarily fixated by the driver, but the necessary information is gathered through peripheral vision. The far point, on the other hand, can be any convenient point located somewhere ahead of the vehicle, from which lateral stability can be easily monitored. The TP of a curve is one of those scenarios, but so is the vanishing point of a straight road (left in the figure) or a lead vehicle (on the right side). The model can easily switch between different far points depending on the situation.

The model then attempts to keep both the near and far points stable, that is $\dot{\Theta}_{near} \approx 0$ and $\dot{\Theta}_{far} \approx 0$, and the near point in the center of the lane, $\Theta_{near} \approx 0$. No restrictions are placed on the far point location. In a validation experiment, the model was shown to accurately represent human steering behavior at a constant speed, even when only a small part of the road was visible. In addition, separately occluding parts of the road resulted in similar behavior as that observed by Land and Horwood (1995) in real driving.

One major issue with this model is that it does not contain a separate open-loop component that provides predictive steering, and is therefore not capable of reproducing steering behavior under total visual occlusion. The models of Donges (1978) and Hildreth et al. (2000) described above do show this capability, but the main advantage of the model by Salvucci and Gray (2004) is that is able to accurately reproduce human steering in a simple way, using only two salient visual features of the road ahead. Neumann and Deml (2011) provided further experimental proof that this model can reproduce human behavior, but also note that no conclusions can be drawn about whether the drivers actually use the TP as the far point, or in fact use any other point on the future path.

Sentouh, Chevrel, Mars, and Claveau (2009b) note that the models of Donges (1978) and Salvucci and Gray (2004) do not incorporate any modeling of how the driver uses kinesthetic information in the control of the steering wheel. This type of information is essential for models used for driver assistance systems, as explained in the following section. In order to remedy this, a new driver model was proposed that, like its predecessors, uses a two-level model for the driver's steering behavior but is augmented with a high-frequency compensatory part that uses kinesthetic feedback.

The developed model assumes the driver's preview behavior is guided by the TP of the curve, while visual compensatory control is achieved using the near point, a point on the center line

of the road a short distance ahead of the vehicle. The points are shown in figure 2-3. The vehicle dynamics model for lateral handling is a bicycle model that is extended to enable lane tracking and to model the feeling of the steering system. The outputs of this model are Θ_{far} (the angle between the heading direction and the curve TP), Θ_{near} (angle to the near viewpoint), both shown in figure 2-3, and δ_d (the steering wheel angle).

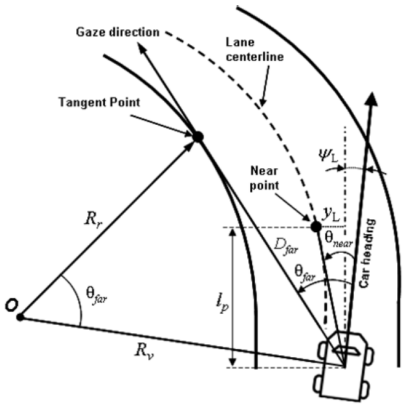

Figure 2-3: Preview information used in driving model. (Sentouh et al., 2009b)

The preview tracking is achieved by a simple gain K_a applied to Θ_{far}. The visual and kinestethic compensatory steering models are described by transfer functions with gains, and lead and lag constants in addition to the human inherent time delays for a total of 11 parameters to be identified. Using grey box identification on test track data, an 88% model fit to the the driver output torque of validation data was obtained.

van der El, Pool, Damveld, van Paassen, and Mulder (2015) developed a general model of the human controller in preview tasks, inspired by the well-known cross-over model for compensatory tracking developed by McRuer, Graham, Krendel, and Reisener Jr. (1965). While it is not specific to steering tasks, the conclusions drawn in this work agree with the two level model of steering, and help explain how the human uses the far and near region for steering control. The model was validated to show that the human controller uses two types of response: the far preview information is low-pass filtered and used for feedback control to track the low frequency component of the desired path, while the near information is high-pass filtered and used in feedforward control to account for high-frequency oscillations near the target. Interestingly, this corresponds well with the vision experiments performed by Land and Horwood (1995), which showed that when only the near region was visible to drivers, the control behavior oscillated very rapidly while maintaining an appropriate lane error. Only showing the far region resulted in accurate tracking of the low-frequency oscillations of the target, but with worse in-lane performance.

2-1-2 Where do drivers actually look

MacAdam (2003) notes that during driving visual cues are of the highest importance, accounting for 90% of the information used. In the previous section an overview of the preview models used in literature is provided, but they do not answer the question of where drivers look when they steer. This section provides a short overview of the current debate on what visual information is actually relevant for curve driving.

Since Gibson (1958) first postulated that humans steer by using certain properties of the optical flow field, a large body of work has been dedicated to discovering the way that humans perceive heading. The main idea is that by keeping the focus of expansion of the optical flow on a point that the observer wishes to travel to, the correct heading will be maintained. However, Wann and Wilkie (2004) mentions one big issue with this reasoning: the optical flow is only equivalent to the actual Retinal Flow (RF) perceived at the back of the eye when the observer has a stable gaze position. When a driver fixates on a point that lies on the side of the current path, as happens in curve driving, or moves his eyes while in motion, the heading direction is no longer clearly retrievable from the RF without using signals from other sources as corrections. In addition, Li and Warren (2002) proved experimentally that humans can control locomotion using only retinal information.

Using these arguments, Wann and Wilkie (2004) developed a model of visual steering control without recovering heading information. In this model, drivers fixate a point that they want to travel through while moving on a constant curvature path. If the vehicle speed is constant, then the change in the angle between the body axis and the direction of gaze, or Visual Direction (VD), will also be constant. One can imagine this as the fixating point rotating towards being straight ahead of the observer at a constant rate. If the gaze is fixated, RF can also provide steering cues. Points that lie on the Future Path (FP) of the trajectory will move vertically in a straight line towards the observer, as shown in figure 2-4 B. If a steering error is present, the flow lines will curve in the opposite direction of the error. This is shown in figure 2-4 A and C.

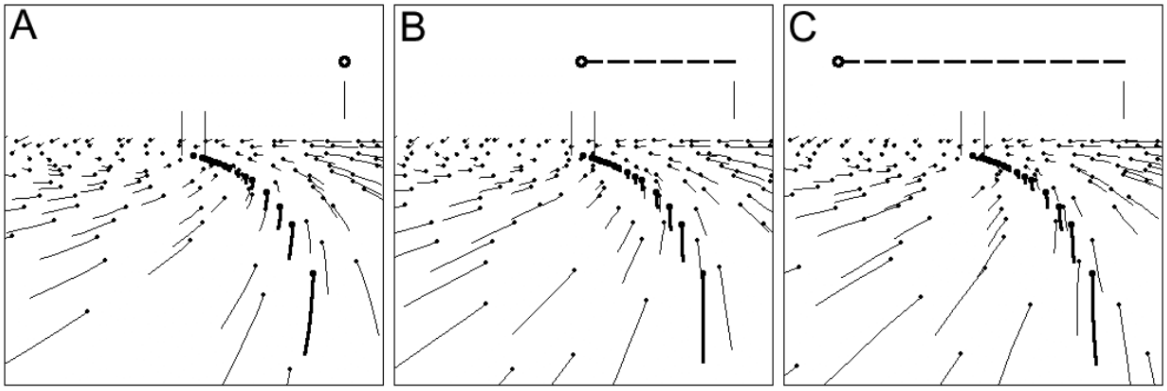

Figure 2-4: Retinal flow field for steering towards a target at constant speed. In all cases the initial heading is the same, and the observer fixates the same target. The circle indicates the current heading due to steering, making A an understeering situation, B correct steering, and C oversteering. (Wann & Wilkie, 2004)

Lappi (2014) provides an overview of the past 20 years of research into visual models of curve driving, focusing on studies of real driving. The starting point of most works has been the work of Land and Lee (1994), who introduced the concept of a TP on the inside lane edge that drivers use to guide their driving strategy. However, in more recent times this concept has been questioned with increased frequency, with many authors suggesting that drivers focus on points located on their FP instead.

Combining several previous studies, Lappi (2014) compiled a list of seven general principles of visual driving behavior in real driving:

1. Gaze behavior is repeatable for specific tasks, both withing and across subjects.
2. Gaze fixations are focused on points that are immediately relevant to the task at hand.
3. Each individual fixation has a specific functional role, even if that role is sometimes not clear on first analysis.
4. Each eye movement is linked to the information that a specific part of a task requires.
5. Drivers tend to minimize the use of short-term memory for their driving information, rather taking the required visual information from the scene as it becomes necessary. The use of short-term memory seems to increase with driver experience.
6. Skilled drivers show preview behavior by anticipation fixations to objects that will be relevant in future for short intervals in between the regular *just in time* fixations.
7. Humans integrate information obtained about the visual scene across saccades, allowing the use of a so-called *visual buffer* that allows for driving under short periods of visual occlusion. A saccade is a rapid involuntary eye movement that can be used to correct for drift of the retina during a tracking task.

In general, TP models assume that the the TP is the target of the driver's gaze, and the driver explicitly uses it as the source of preview information. On the other hand, FP models argue that the driver tracks a target point on the FP, using this point to obtain the preview information. One important note is that points on the FP are close enough to the TP that when focusing on them, they can still show TP *orientation*.

Most real driving studies of driver gaze behavior have clearly shown that drivers exhibit TP *orientation*, that is, drivers show the highest gaze frequency in an Area Of Interest (AOI) around the TP. However, as stated above and contrary to what most of these studies conclude, while this behavior does support the TP model, it does not contradict the FP hypothesis.

Both TP and FP models fall into two categories: steering point models and visual flow models. A steering point is a point that drivers use as a direct reference for steering, as opposed to using it to create a more complex mental model from which to retrieve steering references, as happens in visual flow models.

Itkonen, Pekkanen, and Lappi (2015) conducted a further experiment, measuring eye movements in a way that enables the differentiation of TP and FP behavior. The results clearly showed that when instructed to drive naturally drivers do not fixate the tangent point. In addition, when instructed to look at the tangent point during the curve, drivers where still able to successfully navigate their turn, but their gaze behavior was significantly different than in the natural condition. The authors recognize however that accurate models on where on the FP drivers look do not exist yet. Furthermore, gaze behavior on curve entry could not be analyzed using the same method, leading the authors to speculate on the possibility that TP information could be used in the approach and entry phase of cornering.

In conclusion, no consensus exists of yet on exactly where drivers look and what information is useful in cornering. Models that use either TP or FP information can, at this point in time, represent actual driving behavior with similar accuracy.

2-1-3 The importance of neuromuscular modeling

In addition to knowledge about how drivers perceive turns, Abbink, Cleij, et al. (2012) argue that for designing shared control it is essential to have information about the driver's Neuromuscular System (NMS) in order to reduce conflicts that can arise between the automation and the human. If the designed assistance torques do not correspond with the driver's neuromuscular behavior, any beneficial effect of the assistance system is eliminated and performance degrades.

In the driver model developed by Sentouh et al. (2009b), neuromuscular information is incorporated in the kinestethic compensatory feedback system. The driver's arms are modeled as a first-order transfer function. In addition, the way that the feedback torque from the steering column is received through the muscles and joints is modeled, as is the driver's compensation for this feedback. The diagram of this model is shown in figure 2-5. The near and far information, obtained according to the information in the previous sections, as well as the current steering angle, serve as inputs to the driver model.

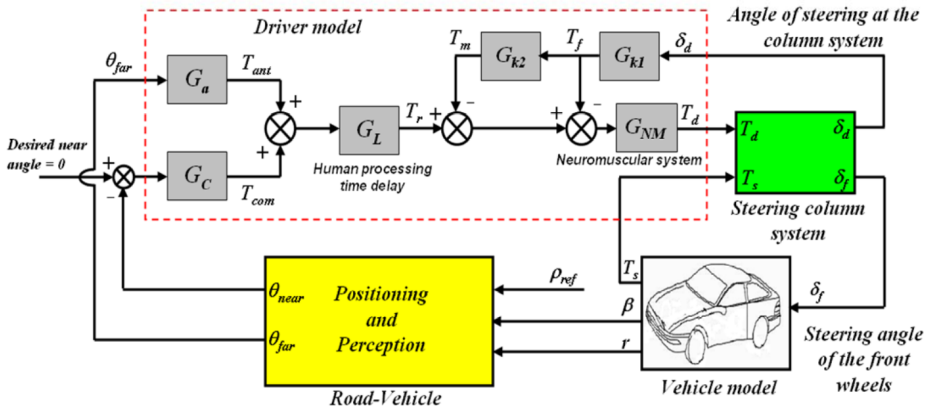

Figure 2-5: Road-vehicle-driver model structure, modeling the human driver as a combination of gains and time delays. (Sentouh et al., 2009b)

Cole (2012) provided a general description of how the human neuromuscular system generates motion. Muscles are activated by the alpha motor neurons, located in the spine. Usually, to start a movement the alpha motor neurons receive signals directly from the motor cortex in the brain. However, there is a second type of activation of the alpha motor neurons, called the stretch reflex. The muscles contain a type of fibers called muscle spindles whose primary function is to provide information about changes in length of muscles. A second class of motor neurons, Gamma motor neurons, can adjust the length of these spindles depending on the brain's expectation of muscle extension. When the actual length of the muscle differs from this expected length, the stretch reflex is activated. The stretch in the muscle spindle causes increase alpha motor neuron activity, resisting the stretching action in order to achieve the expected length. Even though there is still a lack of understanding about the precise function of the stretch reflex, it provides additional muscle stiffness at low frequencies down to zero.

In order to increase this understanding, Cole (2012) developed a driver-vehicle model to study the effects of steering torque feedback, including the dynamics of the arm and the brain's cognitive processing. In this application the vehicle is modeled using a bicycle model

on which lateral disturbance forces can act on three points: the center of mass, and the rear and front axles. Three separate cases were studied, as described below.

Initially, parameters for the driver neuromuscular dynamics were identified in tensed and relaxed states, without taking into account the cognitive path-following control, but including the human stretch reflex described above. The response of the different relaxation states to external disturbances when traveling in a straight line at constant speed were analyzed. Tensing the arm muscles increased the damping of the arms, while the stretch reflex increased their stiffness. When faced with the lateral disturbances, there was no significant difference between the relaxed and tensed states, but the reflex action was found to have an effect, depending on where the disturbance force was applied. The reflex behavior made the total vehicle dynamics behave more similarly to a system with fixed steering, while its absence lead to behavior more similar to hands-free steering.

Then, a path following controller was implemented to model the generation of the alpha and gamma motor neuron signals by the brain. This controller included a cost function that allowed for a tradeoff between the accuracy of the path-following and the amount of control activity. The effects of including the steering wheel feedback torque that arose from the contact of the front tires with the road was evaluated. It was found that when accuracy was preferred, there was no difference between the condition including feedback and the condition without. However, when the focus shifted towards minimizing control activity, steering torque feedback was found to reduce the response bandwidth of the path-following response. This occurs because when there is steering feedback, muscle activation is needed to counteract it. Since the aim is to reduce control activity in detriment of accuracy, the controller will naturally sacrifice accuracy, leading to a smaller bandwidth. The tensed or relaxed state, and the presence of the stretch reflex or a cognitive delay had little to no influence on the results. When reacting to a disturbance, the presence of torque feedback, stretch reflex, and cognitive time delay were all shown to have strong effect on the lateral displacement response of the vehicle. The tensed or relax state had no significant influence.

Finally, the influence of torque and angle overlays on the pinion of the steering system, as used in many assistance systems, on the neuromuscular system was studied. For both cases, a unit step overlay was introduced and the effects analyzed. The inclusion of steering torque feedback was found to reduce the disturbing effect of both overlays, while the stretch reflex reduced the effect of the torque overlay, but increased the effect of the angle overlay. An experiment in a driving simulator was performed where drivers were instructed to drive a straight path, with step angle overlays occurring at random times. Furthermore, drivers where told to either tense or relax their arm muscles in advance of the occurrence of the overlay. The results of this experiment were consistent with the prediction made by the model including the stretch reflex. In addition, the subjects instructed to contract their arm muscles showed a stronger reflex response than the relaxed subjects. However, this experiment showed a large variability, both between and within subjects.

Benderius (2014) also conducted a simulator experiment on the human stretch reflex, in this case with distracted drivers in a head-on collision situation. Just before the collision, an assistance torque intended to help avoid the obstacle was applied to the steering wheel. It was found that both the driver's stretch reflex and a cognitive mechanism of distracted drivers actively opposed this assistance torque, resulting in a larger amount of collisions. This led the author to question the usefulness of steering wheel torque interventions in the case of

distracted drivers.

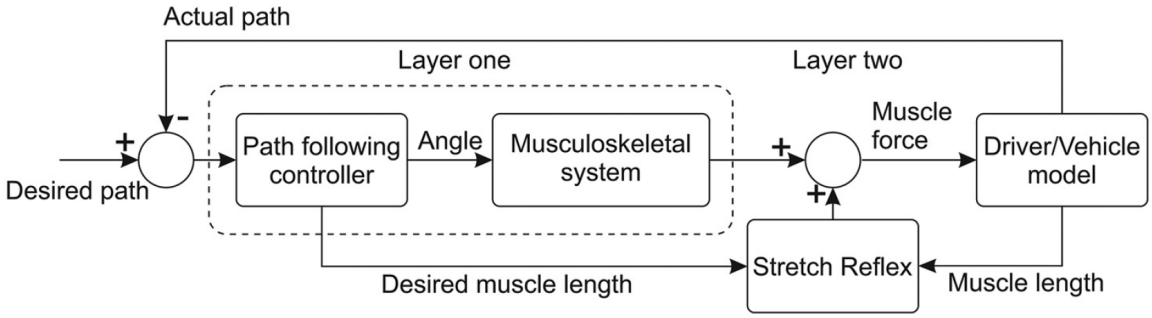

Figure 2-6: Neuromuscular driver/vehicle model structure. (Mehrabi et al., 2014)

Mehrabi, Sharif Razavian, and McPhee (2015) developed a complete 3D model of the human arm, including 15 different muscles, for use in research on steering assistance systems. The model was experimentally validated using electromyography of a driver's arm while using a driving simulator. The general structure of the model is shown in figure 2-6 (Mehrabi et al., 2014). The model consists of three fundamental parts. The first level is the path planning module, that results in the necessary steering angle for the vehicle to achieve the desired path. This is implemented as a Model Predictive Control (MPC) controller that uses a simple internal vehicle model to find the optimal steering wheel angle. The second part consists of the model of the arm, that generates the necessary muscle activations that result in the steering angle from the path-following module. This is achieved by minimizing the steering wheel angle tracking error. Since the arm is a highly redundant system, an extra criterion of minimizing some form of muscular effort like fatigue or used force in added. In order for the model to be able to predict what the optimal muscle actions will be, the kinesthetic system is modeled as an observer that estimates the arm positions and the expected torque on the steering wheel. Finally, the last level describes a stabilizing function characterized by the stretch reflex, which involuntarily compensates for external disturbances or errors in the internal models of the driver.

Based on this, Mehrabi et al. (2015) performed an experiment to investigate the reaction of the model to a one second step torque overlay disturbance on the steering wheel during a lane-change maneuver, with the driver model in relaxed and tensed condition. In the relaxed state, the observer does not detect the disturbance in time to react the it before it ends, while when tensed the model attempts to reject the disturbance and follow the same path as taken without any disturbances. The stretch reflex acts before the voluntary correction has time to exert any force in both situations.

Finally, one essential thing to note is that the studies mentioned in this section all have one thing in common: they do not mention the Golgi Tendon Organ (GTO) reflex. This mechanism is often described as the opposite of the stretch reflex, and is essential for the effectiveness of HSC (Abbink & Mulder, 2010). Just as the muscle spindles measure muscle length, the GTO measure the force on the tendons (Smisek, van Paassen, Mulder, & Abbink, 2013) and relax the muscles in case the tension becomes too large for the tendon to bear. This reflex action can be exploited for the uses of HSC, as described by Abbink (2006) for application to a haptic gas pedal in a car following task. In this work, Abbink describes

that when drivers agree with and/or trust in the assistance provided, they will increase their admittance, that is, they will intentionally give way to the assistance forces provided.

2-1-4 Motor primitive based models

In recent times more attention has been devoted to linking steering behavior with natural human movements. Flad, Trautmann, Diehm, and Hohmann (2013) developed a driver model that switches between elements of a set of fundamental building blocks, or motion primitives, to describe the neuromuscular steering behavior as a grey-box model.

Building on the current state of the art of human movement control, the model describes a finite set of patterns for the neuromuscular system during steering, called *movemes*, that have the steering wheel angle as output and do not take any input. Each *moveme* can be described by a state-space model of the form $\dot{x}_p(t) = A_i x_p(t) + b_i$, where x_p is the state vector that contains the steering wheel angle δ and $\dot{\delta}$. Only $\{A_i, b_i\}$ differ for each *moveme*, and these parameters are driver-specific and obtained using an identification process described in Diehm, Maier, Flad, and Hohmann (2013).

A switching mechanism activates the correct *moveme* to achieve the steering behavior desired by the higher level cognitive systems of the driver. Flad et al. (2013) described the switching mechanism using a MPC framework, relying on the driver's internal models of the collection of *movemes* and of the vehicle's lateral behavior. These models are used to determine the ideal trajectory for a finite time horizon T_s, and after a time T_c within this horizon, the trajectory is re-calculated. The objective function used has as main goal the minimization of the lateral deviation from the intended trajectory, but also includes: the error in the vehicle yaw angle, weighed more heavily by experienced drivers; the number of *moveme* switches, which allows for the reproduction of human error neglecting behavior until a certain maximum is reached; and the steering wheel rate, as a measure of driver comfort.

A real driving experiment was performed with 6 participants, on a lane change and a slalom course at a fixed speed. The Root Mean Square Error (RMSE) of the lateral position in lane varied from $0.047m$ to $0.080m$, while the errors of the steering wheel angle were in the range of 5.3 to 10.3 degrees. The performance of the model was best when the set of individually identified *movemes* for each driver was used, but it was also shown to be possible to use *movemes* from a different driver to achieve worse, yet acceptable results. In addition, the model was used to predict the future steering behavior for prediction times up to 12 seconds, by increasing T_s and not recalculating the predictions after T_c. After this prediction time, the lateral position error for the median driver was $0.023m$, showing that the model can accurately predict human steering behavior even at moderately long prediction times.

Inga, Flad, and Diehm (2015) argued that practical application of the MPC framework is not ideal due to the high computation times involved. Instead, a Hidden Markov Model (HMM) was used to switch between *movemes*, yielding the probability that the driver will each *moveme* in the current driving situation.

Using a similar philosophy, Benderius and Markkula (2014) analyzed a large volume of driving data in an effort to show that drivers' control of the steering wheel follows the same kind of pattern as human reaching movements. More specifically, this means that there is a linear relationship between the steering wheel rate and the the corresponding steering wheel deflection, resulting in a bell-shaped pattern of steering rate over time, as shown in figure 2-7. In

addition, these patterns can be used as motor primitives to describe more complex steering movements. Most steering movements were explainable by bell-shaped rate to time relationships. The movements that were not covered by one such pattern could be explained by superimposing multiple patterns. This leads to the conclusion that driver steering correction behavior might not be governed by a continuous closed-loop control model, as most previous literature shows, but instead by many short bursts of open-loop control. Gordon and Zhang (2015) also found evidence that steering behavior in lane-keeping tasks follows a pulse-like behavior, and developed a model that accurately fit experimental data.

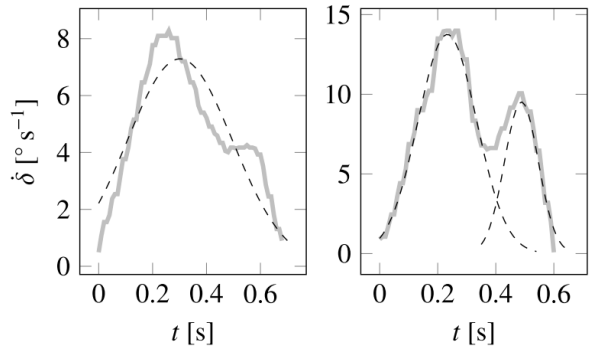

Figure 2-7: Typical patterns of steering rate over time for steering movements, both in real world and simulated driving. (Benderius & Markkula, 2014)

Since the introduction of the concept of a remnant by Tustin (1947), it has been considered as a type of neurological noise or error signal that almost all developed models cannot account for. By explaining steering as a type of reaching behavior, Benderius (2014) showed that the error resulting from the remnant can be eliminated. In this work, reaching incorporated in a satisficing rather than optimizing behavioral framework, which is considered more realistic for human movement.

With regards path planning, it was found that the two-point model proposed by Salvucci and Gray (2004) performs well in predicting steering behavior. However, this model suffers from parameter redundancy, that is, the same behavior could be explained by multiple parameter sets. This model uses a near and a far aim point that driver use to guide their steering. Benderius (2014) argues that this is redundant, and that the two points can be replaced by an egocentric reference frame and a single aim point angle. This angle can be described as the angle between the current vehicle heading and the driver's desired angle. The driver uses near field visual information, gathered primarily through peripheral vision as described by Land and Horwood (1995), to generate the reference frame. In this way, a near point is no longer used explicitly, decreasing the number of model parameters.

The above arguments on steering wheel control and planning behavior are combined in the *aim point correction model*, which contains four tunable parameters, of which only one is driver-dependent. This parameter is modeled as a gain k_s that describes both the driver and the urgency of the situation. The other parameters are the aim point $P_a = (x_a, y_a)$, the reaction time t_r and the sensation threshold T_s. The model seeks satisficing behavior by providing steering corrections triggered by the driver's sensation of the aim error $\eta(t)$ going above a certain threshold T_s at the correction start time t_{0_i}: $\eta(t_{0_i}) > T_s$. In addition, the driver only starts a new correction when he is able to react to the previous one, that is, when

$t_{0_i} > t_{0_{i-1}} + t_r$. The driver's sensation of the aim point error is defined as $\eta(t) = k_s(t)\psi_\epsilon - \delta_t$. Here δ is the current steering wheel angle, and ψ_ϵ is the aim error described by equation (2-2), where y is the lateral offset of the driver, and ψ_h is the current heading of the driver.

$$\psi_\epsilon = \arctan\left(\frac{y_a - y(t)}{x_a}\right) - \psi_h(t) \tag{2-2}$$

The output of the model, the current steering wheel rate, is then defined as the sum of all applied steering corrections, $\dot{\delta}(t) = \sum_{i=1}^{n} \dot{\delta}_i(t_i)$. Each steering correction $\dot{\delta}_i(t_i)$ is described by a bell-shaped profile as shown in equation (2-3). $\dot{\delta}_m = k\eta(t_{0_i})$ is the maximum steering wheel rate, and $t_i = t - t_{0_i}$ is how much time has passed since the start of the correction. The constants k, b, and σ were determined in Benderius and Markkula (2014).

$$\dot{\delta}_i(t_i) = \dot{\delta}_m \exp\left(-\frac{(t_i - b)^2}{2\sigma^2}\right) \tag{2-3}$$

The model was able to accurately reproduce human driving behavior in three different scenarios: a double lane change, a head-on collision scenario, and a lead vehicle braking scenario. In addition, it was able to reproduce the high-frequency peaks that previous models attributed to the remnant. Work still remains to be done in proving that the model behaves well in a routine cornering scenario. In addition, Benderius does not explicitly define the methods for selecting an aim point, and indeed this is still the source of many questions in other literature. However, it is assumed that any salient point in the driver's desired path can be used as an aim point, and the aim point can change depending on the developing situation.

The biggest issue concerning this model is that it only provides steering angle, and not the torque on the steering wheel. In order for it to be applicable to HSC it is essential to add a model of the steering system, including the torque feedback resulting from the interaction of the driver with the vehicle.

Kolekar (2016) developed a driver model, based on the principle of steering as reaching, that is capable of accurately capturing steering wheel torque in both routine and emergency scenarios. The model uses optimal feedback control, incorporating the driver's internal model of the task and preview information In addition, the model captures the inherent variability of human steering behavior by modeling the signal dependent noise present in perception and motor actions. Interestingly, this model is described as a generalized version of the model of Benderius (2014) that incorporates closed-loop corrections.

2-1-5 HSC applications

While there exists a large body of work on driver modeling, and many of these models mention their usefulness for implementation in shared control, actual implementations of these models in a curve driving HSC environment are few in literature.

In Boink, van Paassen, Mulder, and Abbink (2014) and previous related works, a very simple model that attempts to minimize the lateral error to the center line at a certain look-ahead time is used, which results in significant conflicts between the driver and the assistance system.

Saleh et al. (2013) describe a shared control system based on the two-point driver model of Sentouh et al. (2009b) described previously, including neuromuscular information. This systems showed benefits of approximately 15% in reduction of the risk of lane departure, and a reduction of the mean deviation to the center line of almost 30%. The authors note that driver-dependent factors, including speed, could be the cause of the conflicts of the driver with the assistance torques that occurred during 20% of the driving time.

2-1-6 Conclusions

In the above discussion, it has become clear that for the generation of an appropriate reference for HSC, a model needs be able to accurately capture both the driver's intention, and the way that this intention is translated into actions.

In terms of driver intention, that is, the manner in which drivers interpret the available information in the visual scene and relate it to their goal, it has become clear that it is essential to include preview and compensatory modes. Section 2-1-2 shows that literature agrees that visual information is obtained through the observation of visual angles. Since current literature has not yet provided a definitive conclusion on whether TP or FP is the source of preview information, the choice was made to use the angle to the TP due to the ease of identifying it for any corner. In the work of Salvucci and Gray (2004) it is clear that any salient point in the scene can be used as a source of preview information, and the TP is unmistakeably such a point. The compensatory information is used to stabilize the steering behavior on the desired path to the far point. The ideal choice for this is the center of the current lane at a certain preview time ahead, since this provides a simple access to information about the current in-lane error. This means that the models to use for evaluation changes with speed should at least be partially based on the two-point approach of Salvucci and Gray (2004).

Two completely distinct approaches to modeling the actions of the driver have been discussed: either by modeling the neuromuscular system as a series of gains and time-delays, or by treating steering as an equivalent to the human reaching task, either as a sum of open-loop corrections of by applying optimal preview control. Both of these approaches have their merits: the first one provides clear parameters that can help understand and identify the consequences of speed changes, while the second one is able to capture the variability and satisficing behavior properties of human steering. It is therefore interesting to find out what differences will arise when applying both models in variable speed scenarios.

The model proposed by Sentouh et al. (2009b) and Saleh et al. (2013) combines a two-point visual model with a model of the neuromuscular system, making it an ideal candidate for further analysis. A slightly modified version of this model, to account for speed variation (Saleh, Chevrel, Mars, Lafay, & Claveau, 2011), was implemented in simulation. Results and further discussion on this will be presented in chapter 3.

In terms of steering as reaching, the simplicity of the open-loop model of Benderius (2014) shows much promise, but before any implementation can be considered it must be augmented with a model of the interaction of the human with the steering system and the road, in order to be able to generate steering torques instead of angles. Kolekar (2016) developed a model that uses optimal preview control to model steering as a closed-loop reaching tasks. Due to

time constraints it has not been possible to implement this model in simulation, but it will surely be the focus of further research.

2-2 Curve speed choice

Having described steering at constant speed, we now wish to know how this behavior changes with speed. However, when talking about changes in corner driving behavior with speed, it is important to first know how speed actually varies in corners. That is the question that this section aims to answer.

The speed choice of drivers is influenced by a multitude of factors, but in general drivers tend to lower their speed in preparation for upcoming turns in some way. Lechner and Perrin (1993) convincingly showed that the actual behavior of humans lies far below the dynamic capabilities of the vehicles they drive. Over the years, many different models have been developed in order to explain the choices drivers make. In general, these models can be divided into two general categories: those that are based on maintaining a certain margin of error, and those based on observed human motion behavior.

This section will begin by providing an overview of studies providing data about curve speed, as a general observation of driving behavior. Then, an overview of models based on safety margins is presented, followed by an explanation of models based on human movement control. The sections finishes with a short overview of the importance of including neuromuscular information in speed control models.

2-2-1 Speed adaptation in naturalistic driving

In literature, driving velocity data is mostly collected in two ways. It is usually related either to road curvature, taking into account more or less of the road's other geometric features, or to the corresponding vehicle lateral acceleration.

The bulk of the research of driver speed choice against road curvature is in the field of roadway design and road safety. Velocity is recorded in road curves and compared to radius, in an attempt to obtain a velocity profile, or in many cases only the 85th percentile of the speed profile. While this application is quite different from the field of driver assistance systems, the obtained data is useful in order to obtain a first idea of how fast drivers corner, and for comparison purposes with simulator data.

Studies such as Turner, Woolley, and Cairney (2015), Bosetti, Da Lio, and Saroldi (2013), Shino, Yoshitake, Hiramatsu, Sunda, and Kamata (2014), Cafiso and Cerni (2012), among others, showed that in general, corners with small radius are taken at low speeds. Speed increases in a curvilinear fashion with radius, sharply up to radii of approximately $100m$. In the range of radii from $200m$ to $300m$, the slope of this variation begins to decrease, and above radii of approximately $300m$ the speed stops varying with radius. Figure 2-8 shows this variation in a double log-scale plot, using data obtained on real roads in Italy (Bosetti et al., 2013). The horizontal line on this plot corresponds to a curve radius of $300m$.

There are a large amount of conflicting theories on what visual information drivers do use for evaluation and predicting future curves, but there is a consensus that humans have some

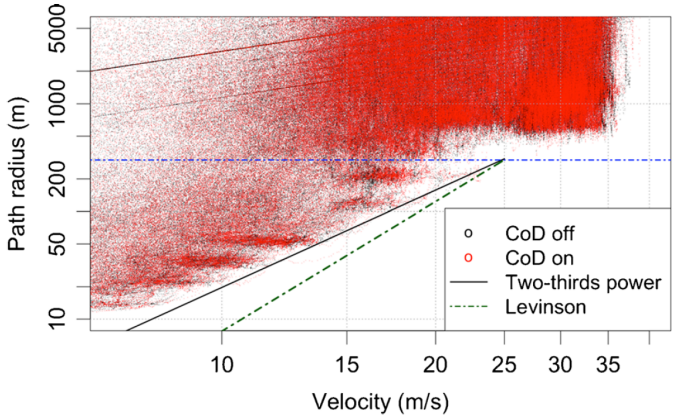

Figure 2-8: Logarithmic variation of longitudinal speed with curve radius from naturalistic driving data. (Bosetti et al., 2013)

way of predicting a margin of safety that they must keep to safely negotiate a turn. Lechner and Perrin (1993) argue that longitudinal speed, lateral and longitudinal accelerations, and steering wheel movements are the most relevant parameters for collecting data on curve driving.

Ritchie, McCoy, and Welde (1968) were among the first to investigate the relationship between lateral acceleration and longitudinal speed, and data on this has been collected by many studies since. Figure 2-9 shows this relationship for driver data obtained on public roads. The maximum lateral acceleration increases with speed up to a velocity of approximately $10m/s$, after which it decreases again. This shows that at low speeds drivers tend to allow larger lateral accelerations than at high speeds. In this figure, the dotted and dash-dotted parabolas represent the lateral acceleration that a vehicle would produce while taking a turn with a constant radius of $10m$ and 600m respectively. These lines make it easier to distinguish the two different behavior regions mentioned above. The points under the second parabola clearly point to these trajectories being driven at constant speeds, while for the points above it show a trade-off between the two variables. The maximum lateral acceleration presented in this figure agrees with the $0.5g$ maximum limit of lateral acceleration on rural roads found by Lechner and Perrin (1993), and with a majority of the lateral acceleration studies performed up to this point.

A majority of the examined works assume that speed is constant in corners, and deceleration occurs entirely on the straight sections tangent to curves. This is a very useful assumption for modeling but, in a study using GPS data on public roads, Pérez Zuriaga, García García, Camacho Torregrosa, and D'Attoma (2010) found that at least 7% of deceleration occurs in the curve. These findings were confirmed by Montella, Pariota, and Galante (2014), who performed a study with 39 subjects driving an instrumented vehicle, and found that approximately half of the observed decelerations continue into the curve. The percentage of deceleration within the curve increases with radius, but interestingly all but 4% of the decelerations ended before reaching the middle of the curve.

Seemingly in contrast to this, the data of Lechner and Perrin (1993) and Bosetti et al. (2013), among others, show that in most situations, drivers tend to avoid combining longitudinal and lateral acceleration, especially when decelerating. This results in a mushroom-shaped

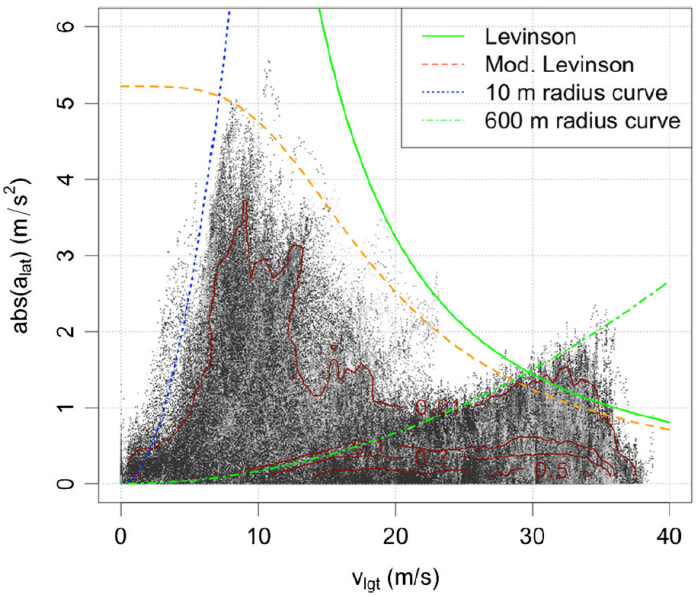

Figure 2-9: Relationship between longitudinal velocity and lateral acceleration in naturalistic curve driving (Bosetti et al., 2013)

g-g plot as shown in figure 2-10 (Bertolazzi, Biral, Da Lio, Saroldi, & Tango, 2010). This apparent difference can be explained by the fact that drivers tend to cut corners, approaching the middle of the turn in a trajectory that is as straight as possible (Mars, 2008). This results in deceleration behavior with low associated lateral acceleration occurring within turns. In addition, when dividing the data into the regions of low and high curvature described above, the considered studies show that the trajectories associated with low curvature roads are the ones where lateral and longitudinal acceleration are more frequently combined.

Moon and Yi (2008) analyzed driver's longitudinal acceleration limits in car-following driving, and concluded that 90% of the observations were in the range of -1.03 to $0.91 m/s^2$. Bosetti et al. (2013) performed a similar analysis for curve driving, and found comparable results, with a range of -0.89 to $0.96 m/s^2$ for the same percentage of observations.

Having discussed and found trends in the data available in literature, it is time to move on to the state of the art of curve driving speed models. The next two sections will provide a comprehensive overview.

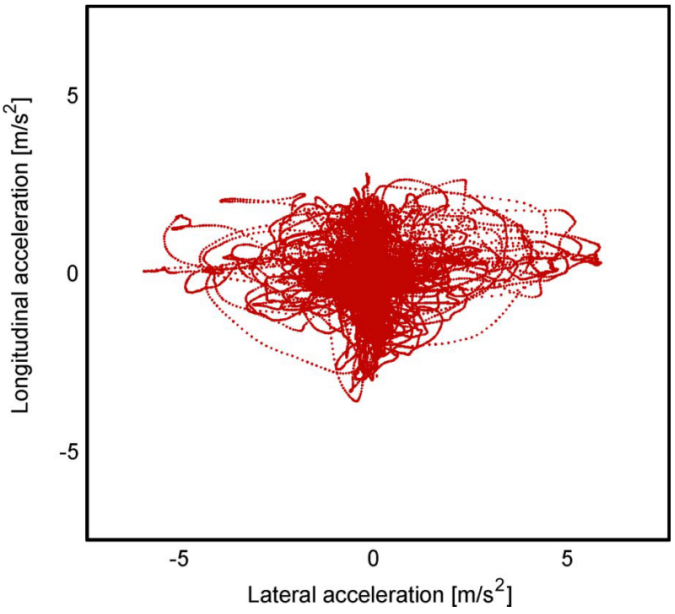

Figure 2-10: Typical g-g diagram for a driver faster than average on public roads. (Bertolazzi et al., 2010)

2-2-2 Models based on safety margins

In the context of road design and road safety, many models exist for the speed at which a driver can safely negotiate a turn given the geometrical characteristics of said turn. While this is a useful limit for assistance systems to take into account as an upper boundary, it does not provide information about a driver's desired speed. Therefore, as argued by Zhang, Xiao, Wang, and Li (2013), it is not directly usable for the design of assistance systems. In this work the focus lies on how the drivers themselves choose a speed, depending on their own preferences of driving style, risk, or safety margins. To this effect, this section summarizes previous research on drivers' speed selection for cornering.

Many studies since, and including, Lechner and Perrin (1993) have shown that human speed choice behavior is, in general, divided into two large categories. These categories depend on the type of road: motorway-like wide roads with a central divider and large ($\sim> 300m$) curve radii, and two-lane roads with small curve radii. Curves of large radius are usually taken at constant speed, that is, drivers do not need to adapt their speed to the turn and behave like they would on straight road segments. On the other hand, on country roads with tight curves drivers perform some sort of tradeoff between speed, comfort and lateral error.

Bosetti et al. (2013) speculate that drivers still perform this tradeoff on motorways, but prefer higher speeds due to the larger lane widths and an increase in perceived safety. However, this hypothesis could not be proved as in their data no drivers drove fast enough to necessitate tradeoff, and therefore all drivers took motorway curves at constant speed. Shino et al. (2014) and Shao, Xu, Li, and Yang (2015) also noticed that drivers tend to switch to a constant speed driving mode as the curve radius increases, for any type of road. Takahashi and Akamatsu (2012) go as far as only considering road sections with radii smaller than $300m$ as curves.

The remainder of this section focuses on curves for which drivers do need to adapt their speed. As seen in the previous section, when curve radius decreases, so does speed. Many different explanations have been offered for the manner in which humans adapt their speed to corners, but the consensus is that some form of tradeoff between a lateral safety or comfort margin and longitudinal speed occurs.

Ritchie et al. (1968) were one of the first to investigate this tradeoff. In a driving study with 50 subjects it was shown that as lateral acceleration increases, longitudinal speed decreases. This lead to the conclusion that drivers mainly use the lateral force as a cue to decide how fast to take a corner. Herrin and Neuhardt (1974) found similar results for drivers on unfamiliar roads.

Godthelp and van Winsum (1996) argue that this relation is a result of the driver's effort to minimize steering errors. Sharper curves or lower steering competence will increase steering errors, and drivers compensate for this by reducing their speed. In order to achieve this regulation, drivers strive to keep a constant Time to Line Crossing (TLC). The TLC represents the amount of time it will take for the vehicle to cross the edge of the current lane, if the control inputs remain constant.

Speed is traded off with curve radius and steering competence in order to keep a constant TLC, independently of these two parameters. Experimental results agreed with this hypothesis. In addition, both drivers with low and high steering competence were found to maintain the same TLC safety margin, with the former lowering their speed to achieve this margin. Conversely, drivers with a higher steering competence showed less steering error, and drove faster.

The TLC hypothesis was tested by simulation by Reymond, Kemeny, Droulez, and Berthoz (2001), using a model based on Godthelp and van Winsum (1996). In the experimental data collected by Reymond et al. the maximum lateral acceleration decreases much more with speed than in the TLC based simulated model. It is important to note that this experiment, which occurred on a closed test track without other traffic, showed maximum lateral accelerations in the order of $6 - 7m/s^2$, while other experiments performed on public roads (Bosetti et al., 2013; Levison, Bittner, Campbell, & Schreiner, 2002) do not exceed $\sim 4m/s^2$.

Since the TLC model did not accurately represent the experimental results, a new model was developed from the idea that drivers' speed choice is based on adjusting a safety margin in lateral accelerations. Therefore, before entering a curve, the driver will adjust the speed in order to stay below a certain value of lateral acceleration. This maximum value Γ_{max} depends on the driver. The driver also uses a safety margin for the path curvature deviation ΔC_{max}, in case of errors in steering, obstacles, or other deviations. At slow speeds, the lateral acceleration is limited by physical factors such as the maximum steering angle δ_{max}, and the wheelbase of the vehicle, L. The resulting envelope for the maximum lateral accelerations is shown in figure 2-11 (Reymond et al., 2001). The results of the driving experiment are shown to fit in this envelope.

Reymond et al. note that since the experiment was performed on a closed test track, the lack of traffic and other uncertainties of driving on public roads can influence the choice of Γ and ΔC. Bosetti, Da Lio, and Saroldi (2015) adapted these parameters to their results and obtained an acceptable fit.

On the other hand, Shino et al. (2014) used the same TLC model as Reymond et al. (2001), and confirmed experimentally that TLC is independent of curve radius for small radii. As the

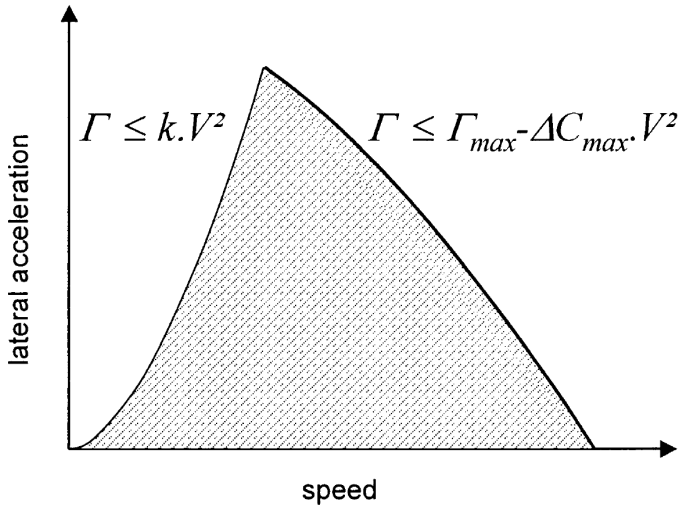

Figure 2-11: Lateral acceleration envelope obtained from model. (Reymond et al., 2001)

radius increases, the curve segments becomes more similar to a straight road, and the speed approaches a constant value. This means that, as seen before, the speed choice model is no longer valid. At radii under $200m$ the model was shown to be a good fit.

2-2-3 Models based on human movement control

In human motion a relationship between velocity and curvature exists: the speed of the movement is related to the path curvature as described in equation (2-4), where v is the tangential velocity, C the path curvature and α is a velocity gain factor. This relationship is called the two-thirds power law, as described by Flash, Meirovitch, and Barliya (2013).

$$v \leq \alpha C^{-\frac{1}{3}} \tag{2-4}$$

Humans tend to produce smooth trajectories in their movements. Investigating this led to the development of the minimum-jerk principle, described by Viviani and Flash (1995). This model states that in order to determine a trajectory, humans select a combination of motions from the multitude of possible motor primitives that minimizes the jerk in the movements. Flash et al. (2013) showed that in description of hand tracing of ellipses, the minimum jerk trajectory shows an exponent that is practically indistinguishable from the one used on equation (2-4).

Bosetti et al. (2013) found that these same principles also apply for humans driving cars around turns. They argue that vehicle control is simply a particular case of human movement control, and that the relationships between lateral acceleration and speed described in previously are analogous to the two-thirds power law. When driving through curves, the minimization of steering errors described by Godthelp and van Winsum (1996), or the acceptable path curvature variance described by Reymond et al. (2001), are illustrations of the minimum jerk model of human movements.

Bosetti et al. (2013) and Bosetti et al. (2015) describe an experiment with 24 subjects on public roads in Italy, where the obtained data is compared to the two-thirds power law, the model developed by Levison (2007), and the model and results of Reymond et al. (2001) described above. This comparison is shown in figure 2-12. (Bosetti et al., 2015)

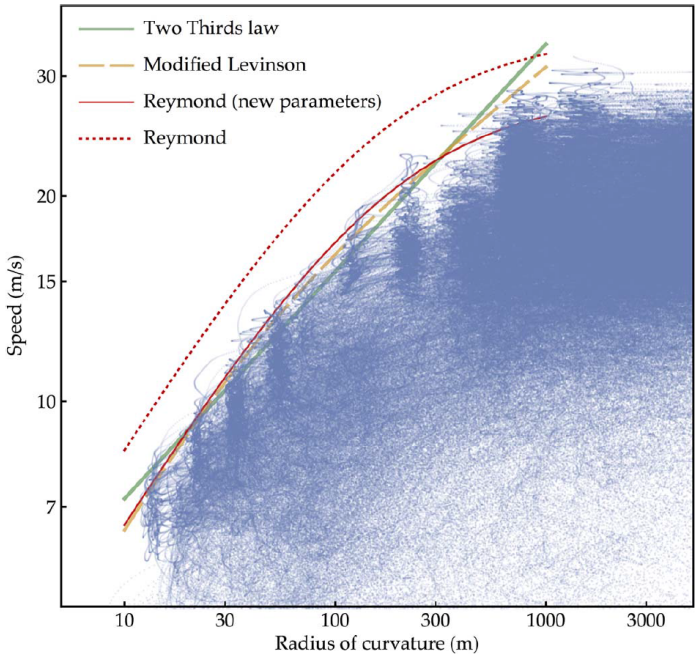

Figure 2-12: Comparison of three curve speed choice models to experimental data. (Bosetti et al., 2015)

The two-thirds power law with $\alpha = 3.70m^{2/3}/s$ proved to be a very good fit to the obtained data. Levison's original criterion is a worse fit than the two-thirds power law. The authors developed a new criterion that is asymptotic to Levison's but models the low speed behavior better. This modified Levison's criterion is shown in equation (2-5), where C is the path curvature and a_0 and v_0 are fitting parameters that describe the data. This model was found to be only a slightly better fit to the experimental data than the two-thirds power law, by describing a slight deviation from a straight line shown by the data.

$$v \leq v_0 \sqrt[4]{\sqrt{\frac{a_0^2}{C^2 v_0^4} + \frac{1}{4}} - \frac{1}{2}} \tag{2-5}$$

Reymond's model does not fit the obtained data. The experimental data on which it is based is very different to Bosetti et al.'s data, having much higher maximum lateral accelerations. As mentioned above, this is most probably due to the fact that the experiment was performed on a closed test track. By adapting the parameters to the new data however, an acceptable fit can achieved. This model also captures the constant speed part of the data at higher radii, but this straight line behavior can also be explained by the fact that it occurs at approximately the legal speed limit.

2-2-4 Neuromuscular dynamics of gas pedal use and HSC applications

As mentioned for the steering task, driver models for use in HSC should also be able to explain the interactions between the human and the control surface through models of neuromuscular behavior. However, as opposed to the steering task, there is not a large amount research into the neuromuscular dynamics of gas and brake pedal use for speed adaptation.

Abbink (2006) provides a comprehensive overview of the dynamics of the human leg when actuating a gas pedal in a car following task. The developed model relates the inverse of the Time To Collision (TTP) to the lead vehicle to forces on the gas pedal. An assistance system based on this information was shown to decrease the workload of drivers in car-following tasks by making the driver adopt a force-task strategy. Mulder, Mulder, et al. (2008) showed that driver prefer stiffness feedback to force feedback during the car following task. Jamson, Hibberd, and Merat (2013) developed an assistance system based on the work of Mulder, Mulder, et al., adapting the haptic gas pedal for eco-driving. Their results showed that a force-feedback task was preferred when the target is a set speed. The design of a similar system to provide information about the criticality of the cornering task is certainly an interesting future research topic.

Park and Sheridan (2004) studied the dynamics of the braking task and found many similarities with the open-loop reaching task, where the initial braking motion is described as a pre-programmed motion that does not rely on any closed-loop feedback until after the initial force is applied. Building on this notion, they developed a model of the braking system as a teleoperator, extending it to a system that detects lower grip areas of the road and softens the impedance of the brake pedal to ensure full ABS activation in these conditions. For most drivers this improved their perception of the road, allowing them to judge the available grip for braking more effectively.

2-2-5 Conclusions

In literature, a large collection of models explaining human speed adaptation exist. The vast majority of these models are simply based on fitting the data, and are used in roadway design. While they can capture the variation of driver speed with a large variety of road features, they do not attempt to explain how a driver actually uses this information, and the model parameters do not provide significant insights into driver behavior.

It must be noted that all the described models require an estimation of curvature. While the relationship between curvature and speed is certainly interesting in order to discover patterns of driving behavior, humans are notoriously poor judges of road curvature (Fildes & Triggs, 1984). Due to this, a realistic model of human speed choice cannot require the estimation of road curvature. In the examined literature, no models were found that do not require it. One promising approach to solve this problem is to use the Extended Tangent Point (ETP), which is the point at the intersection of the visual line that passes through the TP with the lane boundary on the opposite side, as shown in figure 2-13. The angle between the visual direction on the road boundary at the ETP can provide valuable information about how much the curve opens up and subsequently about what speed is required to safely negotiate the corresponding turn. However, this approach has not yet been confirmed by published experiments, and therefore further research is necessary.

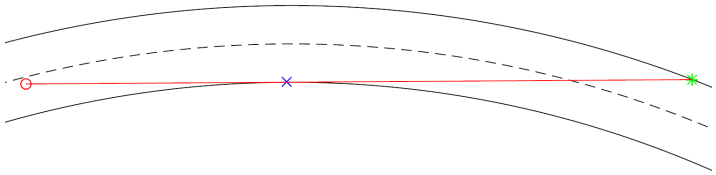

Figure 2-13: Example of ETP. The red circular marker represents the vehicle position, the blue cross the TP, and the green asterisk the intersection of the line passing through the previous two points with the road boundary, called the ETP.

In terms of driver's slowing down behavior, in a vast majority of cases all deceleration is done before the middle of the curve is reached. Drivers tend to use accelerations smaller than $1ms^{-1}$ in absolute value, both when braking into and accelerating out of turns.

2-3 The effect of speed on steering behavior

The body of research into speed effects on steering in curves is, perhaps surprisingly, small. Nonetheless, this section provides an overview of the mentions of the influence of speed on the models described in section 2-1, and of research into steering at variable speeds.

In the work of Donges (1978), the identified parameters of the model were shown to be speed dependent. For the anticipatory part, the anticipation time for the driver to start steering when predicting a change in curvature remains constant, but the initial slope of the steering response increases with vehicle speed. In the compensatory model, the time delay appears to decrease with speed until some lower reaction time limit. This seems logical since the driver has less time to react at higher speeds. Furthermore, the path curvature error becomes more noticeable as speed increases, since it is based on the velocity vector field of the driver's visual field. This leads to a higher gain of the correction to this error.

Hildreth et al. (2000) conducted a simulator experiment were subjects were instructed to correct an initial error in trajectory and return to straight line driving in the center of the road. This experiment was conducted at different constant speeds, and it was found that as speed increased, drivers performed the required maneuver more quickly, but no change in amplitude of the correcting motion was recorded.

Chatzikomis and Spentzas (2009) developed a driver model for evaluating assistance systems, that predicts the driver's longitudinal and lateral control actions based on the heading and position errors to a pre-specified desired path aligned with the center of the road. The lateral control model uses gain scheduling to model the effects of speed on steering action, based on the assumption that the average driver reduced the magnitude of their steering action as the speed increases. However, this assumption is not further justified or proved experimentally.

Saleh et al. (2011) built on the work of Sentouh et al. (2009b) described previously, designing a speed-dependent driver model using the angles resulting from the two point visual model, θ_{near} and θ_{far}, and the current steering angle, δ_{SW}, as inputs. The general structure of the model is shown in figure 2-14. A short description of each part of the model, along with a variation range for each parameter obtained by trial and error, is provided over the next paragraphs.

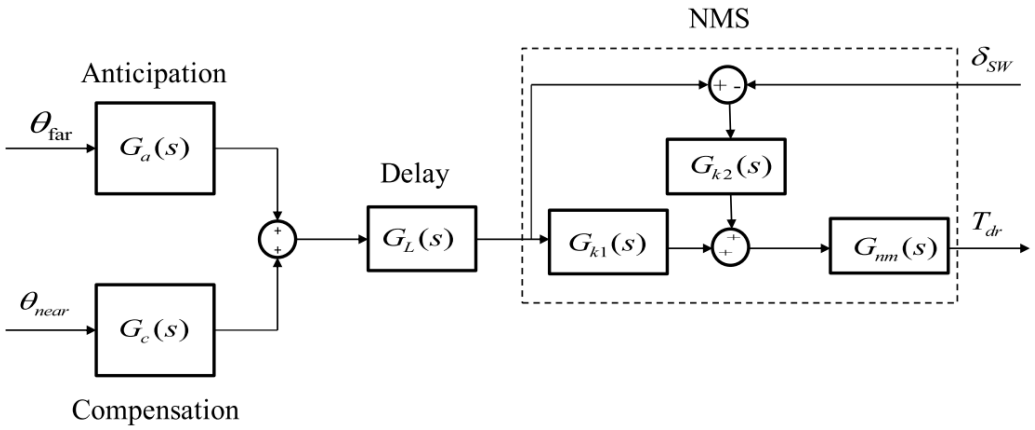

Figure 2-14: Structure of the speed dependent neuromuscular driver model. (Saleh et al., 2013)

The first three blocks of the model represent the visual and central nervous system, of which the anticipatory part is described by a simple gain, as shown in equation (2-6). Values of K_a above 5 lead to over-steering, while values below 2 result in under-steering behavior.

$$G_a(s) = K_a \tag{2-6}$$

The compensation transfer function relating the near point angle to the driver intention, equation (2-7) uses three parameters: the compensation gain K_c, the lag time constant T_I, and the lead time constant T_L. The compensation gain is speed dependent, and the authors describe how with larger speeds drivers rely less on the near point and therefore use less compensation. Values of K_c above 30 lead to instabilities, while at values under 10 significantly reduce the compensation used by the driver, leading to a larger amount of corner cutting. T_I describes the frequency band of the compensatory behavior: too low values (under 0.5) make the model attempt to compensate for all frequencies, resulting in instability; too high values (above 2) filter out the large majority of frequencies, essentially canceling out the compensator behavior. An interesting aside is that the authors note that this parameter could be an indicator of tiredness in a driver, but no further analysis of this is performed in this work. Finally, the lead time constant T_L describes the rate of the compensatory behavior. Small values lead to slow reactions, while large values speed up the behavior and can eventually lead to instabilities. The authors use a range between 2 and 5 for this parameter.

$$G_c(s) = \frac{K_c}{v}\frac{T_L s + 1}{T_I s + 1} \tag{2-7}$$

In addition to the two above described blocks, human information processing has an associated time delay. In this cased it is modeled using the Padé approximation, as shown in equation (2-8). The authors vary τ_p from 0 to 0.1 and note that a too high value will result in instability.

$$G_L(s) = e^{-\tau_p s} \approx \frac{1 - 0.5\tau_p s}{1 + 0.5\tau_p s} \tag{2-8}$$

The result of these three blocks is the desired steering angle by the driver, $\hat{\delta}_{SW}$. The remainder of the model describes the interaction of the human neuromuscular system with the steering wheel in order to generate a torque that will apply this angle to the steering wheel. $G_{k1}(s) = K_r v$ relates the desired angle to a desired torque through an internal model of the steering system stiffness, which varies with speed. Values of K_r below 0.5 result in under-steering, while values above 1.5 cause over-steering and instability. $G_{k2}(s) = K_t$ defines the stiffness of the driver's holding of the steering wheel. The higher this value, the more resistant the driver is to disturbances. Finally, the last block represents the inertia, and passive damping and stiffness of the drivers arms, as shown in equation (2-9). Here, T_N is a neuromuscular time constant, and the authors note that its value has remained constant at 0.1 during many precedent works on the same topic.

$$G_{NM}(s) = \frac{1}{T_N s + 1} \tag{2-9}$$

While the model is speed dependent, and was validated over a large range of speeds, the experiments carried out by Saleh et al. and in subsequent work (Saleh et al., 2013; Mars, Deroo, & Charron, 2014: among others) were performed at constant speed. To the best knowledge of the author, this model has not yet been coupled to a speed controller. In the next chapter, an implementation in simulation of this model together with a speed regulator will be described.

Chapter 3

Simulation results

Before an assistance system can be designed and an experiment can be set up, an evaluation of the previously described literature must be performed. To better understand driver models, and to evaluate how the constant speed models perform when extended with a speed controller, a series of *MATLAB* simulations were performed. This section describes how the models were implemented and provides a description of the obtained results.

3-1 Implementation

An approximately $2000m$ long single-lane road with a width of $4m$, consisting of straight segments and corners varying in radius from $40m$ to $120m$ was designed for use in these simulations. A sample corner with a radius of $50m$ and a deflection angle of 100^o is shown in figure 3-1, including a trajectory followed by the vehicle and driver. In this work, only the results from the actions of the driver model in this turn will be shown, for simplicity. However, the conclusions are valid for the entire road section, including quick successions of turns. The implementation of the Road-Vehicle-Steering (RVS), driver, and speed control models is described in this section.

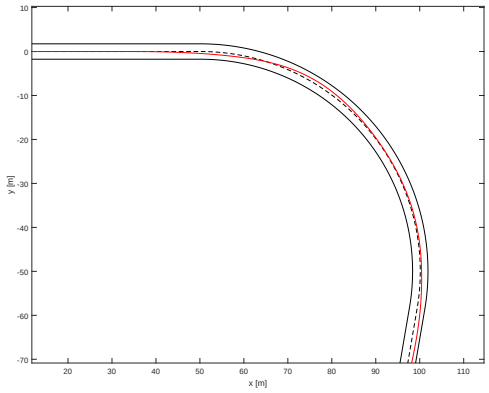

Figure 3-1: Sample corner of the designed road, with a radius of $50m$ and a deflection angle of 100^o. Shown in red is the vehicle trajectory, for a run where the driver model was tuned to prioritize the following of the center of the road. The vehicle travels from the top left to the bottom right of the plot.

3-1-1 Road-Vehicle-Steering (RVS) model

In order to implement any driver model, first one must have a platform to implement it on. In this case, it consists of a RVS model that simulates a vehicle, using a simple bicycle model augmented with a model of the steering system, that travels on a single lane road consisting of straight sections and constant curvature turns.

The vehicle and steering model is a slightly modified version of the one used by Sentouh et al. (2009b), and uses the vehicle parameters that Nguyen, Sentouh, Popieul, and Soualmi (2015) describes for a similar model in straight line driving. The modifications are made to ensure the model can cope with changes in longitudinal speed, and to decouple the tangent and near point detection (road model) from the vehicle model, since the implementation described by Sentouh et al. assumes a vehicle traveling only on a curve, with a constant distance to the TP. It has the states $\mathbf{x} = [\beta,\ \dot{\psi},\ \delta,\ \dot{\delta}]^T$, respectively the current sideslip angle, the current yaw rate of the vehicle, the angle of the steering wheel, and the steering rate. It takes as input the torque exerted by the driver on the steering wheel, T_{driver}.

In addition to the vehicle and steering models, the RVS also determines the road information at each timestep: the far (TP) and near points.

The TP detection algorithm is based on the method developed by Gallen and Glaser (2009), that uses data from an in-vehicle camera to detect zero-crossings of the derivative of the visual angle from the vehicle to the TP (TPA). The method works by taking samples of points on both sides of the road at discrete intervals, calculating the TPA, and finding the point where its derivative passes zero. Figure 3-2 shows how this method works for an example of a left turn. Since the road a vehicle travels on does not only consist of curves but can also contain straight segments, a variable maximum TTP is introduced. If the found point lies further away from the vehicle than this time, the far point is taken as the center of the road at this time ahead.

The speed regulation algorithm described in section 3-1-3 uses the ETP as the indicator of

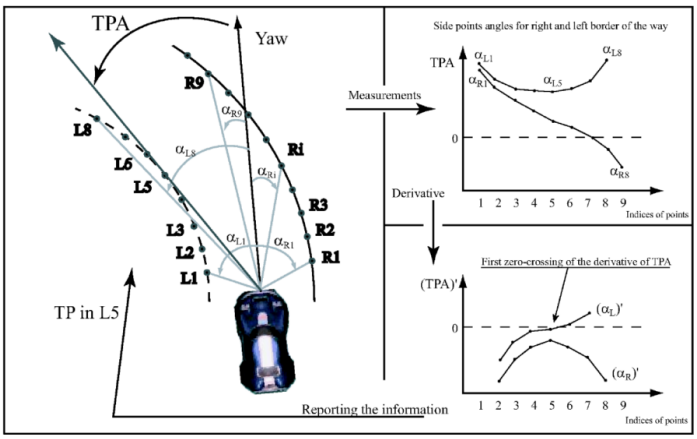

Figure 3-2: Example of the method to find the TP from the road ahead using the derivative of the visual angle to the tangent point (TPA). (Gallen & Glaser, 2009)

the curve speed. Once the TP is found, the line connecting the vehicle to it is extended until it crosses the opposite lane marking. This intersection is the ETP.

This method is preferred over the usage of the value of the road curvature ahead, as is used in most models in literature, due to its realism and applicability to real world driving. This is especially important since human drivers cannot accurately judge curvature, and assistance systems will most likely not have access to accurate enough information from maps.

The near point is found by evaluating the road and finding its center point at the preview distance ahead. The preview distance is simply the distance that will be covered by the vehicle at the current speed during the specified preview time, which is one of the variable parameters of the model. The angle to this point is then calculated and serves as the input for the compensatory part of the driver model.

3-1-2 Driver lateral control model

The driver model used is the only one found in literature that includes a speed dependency: the one first described by Saleh et al. (2011) as an evolution of the model described by Sentouh et al. (2009b). Its structure is described in section 2-3. The inputs are the near and far point angles obtained as described in the previous section, and the current steering angle at the column. The model is implemented using a state-space representation, and the values of the driver parameters are taken from the original paper, except for K_t, since the original value of this parameter (12) appears to cause instabilities when taking high curvature turns at low speeds. The values are shown in table 3-1.

Table 3-1: Initial parameter values for driver model

Parameter	K_a	K_c	T_I	T_L	τ_p	K_r	K_t	T_N
Value	3.4	15	1	3	0.04	1	3	0.01

3-1-3 Speed controller

As discussed in section 2-2, currently no models that allow for a preview judgment of the driver desired speed for an upcoming turn without requiring curvature estimation exist. The use of the ETP as a measure of this was discussed as a promising approach, but at this point more research is necessary to identify exactly how speed is related to this point. In this work it is assumed that drivers maintain a safety margin of 2 seconds in Time to Extended Tangent Point (TETP). This value is chosen based on the work of Boer (1996), who mentions that drivers usually begin to steer into an upcoming turn at a TTP of less than $1.5s$. Since, as mentioned in section 2-2, drivers tend to brake before they enter a turn, a value of 2 seconds is acceptable. The desired speed is then calculated as the speed that would take the vehicle to the ETP in 2 seconds.

The acceleration limits are based on those found for 90% of observations, excluding emergencies, of the experiments conducted by Moon and Yi (2008); Bosetti et al. (2013). The maximum comfortable accelerations are $-0.89ms^{-2}$ for braking and $0.91ms^{-2}$ for accelerating. The desired acceleration is calculated such that the driver reaches the target speed at the tangent point of the curve. As a side-note, if the vehicle happens to leave the road during the simulation, this model will gradually slow down to $5ms^{-1}$ or until the vehicle returns to the road. When not in a turn, the free speed is set to $15ms^{-1}$.

In the future, attention must be given to the values of the time margins that drivers actually keep, especially since they are likely to depend on individual driving style. In addition, it is desirable to model the dynamics of the human leg and pedals system, with a view to the possibility of implementing an assistance system.

3-2 Steering model parameter influence

In this section the parameters of the model will be varied over the range described by Saleh et al. (2011), in order to verify if the conclusions drawn in that work are valid for this implementation of the model including a speed controller. In addition, the preview and maximum TTP parameters will be varied to examine their effect on the model. The parameters are varied individually, that is, all other values remain constant and equal to those in table 3-1 during each run.

3-2-1 Anticipatory gain K_a

The anticipatory gain, K_a, reflects the intensity of the driver's reaction to the anticipatory visual stimulus, the angle to the TP. figure 3-3 shows the effects of varying K_a from 2 to 10 on the lateral position error with regards to the center line (y_{lat}), the steering angle (δ), the steering torque (T_{driver}), and the longitudinal speed (v_{long}). A low value (red line in the figure) will cause the model to under-steer, and in some parts of the road, not shown in the figure, the vehicle will even leave the road. A high value makes the model cut corners more, as evidenced by the cyan and purple lines in the figure. At $K_a = 10$ oscillations in steering angle and torque begin to appear, and even higher values lead to unstable behavior as the model overcompensates for the far point angle. At approximately 100 meters into the turn,

the oscillations cause the vehicle to leave the road on the inside. The observed patterns match the conclusions of Saleh et al..

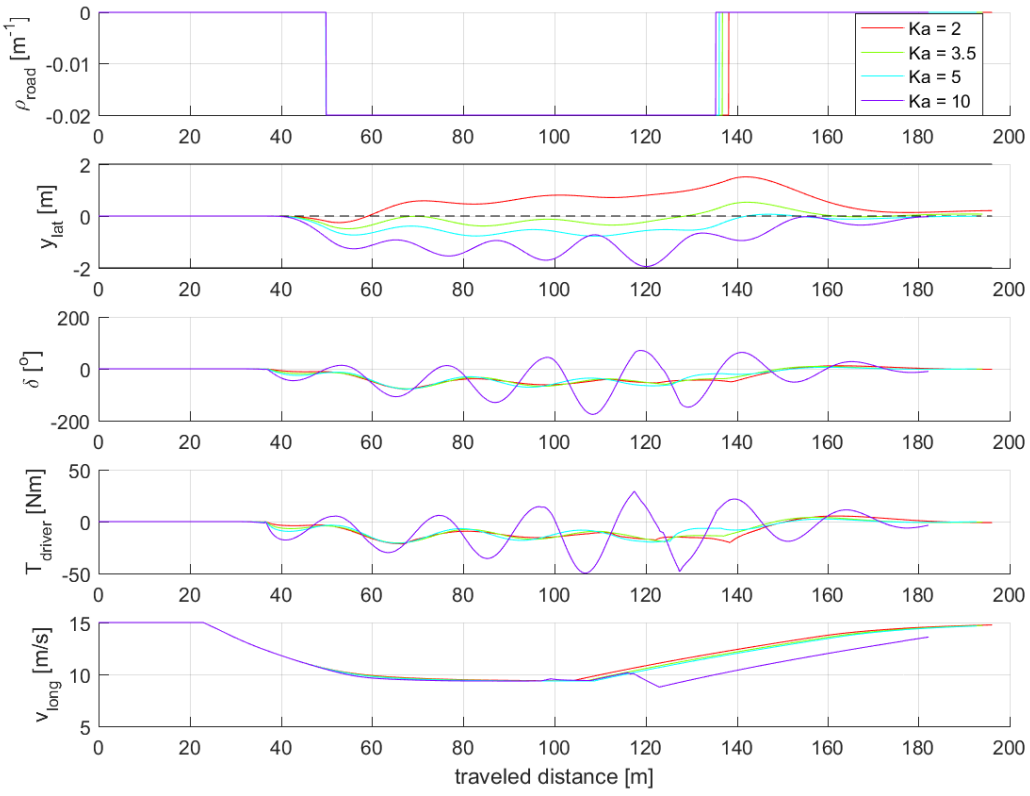

Figure 3-3: Influence of the anticipatory gain K_a on the simulation results. The top plot shows the road curvature, the second the lateral position error with regards to the center line (y_{lat}), the third the steering angle (δ), the fourth the steering torque (T_{driver}), and finally the longitudinal speed (v_{long})

3-2-2 Compensatory gain K_c

K_c represents the importance the driver assigns to staying close to the center of the lane, and the results of its variation are displayed in figure 3-4. The higher this value, the closer the model stick to the central line, and too high values lead to overcompensation and instability. Lower values see larger deviations from the center line, indicating more corner cutting behavior and a wider turn exit. As with K_a, the results agree with Saleh et al..

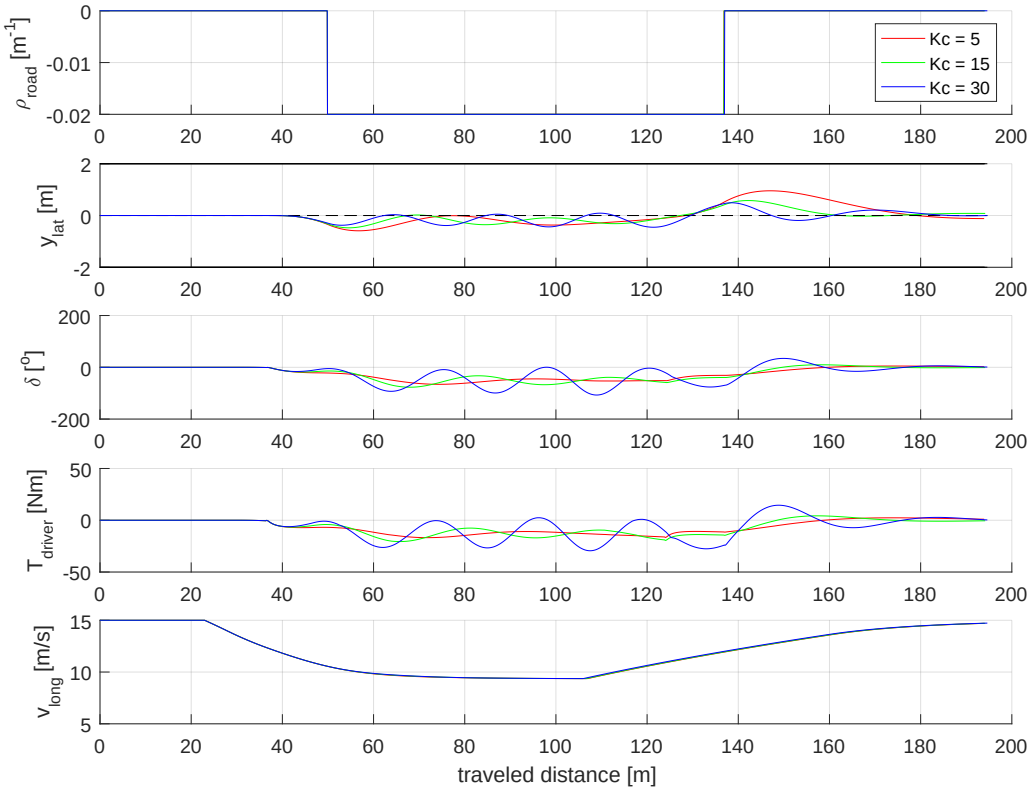

Figure 3-4: Influence of the compensatory gain K_c on the simulation results. The top plot shows the road curvature, the second the lateral position error with regards to the center line (y_{lat}), the third the steering angle (δ), the fourth the steering torque (T_{driver}), and finally the longitudinal speed (v_{long})

3-2-3 Lag time constant T_I

As the name indicates, the lag time constant T_I affects the lag characteristics of the response to the near point. A low T_I causes the model to respond to all the frequencies in the stimulus. This can be seen for for $T_I = 0.1$ in figure 3-5, where in the steering angle and torque plots after the initial turn-in a correction to stay closer to the center of the lane. Higher values result in less compensation and therefore higher deviations from the center and more oscillation. The acceptable values can be lower than the range of [0.5,2] found by Saleh et al., possibly because the speed controller reduces the speed in the turn.

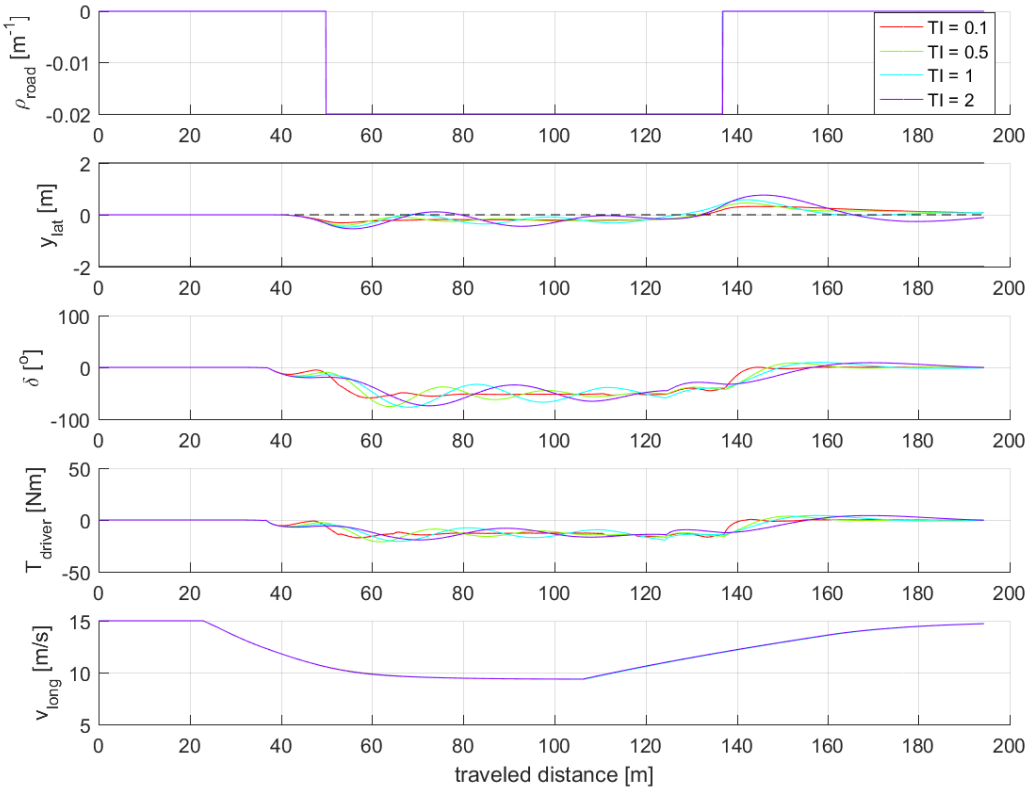

Figure 3-5: Influence of the lag time constant T_I on the simulation results. The top plot shows the road curvature, the second the lateral position error with regards to the center line (y_{lat}), the third the steering angle (δ), the fourth the steering torque (T_{driver}), and finally the longitudinal speed (v_{long})

3-2-4 Lead time constant T_L

T_L has the opposite effect as T_I on the response: higher values make the system respond faster to changes in the compensatory visual angle. In figure 3-6, larger values of T_L result in a steeper and larger magnitude of the torque response of the driver than for lower values. There is an upper limit however, as in the figure a T_L value of 7.5 already leads to significant oscillations. Saleh et al. found acceptable values between 2 and 5, and that agrees with the behavior found in this simulation.

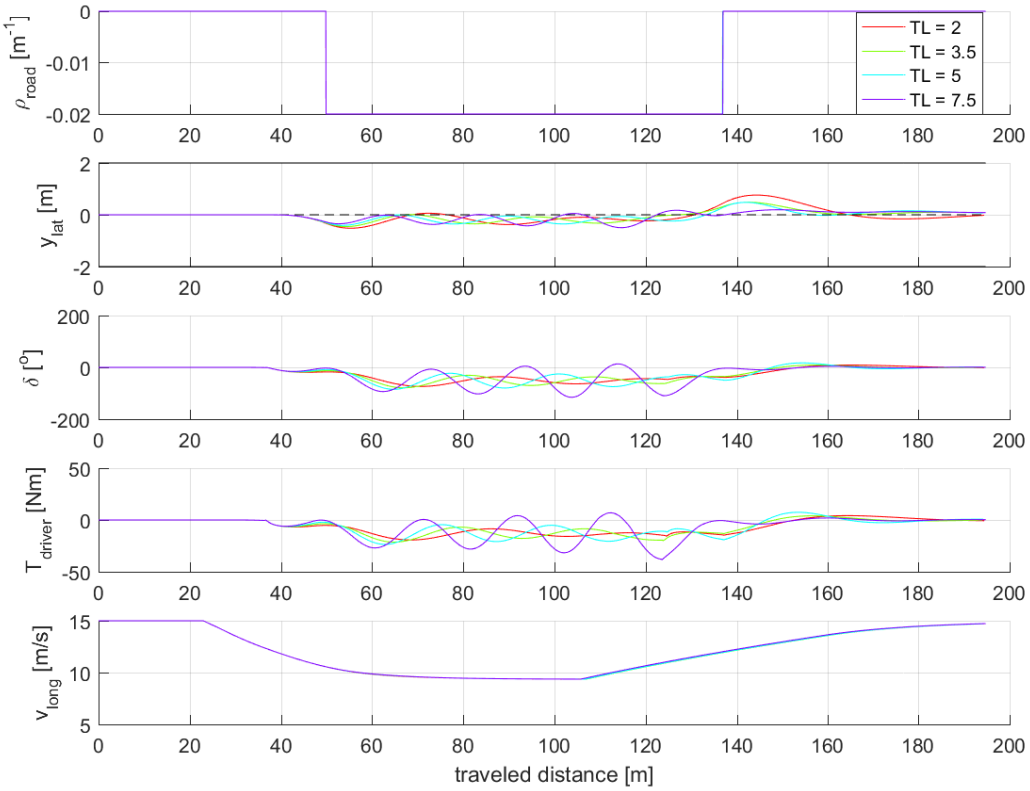

Figure 3-6: Influence of the lead time constant T_L on the simulation results. The top plot shows the road curvature, the second the lateral position error with regards to the center line (y_{lat}), the third the steering angle (δ), the fourth the steering torque (T_{driver}), and finally the longitudinal speed (v_{long})

3-2-5 Time delay τ_p

The effect of the human time delay on the response, shown in figure 3-7, seem quite intuitive. The larger the time delay, the more unstable the response becomes. Saleh et al. found an acceptable maximum of 0.01, and these results confirm this.

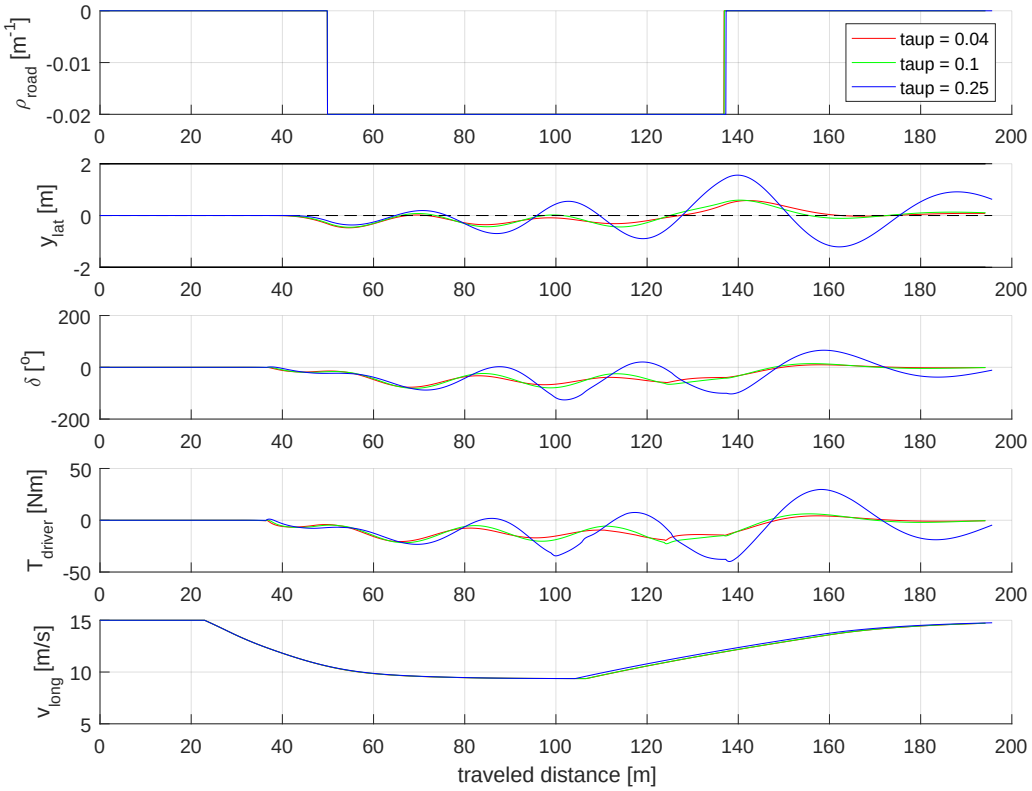

Figure 3-7: Influence of the time delay τ_p on the simulation results. The top plot shows the road curvature, the second the lateral position error with regards to the center line (y_{lat}), the third the steering angle (δ), the fourth the steering torque (T_{driver}), and finally the longitudinal speed (v_{long})

3-2-6 Internal model of steering stiffness gain K_r

The gain of the driver's internal model of the stiffness of the steering system, K_r, affects the torque that the driver exerts on the steering wheel. A low value, as shown by the red line in figure 3-8, results in too little torque being applied, and this slow actions result in the vehicle leaving the road on turn exit after approximately 140 meters. Values above 1.5 result in over-steering and possible instabilities. These results agree with Saleh et al..

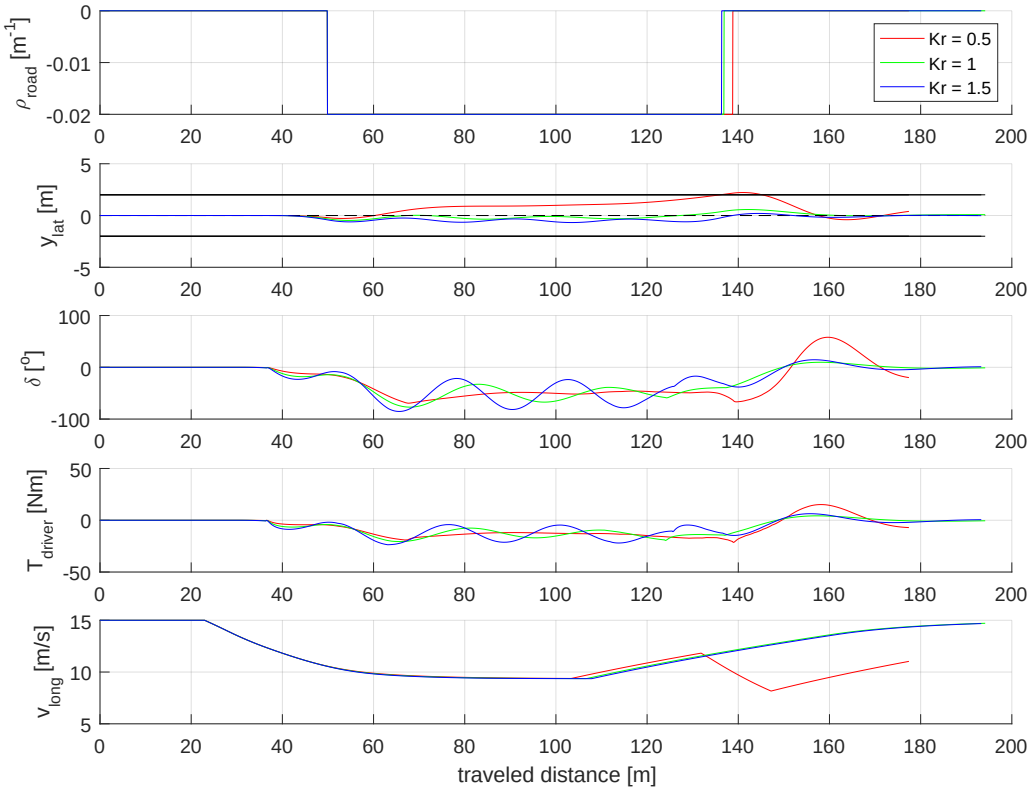

Figure 3-8: Influence of gain of the internal model of steering stiffness K_r on the simulation results. The top plot shows the road curvature, the second the lateral position error with regards to the center line (y_{lat}), the third the steering angle (δ), the fourth the steering torque (T_{driver}), and finally the longitudinal speed (v_{long})

3-2-7 Driver stretch reflex gain K_t

This parameter is the only one whose effect is significantly different in the simulation when compared to Saleh et al.'s results. K_t acts on the difference between the driver's desired steering wheel angle and the actual angle of the steering wheel, representing the human stretch reflex. While in the original work the ideal value was found to be 12, and could increase even further without issue, in the simulation values above 6 already cause instabilities due to too strong reactions of the stretch reflex, as shown in figure 3-9. Saleh et al. argue that this value can theoretically reach infinity, but this would amplify any difference in the desired steering angle and the steering wheel angle at the column too strongly and directly cause instability. This parameter should take values between 0 and 6.

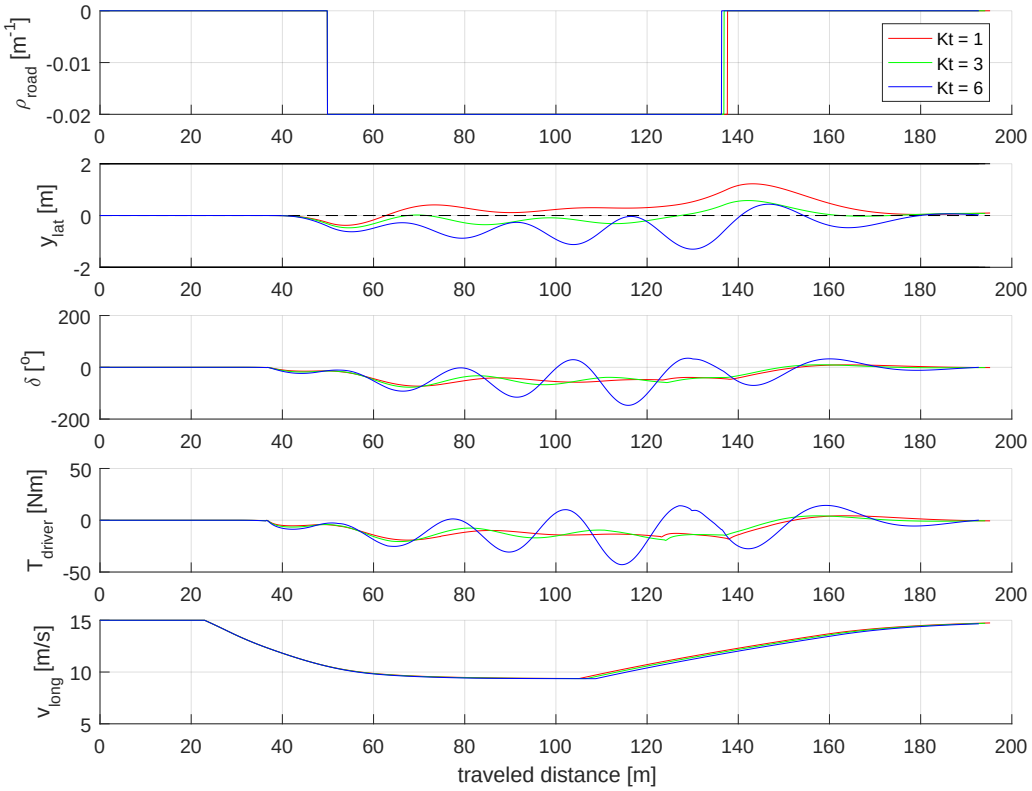

Figure 3-9: Influence of the gain of the driver stretch reflex K_t on the simulation results. The top plot shows the road curvature, the second the lateral position error with regards to the center line (y_{lat}), the third the steering angle (δ), the fourth the steering torque (T_{driver}), and finally the longitudinal speed (v_{long})

3-2-8 Maximum TTP

Having finished the analysis of the parameters of Saleh et al.'s model, the influence of the perception time parameters on the response is also analyzed. We begin with the TTP, which can be seen as a measure of how far before the curve the driver notices the tangent point, and therefore begins to turn in. As would be expected, lower values such as the red line in figure 3-10 result in later steering into the corner, and as a consequence, less corner cutting. In this example, a value of 1 second causes the vehicle to be on the outside of the turn during the entire curve. The magnitude of the steering actions is unaffected.

This parameter also influences the acceleration of the speed controller. A lower value mean that the margin the tangent point is smaller, and therefore a larger braking action is needed to reach the desired speed at the tangent point.

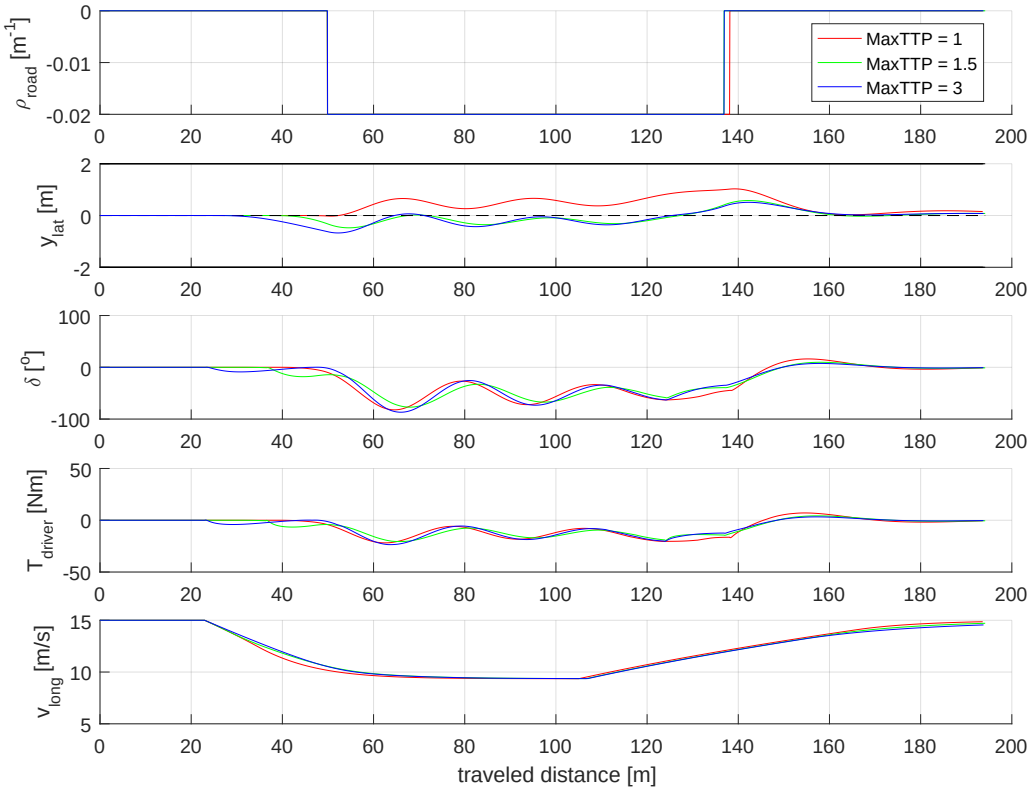

Figure 3-10: Influence of the TTP margin on the simulation results. The top plot shows the road curvature, the second the lateral position error with regards to the center line (y_{lat}), the third the steering angle (δ), the fourth the steering torque (T_{driver}), and finally the longitudinal speed (v_{long})

3-2-9 Near point preview time T_p

The preview time to the near point is the measure of how far ahead of the vehicle the center of the road is used as a source of information. As with the TTP described above, the effects agree with expectations. In figure 3-11 too low values cause instability, as a point too close of the vehicle is taken. A large value essentially removes the effect of the compensatory behavior by making it behave more closely to the preview information, resulting in corner cutting during turns.

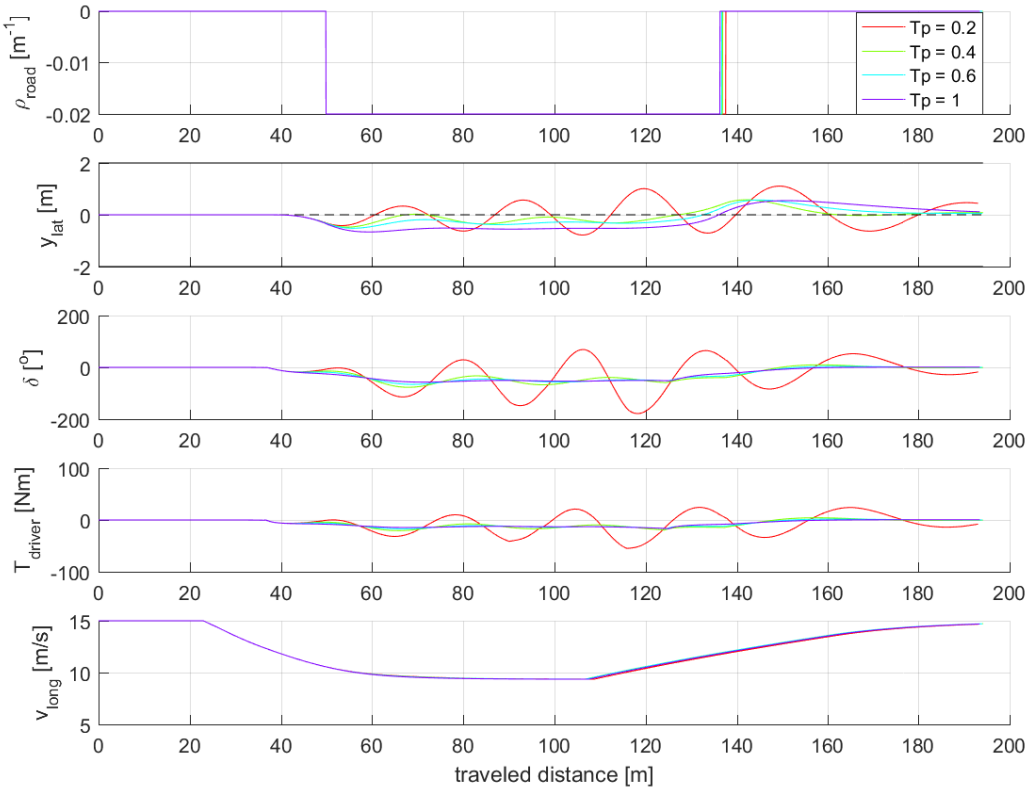

Figure 3-11: Influence of the near point preview time T_p on the simulation results. The top plot shows the road curvature, the second the lateral position error with regards to the center line (y_{lat}), the third the steering angle (δ), the fourth the steering torque (T_{driver}), and finally the longitudinal speed (v_{long})

3-3 Maximum TETP

The safety margin in the time to the ETP only influences the desired speed of the speed controller. In figure 3-12, a 1 second margin causes the vehicle to leave the road on the outside of the turn. In addition, more steering activity is needed to ensure that the vehicle can still take the turn at higher speeds. Margins of 1.5 and 2 seconds are enough for safe curve driving with the default parameters of the driver model.

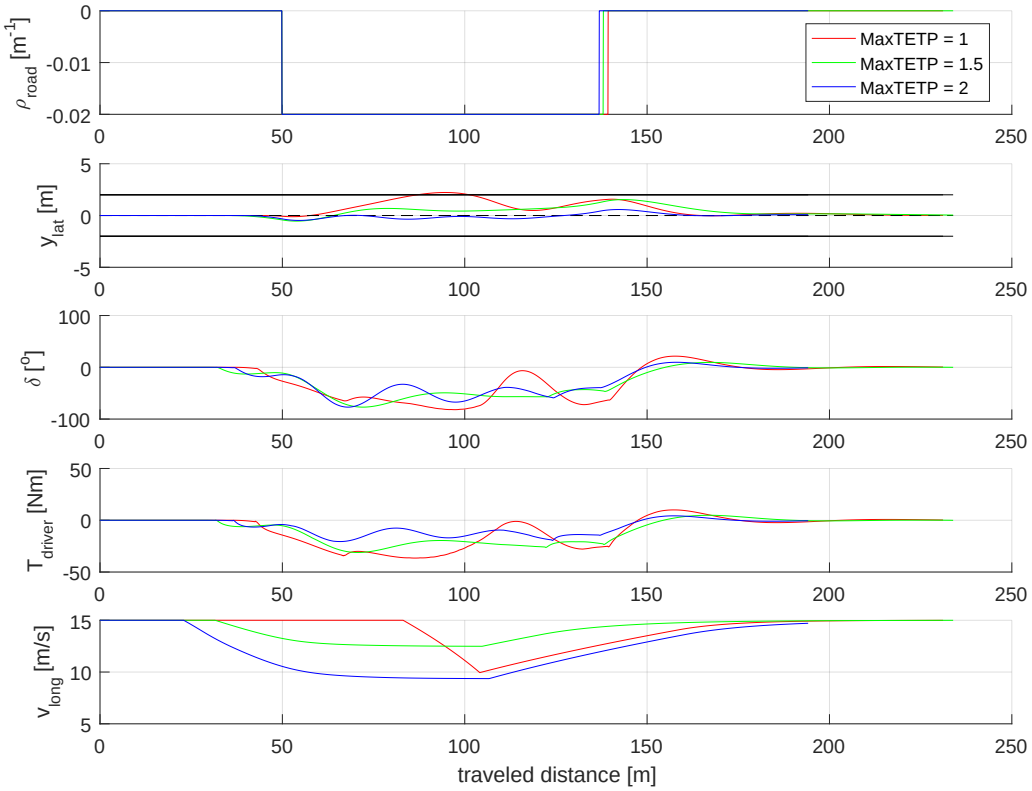

Figure 3-12: Influence of the TETP margin on the simulation results. The top plot shows the road curvature, the second the lateral position error with regards to the center line (y_{lat}), the third the steering angle (δ), the fourth the steering torque (T_{driver}), and finally the longitudinal speed (v_{long})

3-4 Speed influence on steering model

Finally, the effect of the free speed during the straight line segments is shown in figure 3-13. The larger speed results in earlier turn-in and more corner cutting, as well as faster steering actions. Interestingly, the model shows larger magnitudes of steering torque for the higher speeds, contrary to the conclusions of (Hildreth et al., 2000). The task in that experiment was the return to straight line driving and not the negotiation of a curve, which could explain the difference. More experimental validation is needed to determine the realism of the model when changing speed.

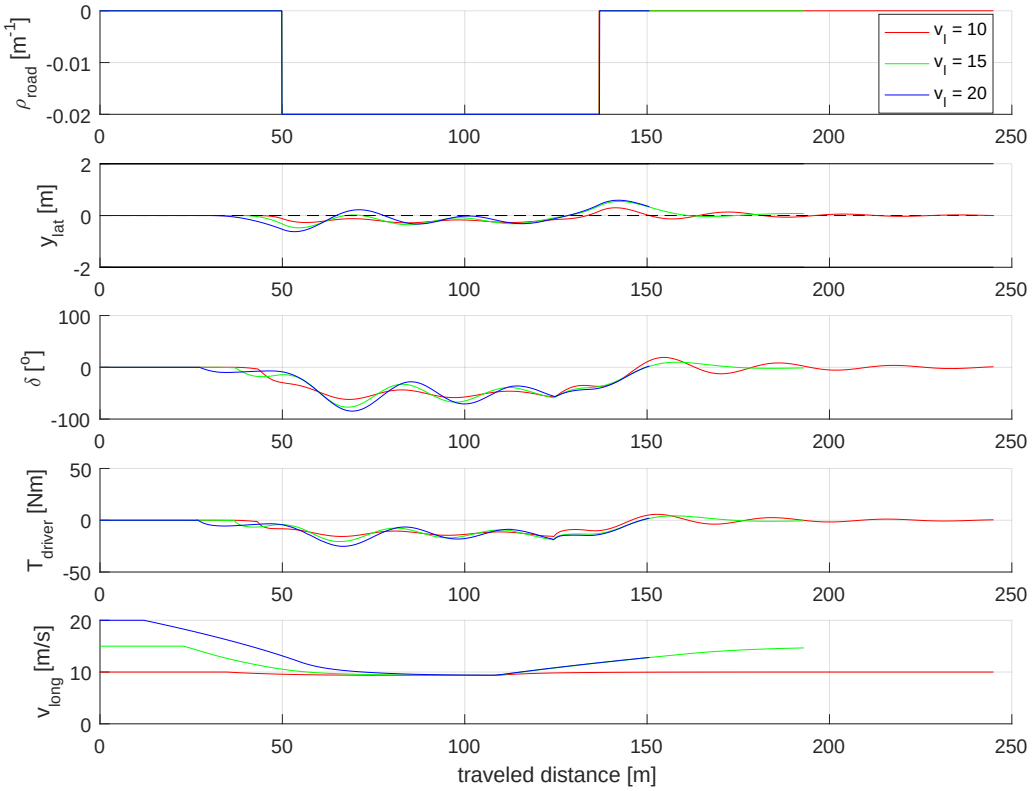

Figure 3-13: Influence of the free speed v_{long} on the simulation results. The top plot shows the road curvature, the second the lateral position error with regards to the center line (y_{lat}), the third the steering angle (δ), the fourth the steering torque (T_{driver}), and finally the longitudinal speed (v_{long})

3-5 Identification of parameters

In order to determine if the parameters of the driver model can be identified, a run with the default parameters was performed, noise was added to the results and a non-linear least-squares method with parameter limit values obtained from the above discussion. The original and identified values of the parameters are shown in table 3-2, and the resulting driver torque plot in figure 3-14. While there is a considerable difference between the parameter values, the resulting torque plot is practically identical. This tells us that the model is over-parametrized. (Xin, 2016) performed identification experiments and reached the same conclusion, identifying the parameters with Variance Accounted For (VAF) values of over 99% for the steering angle and torque but noticing over-parametrization. To mitigate this, Xin simplified the NMS by assuming driving at constant speed. This approach will not work in this case, since the goal is identify variation with speed, and therefore a new approach must be found before further work can be done.

Table 3-2: Identified parameter values for driver model

Parameter	K_a	K_c	T_I	T_L	τ_p	K_r	K_t
Original value	3.4	15	1	3	0.04	1	3
Identified value	2.8838	13.4088	0.8638	2.5452	0.0524	1.2903	2.2855

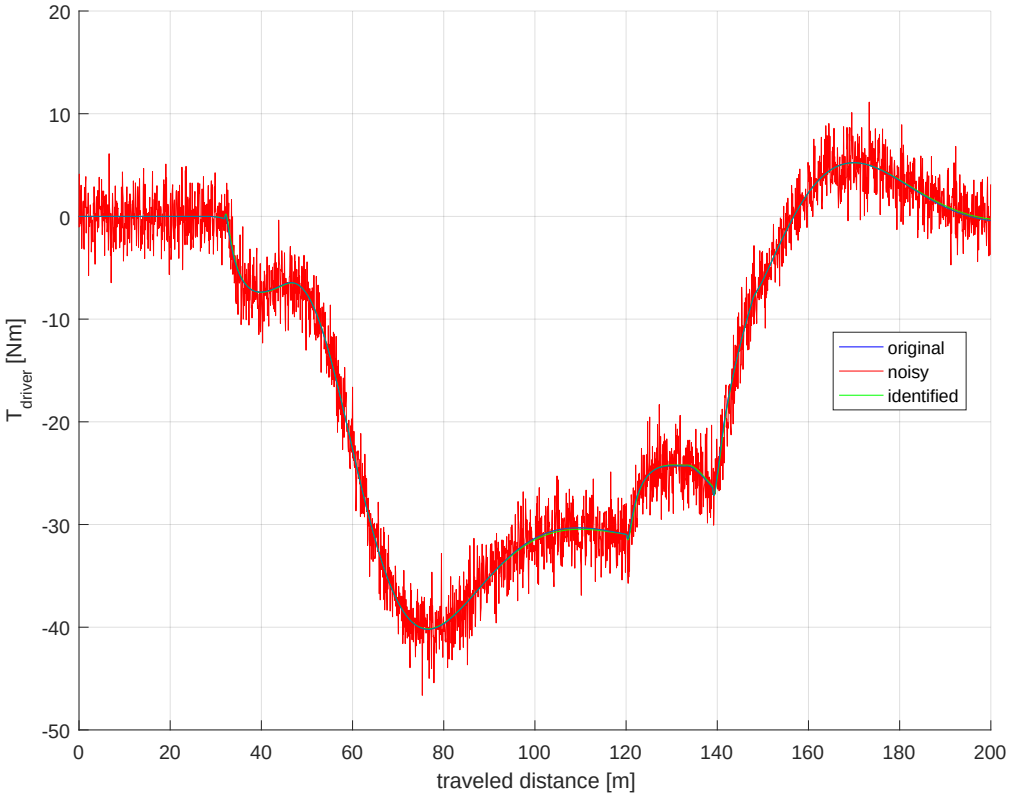

Figure 3-14: Original, noisy, and identified driver steering torques.

3-6 Conclusions

Literature on speed adaptation of steering behavior is scarce, but most agree that as speed increases, anticipation times remain constant, steering rate increases, and preview becomes more dominant than compensatory behavior.

The speed-dependent driver model developed by Saleh et al. (2011) was implemented in a *MATLAB* simulation environment, and the results generally agree with the conclusions from the limited amount of literature available. The model was coupled with a speed controller based on a safety margin to the ETP without significant issues, and the model is now capable of generating variable speed results. The range of the parameters from the original work was tested at variable speeds, and the found values agree in all cases except the gain of the stretch reflex, which cannot reach as high values without the model becoming unstable. In general, the model performs as expected, and the next step is to apply it to available experimental

data to determine its realism. To be able to compare it to real data, identification must be performed to find the values of the driver-dependent parameters. However, the model is over-parametrized, and this must be resolved before any further work on this model can be done.

Chapter 4

Conclusions and future work

While the topic of driver modeling for driving assistance systems has received considerable attention over the past decades, most of the research has focused on constant speed driving. In order to provide better support in the driving task, this research must be extended to take into account the way that drivers actually drive, that is, varying their speed depending on factors such as road geometry and traffic. The central goals of the research of this master's thesis are twofold: to find out whether adapting the haptic shared control reference trajectory based on the vehicle speed improves user acceptance of steering shared control systems, and to gain insight into what factors human drivers take into account when adapting their speed to upcoming turns in the road.

In previous literature, the study of steering has mostly been performed during constant speed driving, and can be subdivided into two different tasks: the perception of the road ahead to generate a steering intention, and the control action that translates this intention to an actual steering movement. Even though discussion remains on where exactly driver look, it is generally accepted that perception follows a two-level model, using visual angles to obtain both preview and compensatory information from the far and near regions of the road, respectively. Less consensus exists on how to model the neuromuscular behavior of the human driver. The most common approach consists of modeling each desired component of the NMS as a transfer function. This has the advantage that the parameters to be identified can be easily explained. In recent years, studies of driver behavior have shifted their attention to the work done on human motion control and more specifically to the task of reaching, which was found to contain many similarities to steering. Benderius (2014) developed a simple open-loop steering correction model based on steering rate patterns, only containing one driver-dependent parameters. While this model is attractive in its simplicity and the fact that is captures the tendency of humans to satisfice instead of optimize, it does not model the application of steering torques, as required for model that can be used as references for HSC. Kolekar (2016) based his model on the framework of Optimal Preview Control, often seen in the field of neurophysiology. In addition to the fact that it links the steering task to the larger field of human behavior studies, this model has the advantages of being able to capture both routine and emergency behavior in one model, and includes the natural

variability of steering. As of yet, the model cannot reproduce satisficing behavior, and as the author notes, this should be the object of future work. Modeling steering as reaching is a recent development, and while they can accurately reproduce steering behavior, these models still require further study.

Humans generally do not drive at constant speed, and tend to adapt their speed to the road situation ahead. The speed choice of drivers has been extensively studied in the context of road safety, and over the past ten years also for driving assistance systems. The vast majority of these models use the curvature of the road a measure of lateral acceleration, and adapt the speed based on safety margins. This usually requires a judgment of road curvature, which is not a task that humans perform well. In the study of car following tasks, the TTP is used a measure of when to brake. Adapting this for the purposes of curve driving, models based on keeping a safety margin in the time to the tangent point or the extended tangent point show promise.

Interestingly, the combination of the two behaviors has not been the subject of much study. The NMS model developed by Saleh et al. (2011) is one of the few that explicitly includes the effect of speed on the steering behavior of the driver, but it is not coupled to a speed controller. In simulation, this model was cascaded with a TETP based speed regulator, and the results agree with the conclusions of previous literature: as speed increases, the anticipation time remains constant, the rate of steering corrections increases, and preview becomes dominant over compensatory behavior, resulting in more corner-cutting. Attempts at identification of the parameters of this model were able to capture the steering behavior, but showed that the model is over-parametrized.

To investigate speed control, identify the changes with speed and the differences between the different neuromuscular models, and implement an assistance system based on this new reference, would go beyond the scope of a Master's thesis project. Therefore further work on this project will focus only on the classical model, leaving the discussion on steering as reaching aside. The initially posed question of *How do drivers combine speed choice and steering behavior during curve negotiation, and how can knowledge of this interaction be applied in the design of haptic assistance?* will be answered by developing, identifying and validating a speed control model based on time to extended tangent point, and combining this with a steering model based on the work of Saleh et al. (2011). The analysis of speed effects on the model developed by Kolekar (2016) will be left to further research.

The first step of the future work will be to test the hypothesis that drivers regulate their speed based on a time margin to the ETP. In order to do this, a speed model with two different modes of reducing speed will be developed. These two modes correspond to the actions of releasing the accelerator pedal and applying the brakes, with drivers using different time margins for each of these modes. Currently available experimental data do not contain sufficient variations in speed due to the large curvatures used, and therefore a new experiment will be set up to enable the identification of the time margins to the ETP.

Once the parameters of this speed model have been identified, it can be connected to a steering control model. The hypothesis of this part of the project is that drivers' performance and/or acceptance of HSC systems will be improved using a HCR driver model that varies with speed, when compared to constant speed models. To test this, an experiment will be designed in which the speed choice is left to the driver and two distinct steering HSC systems are provided. These references differ only in whether the reference depends on the vehicle

speed. Using a high level of haptic authority, the question of whether the inclusion of speed dependency in the used HCR provides significant benefits can be answered.

Bibliography

Abbink, D. A. (2006). *Neuromuscular analysis of haptic gas pedal feedback during car following* (PhD Thesis). Delft University of Technology.

Abbink, D. A., Cleij, D., Mulder, M., & van Paassen, M. M. (2012). The Importance of Including Knowledge of Neuromuscular Behaviour in Haptic Shared Control. In *Ieee international conference on systems, man, and cybernetics* (pp. 3350–3355). Seoul, South Korea.

Abbink, D. A., & Mulder, M. (2010). Neuromuscular Analysis as a Guideline in designing Shared Control. *Advances in Haptics*, 499–517.

Abbink, D. A., Mulder, M., & Boer, E. R. (2012). Haptic shared control: Smoothly shifting control authority? *Cognition, Technology and Work*, *14*, 19–28.

Bainbridge, L. (1983). Ironies of automation. *Automatica*, *19*(6), 775–779.

Benderius, O. (2014). *Modelling driver steering and neuromuscular behaviour* (PhD Thesis). Chalmers University of Technology.

Benderius, O., & Markkula, G. (2014). Evidence for a fundamental property of steering. In *Human factors and ergonomics annual meeting* (pp. 884–888).

Bertolazzi, E., Biral, F., Da Lio, M., Saroldi, A., & Tango, F. (2010). Supporting drivers in keeping safe speed and safe distance: The SASPENCE subproject within the European framework programme 6 integrating project PReVENT. *IEEE Transactions on Intelligent Transportation Systems*, *11*(3), 525–538.

Boer, E. R. (1996). Tangent point oriented curve negotiation. In *Proceedings of the 1996 ieee intelligent vehicles symposium* (pp. 7–12). Tokyo: IEEE.

Boink, R. P., van Paassen, M. M., Mulder, M., & Abbink, D. A. (2014). Understanding and reducing conflicts between driver and haptic shared control. *2014 IEEE International Conference on Systems, Man, and Cybernetics (SMC)*, 1510–1515.

Bosetti, P., Da Lio, M., & Saroldi, A. (2013). On the human control of vehicles: an experimental study of acceleration. *European Transport Research Review*, *6*(2), 157–170.

Bosetti, P., Da Lio, M., & Saroldi, A. (2015). On Curve Negotiation: From Driver Support to Automation. *IEEE Transactions on Intelligent Transportation Systems*, *16*(4), 1–1.

Cafiso, S., & Cerni, G. (2012, dec). A new approach to define continuous Speed Profile Models for two lane rural roads. *Transportation Research Record*, *23-09*(July), 1–22.

Chatzikomis, C. I., & Spentzas, K. N. (2009). A path-following driver model with longitudinal and lateral control of vehicle's motion. *Forschung im Ingenieurwesen/Engineering Research*, *73*(4), 257–266.

Cole, D. J. (2012). A path-following driver–vehicle model with neuromuscular dynamics, including measured and simulated responses to a step in steering angle overlay. *Vehicle System Dynamics*, *50*(4), 573–596.

Diehm, G., Maier, S., Flad, M., & Hohmann, S. (2013). Online identification of individual driver steering behaviour and experimental results. In *2013 ieee international conference on systems, man, and cybernetics,* (pp. 221–227).

Donges, E. (1978). A Two-Level Model of Driver Steering Behavior. *Human factors*, *20*(6), 691–707.

Fildes, B. N., & Triggs, T. J. (1984). The Effect of Road Curve Geometry on Curvature Matching Judgements. *Australian Road Research*, *12*(5), p. 63–70.

Flad, M., Otten, J., Schwab, S., & Hohmann, S. (2014a). Necessary and sufficient conditions for the design of cooperative shared control. In *2014 ieee international conference on systems, man, and cybernetics (smc)* (pp. 1253–1259).

Flad, M., Otten, J., Schwab, S., & Hohmann, S. (2014b). Steering driver assistance system: A systematic cooperative shared control design approach. In *2014 ieee international conference on systems, man, and cybernetics (smc)* (pp. 3585–3592).

Flad, M., Trautmann, C., Diehm, G., & Hohmann, S. (2013). Experimental validation of a driver steering model based on switching of driver specific primitives. In *2013 ieee international conference on systems, man, and cybernetics* (pp. 214–220).

Flash, T., Meirovitch, Y., & Barliya, A. (2013). Models of human movement: Trajectory planning and inverse kinematics studies. *Robotics and Autonomous Systems*, *61*(4), 330–339.

Flemisch, F., Heesen, M., Hesse, T., Kelsch, J., Schieben, A., & Beller, J. (2012). Towards a dynamic balance between humans and automation: Authority, ability, responsibility and control in shared and cooperative control situations. *Cognition, Technology and Work*, *14*(1), 3–18.

Gallen, R., & Glaser, S. (2009). Vision Based Tangent Point Detection Algorithm, Evaluation and Validation. In *Mva2009 iapr conference on machine vision applications* (pp. 518–522). Yokohama, Japan.

Gibson, J. J. (1958). Visually controlled locomotion and visual orientation in animals. *British journal of psychology (London, England : 1953)*, *49*(3), 182–194.

Godthelp, H. (1986, apr). Vehicle Control During Curve Driving. *Human Factors: The Journal of the Human Factors and Ergonomics Society*, *28*(2), 211–221.

Godthelp, H., & van Winsum, W. (1996). Speed Choice and Steering Behavior in Curve Driving. *Human Factors: The Journal of the Human Factors and Ergonomics Society*, *38*(3), 434–441.

Gordon, T. J., & Lidberg, M. (2015). Automated driving and autonomous functions on road vehicles. *Vehicle System Dynamics*, *53*(7), 958–994.

Gordon, T. J., & Zhang, Y. (2015). Steering Pulse Model for Vehicle Lane Keeping. In *2015 ieee international conference on computational intelligence and virtual environments for measurement systems and applications (civemsa).*

Herrin, G. D., & Neuhardt, J. B. (1974, apr). An Empirical Model for Automobile Driver Horizontal Curve Negotiation. *Human Factors: The Journal of the Human Factors and Ergonomics Society*, *16*(2), 129–133.

Hildreth, E. C., Beusmans, J. M., Boer, E. R., & Royden, C. S. (2000). From vision to action: experiments and models of steering control during driving. *Journal of experimental psychology. Human perception and performance*, *26*(3), 1106–1132.

Inga, J., Flad, M., & Diehm, G. (2015). Gray-Box Driver Modeling and Prediction : Benefits of Steering Primitives. In *2015 ieee international conference on systems, man, and cybernetics* (pp. 3054–3059).

Itkonen, T. H., Pekkanen, J., & Lappi, O. (2015). Driver gaze behavior is different in normal curve driving and when looking at the tangent point. *PLoS ONE*, *10*(8), 1–19.

Jamson, A. H., Hibberd, D. L., & Merat, N. (2013). The design of haptic gas pedal feedback to support eco-driving. In *Seventh international driving symposium on human factors in driver assessment, training, and vehicle design* (pp. 1689–1699).

Kolekar, S. (2016). *A Human-like steering model based on sensorimotor control theories* (Master's thesis). Delft University of Technology.

Land, M. F., & Horwood, J. (1995). *Which parts of the road guide steering?* (Vol. 377).

Land, M. F., & Lee, D. N. (1994). Where we look when we steer. *Nature*, *369*(6483), 742–744.

Lappi, O. (2014). Future path and tangent point models in the visual control of locomotion in curve driving. *Journal of Vision*, *14*(21), 1–22.

Lechner, D., & Perrin, C. (1993). The actual use of the dynamic performances of vehicles. *Proc. of the Institution of Mechanical Engineers, Part D: Journal of Automobile Engineering*, *207*(44), 249–256.

Levison, W. H. (2007). *Development of a Driver Vehicle Module for the Interactive Highway Safety Design Model* (Tech. Rep. No. November). U.S. Department of Transportation, Federal Highway Administration.

Levison, W. H., Bittner, A., Campbell, J., & Schreiner, C. (2002, jan). Modification and Partial Validation of the Driver/Vehicle Module. *Transportation Research Record: Journal of the Transportation Research Board*, *1803*, 52–58.

Li, L., & Warren, W. H. (2002). Retinal flow is sufficient for steering during observer rotation. *Psychological science*, *13*(5), 485–91.

MacAdam, C. C. (2003, aug). Understanding and Modeling the Human Driver. *Vehicle System Dynamics*, *40:1-3*(January 2014), 101–134.

Mars, F. (2008). Driving around bends with manipulated eye-steering coordination. *Journal of vision*, *8*(2008), 10.1–11.

Mars, F., Deroo, M., & Charron, C. (2014). Driver adaptation to haptic shared control of the steering wheel. In *2014 ieee international conference on systems, man, and cybernetics (smc)* (pp. 3585–3592). San Diego, USA.

Mars, F., Deroo, M., & Hoc, J.-M. (2014). Analysis of human-machine cooperation when driving with different degrees of haptic shared control. *IEEE Transactions on Haptics*, *7*(3), 324–33.

McRuer, D. T., Allen, R. W., Weir, D. H., & Klein, R. H. (1977). New results in driver steering control models. *Human Factors*, *19*(4), 381–397.

McRuer, D. T., Graham, D., Krendel, E., & Reisener Jr., W. (1965). *Human Pilot Dynamics in Compensatory Systems. Theory, Models and Experiments with Controlled Element and Forcing Function Variations* (Tech. Rep.). Air Force Flight Dynamics Laboratory.

Mehrabi, N., Sharif Razavian, R., & McPhee, J. (2014). A physics-based musculoskeletal driver model to study steering tasks. *Journal of Computational and Nonlinear Dynamics*, *10*(2), 021012–021012–8.

Mehrabi, N., Sharif Razavian, R., & McPhee, J. (2015). Steering disturbance rejection using a physics-based neuromusculoskeletal driver model. *Vehicle System Dynamics*, *3114*(June 2015), 1–23.

Montella, A., Pariota, L., & Galante, F. (2014). Prediction of Drivers ' Speed Behaviour on Rural Motorways Based on an Instrumented Vehicle Study. *TRB 2014 Annual Meeting*, 19.

Moon, S., & Yi, K. (2008, aug). Human driving data-based design of a vehicle adaptive cruise control algorithm. *Vehicle System Dynamics*, *46*(8), 661–690.

Mulder, M., Abbink, D. A., & Boer, E. R. (2008). The effect of haptic guidance on curve negotiation behavior of young, experienced drivers. *Conference Proceedings - IEEE International Conference on Systems, Man and Cybernetics*, 804–809.

Mulder, M., Abbink, D. A., & Boer, E. R. (2012). Sharing Control With Haptics: Seamless Driver Support From Manual to Automatic Control. *Human Factors: The Journal of the Human Factors and Ergonomics Society*, *54*(5), 786–798.

Mulder, M., Mulder, M., van Paassen, M. M., & Abbink, D. A. (2008). Haptic gas pedal feedback. *Ergonomics*, *51*(11), 1710–1720.

Neumann, H., & Deml, B. (2011). The Two-Point Visual Control Model of Steering - New Empirical Evidence. *Digital Human Modeling SE - 55*, *6777*, 493–502.

Nguyen, A., Sentouh, C., Popieul, J.-C., & Soualmi, B. (2015). Shared Lateral Control with On-Line Adaptation of the Automation Degree for Driver Steering Assist System: A Weighting Design Approach. In *2015 ieee 54th annual conference on decision and control* (pp. 857–862). Osaka, Japan.

Park, S., & Sheridan, T. B. (2004). Enhanced Human - Machine Interface in Braking. *IEEE Transactions on Systems, Man and Cybernetics, Part A: Systems and Humans*, *34*(5), 615–629.

Pérez Zuriaga, A. M., García García, A., Camacho Torregrosa, F. J., & D'Attoma, P. (2010). Modeling Operating Speed and Deceleration on Two-Lane Rural Roads with Global Positioning System Data. *Transportation Research Record: Journal of the Transportation Research Board*, *2171*, 11–20.

Reymond, G., Kemeny, A., Droulez, J., & Berthoz, A. (2001). Role of Lateral Acceleration in Curve Driving : Driver Model and Experiments on a Real Vehicle and a Driving Simulator. *Human Factors: The Journal of the Human Factors and Ergonomics Society*, *43*(3), 483–495.

Ritchie, M. L., McCoy, W. K., & Welde, W. L. (1968, jun). A Study of the Relation between Forward Velocity and Lateral Acceleration in Curves During Normal Driving. *Human Factors: The Journal of the Human Factors and Ergonomics Society*, *10*(3), 255–258.

Saleh, L., Chevrel, P., Claveau, F., Lafay, J.-F., & Mars, F. (2013). Shared steering control between a driver and an automation: Stability in the presence of driver behavior uncertainty. *IEEE Transactions on Intelligent Transportation Systems*, *14*(2), 974–983.

Saleh, L., Chevrel, P., Mars, F., Lafay, J. F., & Claveau, F. (2011). Human-like cybernetic driver model for lane keeping. In *18th ifac world congress* (Vol. 18, pp. 4368–4373).

Salvucci, D. D., & Gray, R. (2004). A two-point visual control model of steering. *Perception*, *33*(10), 1233–1248.

Sentouh, C., Chevrel, P., Mars, F., & Claveau, F. (2009a). A Human-Centred Approach of Steering Control Modelling. In *Proceedings of the 21st iavsd symposium on dynamics of vehicles on roads and tracks* (pp. 1–12). Stockholm, Sweden.

Sentouh, C., Chevrel, P., Mars, F., & Claveau, F. (2009b). A sensorimotor driver model for steering control. In *Proceedings of the 2009 ieee international conference on systems, man and cybernetics* (pp. 2462–2467).

Shao, Y., Xu, J., Li, B., & Yang, K. (2015, feb). Modeling the Speed Choice Behaviors of Drivers on Mountainous Roads with Complicated Shapes. *Advances in Mechanical Engineering*, *7*(2), 862610–862610.

Shino, M., Yoshitake, H., Hiramatsu, M., Sunda, T., & Kamata, M. (2014, aug). Deviated state detection method in driving around curves based on naturalistic driving behavior database for driver assistance systems. *International Journal of Automotive Technology*, *15*(5), 749–755.

Smisek, J., van Paassen, M. M., Mulder, M., & Abbink, D. A. (2013). Neuromuscular analysis based tuning of haptic shared control assistance for UAV collision avoidance. *2013 World Haptics Conference, WHC 2013*(April 2013), 389–394.

Takahashi, A., & Akamatsu, M. (2012). Speed Choice Model of Curve Entering Based on Naturalistic Driving Data. In *European conference on human centred design for intelligent transport systems.*

Turner, B., Woolley, J., & Cairney, P. (2015). An analysis of driver behaviour through rural curves: Exploratory results on driver speed. In *Australasian road safety conference.*

Tustin, A. (1947). The Nature of the Operator's Response in Manual Control, and its Implications for Controller Design. *Journal of the Institution of Electrical Engineers*, 190–206.

van der El, K., Pool, D. M., Damveld, H. J., van Paassen, M. M., & Mulder, M. (2015). An Empirical Human Controller Model for Preview Tracking Tasks. *IEEE Transactions on Cybernetics*, 1–13.

van Paassen, M. M., Boink, R. P., Abbink, D. A., Mulder, M., & Mulder, M. (n.d.). Four Design Choices for Haptic Shared Control. *Not yet published*.

Viviani, P., & Flash, T. (1995). Minimum-jerk, two-thirds power law, and isochrony: converging approaches to movement planning. *Journal of experimental psychology. Human perception and performance*, *21*(1), 32–53.

Wann, J. P., & Wilkie, R. M. (2004). How do We Control High Speed Steering? *Optic flow and beyond*, 371–389.

Xin, G. (2016). *Model-Based Individualization of Human-Like Steering Controllers* (Master's Thesis). Delft University of Technology.

Zhang, D., Xiao, Q., Wang, J., & Li, K. (2013, mar). Driver curve speed model and its application to ACC speed control in curved roads. *International Journal of Automotive Technology*, *14*(2), 241–247.